Noradrenergic Circuit Adaptations Underlying Predatory Aggression

Doctoral thesis

to obtain a doctorate (PhD)

from the Faculty of Medicine of the

University of Bonn

Güniz Göze Eren

from Manavgat, Turkey

2026

Written with authorization of

the Faculty of Medicine of the University of Bonn

First reviewer: Dr. James W. Lightfoot

Second reviewer: Prof. Dr. Ilona Grunwald Kadow

Day of oral examination: 15.12.2025

From the Max Planck Institute for Neurobiology of Behavior – caesar

Dedication

To my mother,
who once told me, when I was ten
and imagining that I might become a veterinarian:
“moleküler biyolog ol bari” —
at least be a molecular biologist.

This thesis is for her, for reminding me in difficult moments that trying my best was always enough.

Table of Contents

List of abbreviations

List of abbreviations

5-HT	5-hydroxytryptamine (Serotonin)
AVPR1A	Vasopressin Receptor 1A
COM	Center of Mass
CRISPR	Clustered Regularly Interspaced Short Palindromic Repeats
crRNA	CRISPR RNA
DNA	Deoxyribonucleic acid
Eu	Eurystomatous
F1, F2	Filial 1, Filial 2 (generations)
GFP	Green Fluorescent Protein
HCR	Hybridization Chain Reaction
HDBSCAN	Hierarchical Density-Based Spatial Clustering
HisCl	Histamine gated chloride channel
IQR	Interquartile Range
J2, J4	Juvenile stage 2, Juvenile stage 4
L1	Larval stage 1
NGM	Nematode Growth Medium
OL	Outer Labial (neurons)
OLQ	Outer Labial Quadrant (neurons)
P0	Parental (generation)
PCR	Polymerase chain reaction
PDF	Pigment Dispersing Factor (neuropeptide)
qPCR	Quantitative Polymerase Chain Reaction

RFP	Red Fluorescent Protein
RIM	Ring Interneuron M
RIC	Ring Interneuron C
RIP	Ring Interneuron P
RNA	Ribonucleic acid
RNA-FISH	RNA Fluorescent In Situ Hybridization
RT-qPCR	Reverse Transcription Quantitative Polymerase Chain Reaction
sgRNA	Single-guide RNA
St	Stenostomatous
TE buffer	Tris-EDTA buffer
UMAP	Uniform Manifold Approximation and Projection
UV	Ultraviolet
WT	Wildtype
YFP	Yellow Fluorescent Protein

1. Introduction

1.1. Behavioral Neuroscience: A Brief History of Neuroethology

“ I yearned to become a wild goose and, on realizing that this was impossible, I desperately wanted to have one and, when this also proved impossible, I settled for having domestic ducks.”

— Konrad Lorenz

The modern scientific study of animal behavior finds its roots in the tradition of naturalistic observation, pioneered by early ethologists such as Konrad Lorenz, Karl von Frisch and Nikolaas Tinbergen (Lorenz 1950; Tinbergen 1951; Frisch 1967). Through field studies and comparative approaches, these researchers established a foundation for understanding behavior as an evolved, adaptive trait shaped by natural conditions and evolutionary history. Among these early pioneers, Lorenz brought evolutionary depth to behavioral analysis. He approached behavior as an innate genetically encoded feature, shaped by natural selection and that could evolve similarly to morphological traits (Lorenz 1966). Karl von Frisch demonstrated honeybee communication, famously decoding the waggle dance and demonstrating that bees communicate the location of food sources using a symbolic form of spatial reference (Frisch 1967). Perhaps most enduringly, Niko Tinbergen established four questions which address the causation, development, function, and evolutionary origins of behavior, that have since become a foundational framework within behavioral science (Tinbergen 1951).

In parallel with these developments, advances in physiology and molecular biology also began to transform the study of behavior. The development of electrophysiological recording techniques, molecular genetics, and neuroanatomical tracing enabled researchers to dissect the molecular foundations of synaptic transmission (Katz and Miledi 1965), the electrical basis of neuronal communication (Hodgkin and Huxley 1952), and the role of discrete neural circuits in behavior (Evarts 1968). Additionally, key insights into the molecular mechanisms of neural development, synaptic transmission, and circuit function have been gained through studies in genetically tractable organisms such as *Caenorhabditis elegans*, *Drosophila melanogaster*, and *Mus musculus* (Benzer 1967; Brenner 1974; Capecchi 1989).

Therefore, the model organism approach allowed for precise, mechanistic descriptions of how behavior arises from neural activity and gene function although it is constrained by the behavioral repertoire of these species.

The convergence of ethology with systems neuroscience led to the emergence of neuroethology (Camhi 1941; Hoyle 1984). This field approaches behavior as an outcome of neural organization shaped by evolutionary processes and environmental demands, rather than treating behavior only as an assay for neural function. It aims to understand how the nervous system gives rise to natural behaviors, often by focusing on species with diverse behavioral repertoires across ecologically relevant contexts. Furthermore, species have often been chosen based on the distinctiveness of their behaviors and nervous systems, not on the availability of molecular tools. For instance, electric fish have been studied for their electrolocation and communication behaviors, which rely on specialized sensorimotor systems that allow for high resolution interaction with the environment (Nelson and MacIver 2006), while sea slugs (*Aplysia*) facilitated the detailed study of synaptic plasticity due to their large, easily identifiable neurons (Kandel 2001). These organisms exemplify what is now known as Krogh's principle - for many problems there is an animal on which it can be most conveniently studied (Krogh 1929).

This approach has been particularly productive in revealing how relatively small and evolutionarily conserved neural circuits can produce diverse and flexible behavioral outputs. In crickets, compact auditory and motor circuits generate species specific calling songs used in mate attraction and territorial interactions. This has provided insights into how neural systems that are shaped by reproductive pressures encode communication signals (Huber 1962). In leeches, decision making between crawling and swimming behaviors involves a small number of identified neurons whose coordinated activity has revealed how neural dynamics contribute to behavioral choice in response to environmental cues (Briggman et al. 2005). In *Drosophila melanogaster*, structured neural circuits support behaviors such as courtship and navigation (Thistle et al. 2012), with internal states like hunger modulating behavioral choices through defined neuromodulatory pathways (Sayin et al. 2019).

Furthermore, in many such systems, neural mechanisms are studied not in isolation but in direct relation to the species social behavior and natural habitat.

In recent years, a new subfield has emerged in the form of computational neuroethology, which applies machine learning, computer vision, and high throughput behavioral analysis to the study of natural animal behavior. This approach enables researchers to quantify complex, time varying actions across large populations with a level of objectivity, scale, and precision that was previously unattainable. By automating the tracking and classification of behavior, it becomes possible to discover previously unrecognized patterns and relate them directly to neural activity and underlying genetic and molecular processes involved (Branson et al. 2009; Dankert et al. 2009). For example, unsupervised algorithms have been used to identify distinct behavioral phenotypes, in *Drosophila* larvae across thousands of genotypes, revealing structure in behavior that would have escaped human observation (Vogelstein et al. 2014). This approach has also enhanced the utility of forward genetic screens and enabled richer correlations between behavior and brain function, especially in the context of social and state dependent interactions (Kabra et al. 2013). As computational tools continue to evolve, this integrative framework promises to further connect quantitative behavioral analysis with circuit level neuroscience.

In summary, the study of animal behavior has progressed from observational ethology to molecular neurobiology, with neuroethology serving as a conceptual and methodological bridge. The next step is to integrate evolutionary, physiological, and genetic levels of analysis into a coherent framework for understanding how behaviors arise and evolve.

1.2. Evolution of Behavior: Comparative Species Approach

Studying how behavior evolves offers more than understanding evolutionary mechanisms. It provides a powerful lens for uncovering general principles of how behaviors are generated, structured, and modified. Evolutionary comparisons reveal which features of behavior are flexible and responsive to selection and which are constrained by the architecture of the nervous system (Asahina et al. 2014; Jourjine and Hoekstra 2021).

Consequently, understanding how behavior evolves requires detailed analysis and systematic comparison across related taxa.

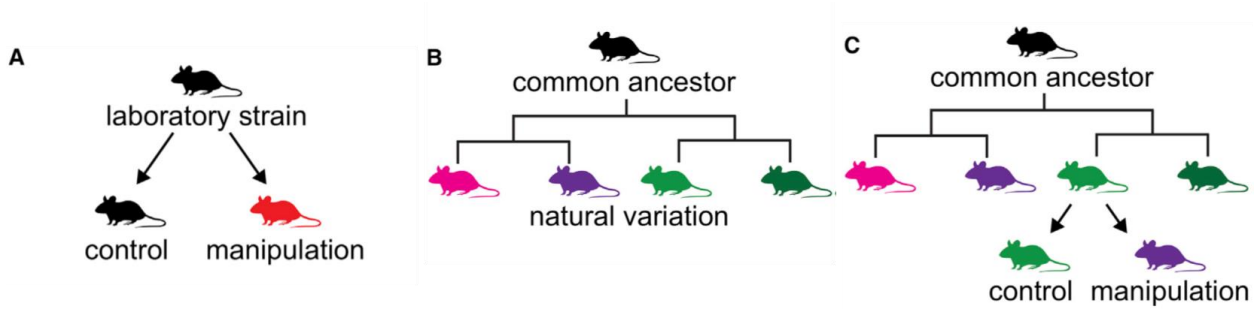

Fig. 1. Integrating manipulative and comparative approaches in behavioral neuroscience. **(A)** Traditional manipulative approaches in laboratory strains test the effects of specific genetic, molecular, or neuronal perturbations by comparing manipulated animals (red) to unmanipulated controls (black). **(B)** Comparative approaches in evolutionary biology examine natural variation in behavior across species or populations that share a common ancestor, correlating behavioral diversity with genetic or neural divergence. **(C)** Integrating these strategies allows manipulative tools to be applied in a comparative framework, for example by introducing targeted manipulations into one species (green) to test whether they can reproduce behavioral traits characteristic of another species (purple). Adapted from Jourjine & Hoekstra (2021).

A well-studied example comes from *Peromyscus* mice, where closely related species show differences in mating behavior and parental care. *P. maniculatus* is promiscuous and exhibits minimal parental investment while *P. polionotus* is monogamous and highly parental. Crucially, the underlying anatomical structures are largely conserved between these species. Instead, their behavioral differences are associated with divergent activity in defined hypothalamic circuits (Bendesky et al. 2017).

In *Drosophila*, comparative studies across species and strains have revealed variation in aggression, courtship, and locomotor behaviors, even when overall brain anatomy and genetic architecture remain conserved. For instance, differences in male courtship song structure between *D. melanogaster* and *D. simulans* are linked to changes in the temporal dynamics of central pattern generators, despite shared underlying motor circuits (Moulin et al. 2001). Aggression levels also vary across strains and species, often correlating with

differences in the expression or sensitivity of neuromodulators such as octopamine (Asahina et al. 2014). Similarly, foraging strategies and activity rhythms show genetic variation within *D. melanogaster* populations, shaped by natural alleles of the foraging gene, *for* (Allen and Sokolowski 2021; Hernández et al. 2021). These findings suggest that behavioral divergence can result from relatively subtle modifications in circuit connectivity, gene expression, or sensory tuning, allowing evolutionary change to act on a modular and accessible system (Dai et al. 2008; Coleman et al. 2024; Ye et al. 2024).

Similarly, in birds, song learning and vocal production offer a rich system for tracing behavioral divergence onto conserved forebrain circuits, where developmental and hormonal modulation shapes species specific repertoires (Brainard and Doupe 2002; Benichov et al. 2016).6). Comparative studies of taste receptor evolution also reveal how ecological specialization drives sensory and behavioral change. Hummingbirds, which evolved from insectivorous swifts, have repurposed ancestral umami taste receptors to detect sugars, enabling their adaptation to a nectar feeding niche (Baldwin et al. 2014). Similarly carnivorous birds such as penguins have lost multiple taste receptors including sweet and umami through pseudogenization of taste receptor genes (Zhao et al. 2015). These examples highlight how behavioral divergence can result not only from changes in neural circuitry but also from molecular alterations in sensory input pathway.

These examples demonstrate a recurring theme, behavioral divergence can arise through subtle modifications in circuit dynamics or gene expression without a complete rewiring of the nervous system. This insight is particularly powerful when extended to model invertebrate clades, such as the nematodes *C. elegans* and the well-established comparative species *Pristionchus pacificus* (Sommer and Lightfoot 2022). Despite sharing a highly stereotyped body plan and broadly similar nervous system organization, these species differ in key behavioral strategies including foraging, predation, and social interaction (Hong and Sommer 2006; Wilecki et al. 2015; Hong et al. 2019; Lightfoot et al. 2019, 2021; Moreno et al. 2019; Hiramatsu and Lightfoot 2023). Their tractability, combined with deep genomic resources and well characterized connectomes, makes them an ideal comparative system

for dissecting how behavioral evolution unfolds at the level of genes, circuits, and behavioral function (Bumbarger et al. 2013; Cook et al. 2019, 2025).The next sections will examine these two species in more detail, outlining their behavioral repertoires, ecological settings, and the molecular and genomic tools that make them uniquely suited for evolutionary analysis.

1.3. Invertebrate Neuromodulation and Behavior

In invertebrates, neuromodulators such as serotonin, dopamine, octopamine, and tyramine play central roles in shaping behavioral states. Rather than conveying rapid, point to point signals, neuromodulators reconfigure entire circuits to reflect changes in internal state, motivation, or environmental context (Marder 2012); (Bargmann 2012)). This capacity for dynamic reorganization is essential for behavioral flexibility, allowing animals to adapt the same neural circuits to multiple purposes depending on current needs.

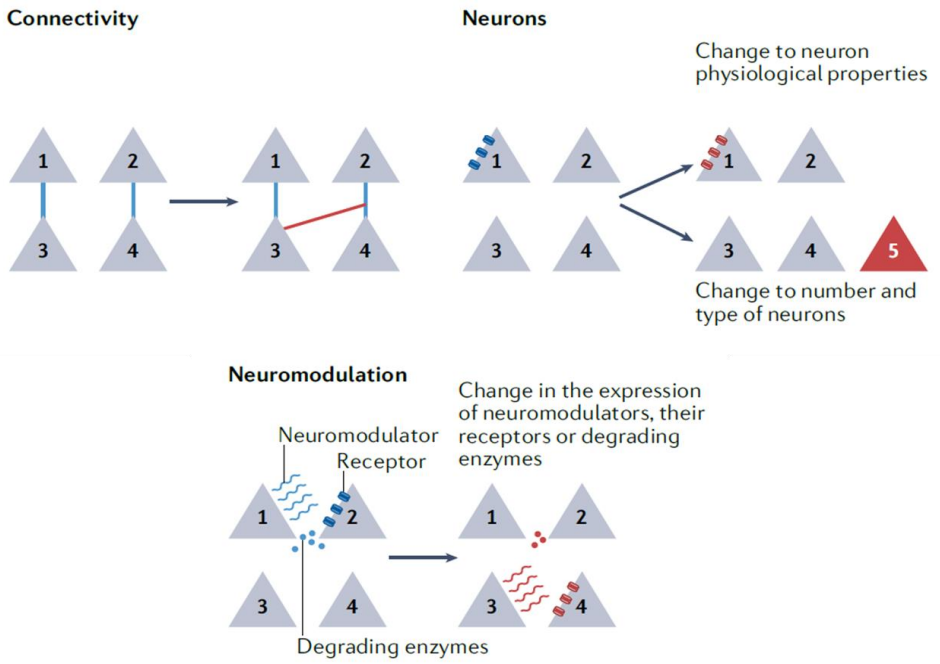

Fig. 2. Evolutionary routes for neural circuit change. Neural circuits can evolve through modifications at multiple levels. Connectivity: synaptic wiring among homologous neurons may change while overall circuit motifs are conserved. Neurons: evolutionary changes may also affect neuron properties directly, including alterations in physiological characteristics, or in the number and type of neurons present. Together, these mechanisms provide a substrate for behavioral plasticity and diversification across species. Neuromodulation: shifts in the expression of neuromodulators, their receptors, or degrading enzymes can alter circuit gain and state dependent responsiveness. Adapted from Roberts, Pop & Prieto-Godino (2022).

Serotonin (5-HT) regulates a broad range of behaviors including feeding, locomotion, and social interaction. In *C. elegans*, serotonin synthesis is dependent on the activity of the enzyme tryptophan hydroxylase (TPH-1). Serotonin subsequently promotes feeding by acting through G-protein coupled receptors such as SER-5 and SER-7, which increase cyclic-AMP and activate protein kinase A pathways, leading to increased excitability of pharyngeal and sensory neurons ((Flavell et al. 2013); (Dag et al. 2023). It also modulates locomotor circuits via the MOD-1 receptor, a serotonin gated chloride channel, which hyperpolarizes interneurons and reduces movement during satiety (Ranganathan et al. 2001a). These context dependent effects are achieved through differential receptor expression and cell specific downstream signaling cascades.

Dopamine, another conserved biogenic amine, is closely tied to reward evaluation, arousal, and experience dependent plasticity. In *Drosophila*, dopaminergic neurons project to the mushroom bodies, where they modulate synaptic plasticity underlying learning and memory (Caron et al., 2013; Liu et al. 2012; Waddell 2013). Dopamine acts through D1-like receptors (DopR1) and D2-like receptors (DopR2), which regulate cyclic-AMP levels and influence both short term decision making and longer term motivational state (Sayin et al. 2019). These receptors modulate synaptic strength and responsiveness to sensory cues, affecting how stimuli are evaluated in behavioral contexts such as exploration and foraging. In *C. elegans*, dopamine also links sensory cues to behavioral state. It is synthesized by the tyrosine hydroxylase, CAT-2 and it plays a key role in adapting gait during transitions between crawling and swimming, dopaminergic neurons respond to mechanical input from body bends, allowing the animal to adjust its motor patterns based on environmental context (Vidal-Gadea et al. 2011). Dopamine also contributes to nonassociative learning, such as habituation to repeated mechanical stimuli, by regulating neuronal responsiveness within sensory circuits (Kindt et al. 2007).

Octopamine is functionally analogous to vertebrate noradrenaline and acts as a general arousal signal in many invertebrates. In *Drosophila*, octopamine is released from ventral unpaired median (VUM) neurons and binds to α- and β-adrenergic like receptors, which activate intracellular signaling pathways including cAMP and phospholipase-C (Roeder 2005). These pathways increase intracellular calcium and enhance synaptic release, promoting aggression, courtship initiation, and locomotor readiness depending on the circuit context. In *Caenorhabditis o*ctopamine is synthesized by the tyramine β-hydroxylase TBH-1 and is known to function in arousal, locomotion, and learning by acting on specific G protein coupled receptors such as SER-3 and SER-6. It modulates synaptic transmission and behavioral responsiveness particularly under starvation and stress conditions (Suo et al. 2006).

Tyramine, a precursor to octopamine, was once thought to serve only as a biosynthetic intermediate but is now recognized as a distinct neuromodulator with its own receptors and

behavioral roles. It acts through TAR1 and TAR2 receptors, which are coupled to G-protein signaling (Kutsukake et al. 2000). In *Drosophila* larvae, tyramine suppresses locomotion through inhibitory signaling to motor neurons, whereas octopamine enhances it (Saraswati et al. 2004).The balance of these systems shapes motor output in a state dependent manner. In *C. elegans* tyramine is synthesized by the tyrosine decarboxylase enzyme TDC-1 and is released from the RIM and RIC neurons. It has been shown to regulate reversal and escape behaviors in response to sensory cues. This activity includes inhibiting forward locomotion and promoting rapid reversal and turning through inhibitory control over cholinergic motor neurons (Pirri et al. 2009).

These systems highlight how neuromodulators act not just as on off switches but as tuning mechanisms, adjusting circuit gain, temporal dynamics, and sensory responsiveness (Zhang et al. 2008; Li et al. 2011; Inagaki et al. 2012).They function as context sensitive regulators that enable nervous systems to flexibly prioritize behaviors such as feeding, egg laying, or withdrawal. Invertebrate nervous systems frequently employ neuromodulation to allow sensory inputs to be interpreted in light of physiological state and past experience. This enables a relatively small and evolutionarily constrained neural substrate to support a wide range of behaviors. From an evolutionary perspective, neuromodulation offers a solution to the challenge of behavioral plasticity, it allows new behavioral strategies to emerge without requiring larger numbers of neurons or the higher metabolic cost associated with more complex circuit architectures. This molecular architecture of modulation makes behavioral control both flexible and evolvable, providing a key mechanism by which species can diversify behavioral strategies while retaining conserved neural substrates.

The study of neuromodulatory control in invertebrates offers more than insights into species specific behaviors. It provides a mechanistic foundation for understanding how nervous systems organize flexible responses to changing internal and external conditions. Because many of the core signaling pathways, monoaminergic modulation and G-protein coupled receptor cascades are conserved across phyla, invertebrate models serve as tractable systems for uncovering principles that also apply to vertebrate brains (Bargmann

2012; Marder 2012). Key features such as state dependent gating, neuromodulatory tuning of excitability, and behavioral prioritization through circuit level reconfiguration are also found in mammalian systems, where similar processes underlie attention, motivation, hunger and other affective states (Aston-Jones and Cohen 2005; Yang et al. 2024). As such, insights from organisms like *Drosophila* and *C. elegans* continue to inform a broader understanding of how neural circuits generate adaptive, context sensitive behavior across evolutionary time scales.

1.4. *C. elegans* as a Model for Behavior

The nematode *Caenorhabditis elegans* was established as a model organism by Sydney Brenner in the 1960s with the aim of bringing genetic and molecular approaches to complex biological problems such as development and nervous system function (Brenner 1974). It was chosen for its small size, transparent body, rapid generation time, and relatively simple anatomy. These features made it uniquely suitable for both large scale genetic screens and high resolution cellular and behavioral analyses.

Adult *C. elegans* hermaphrodites possess exactly 302 neurons, all of which were originally reconstructed through serial section electron microscopy (White et al. 1986). More recently, complete connectomes have been mapped across both sexes and developmental stages, offering an unparalleled view of neural architecture throughout the life cycle (Cook et al. 2019, 2020; Witvliet et al. 2021). Its developmental lineage is also fully known (Sulston and Horvitz 1977), and its genome was the first from a multicellular animal to be completely sequenced (Consortium* 1998). The availability of precise cell fate maps and powerful genetic tools, including RNA interference (Fire et al. 1998) and transgenic markers such as GFP (Chalfie et al. 1994), allows for detailed dissection of gene function and neural circuitry.

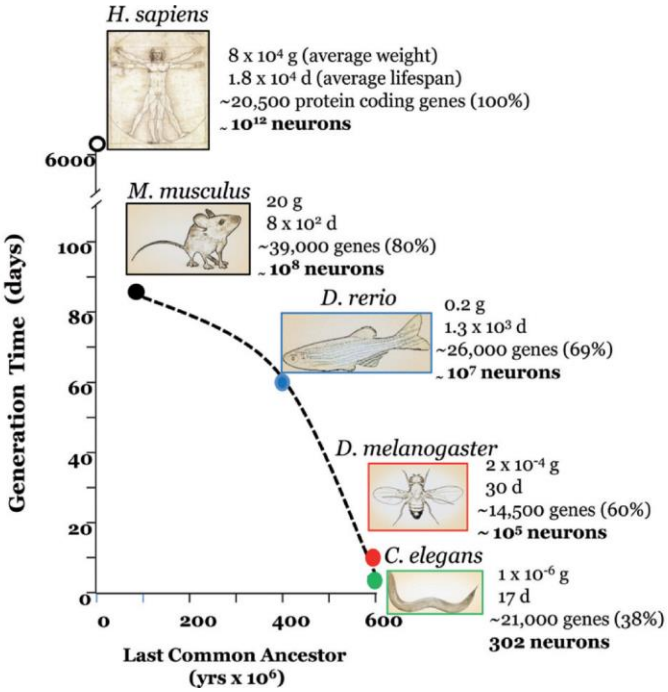

Fig. 3. Comparative features of major genetic model organisms used in behavioral neuroscience. The four principal genetic models, *Mus musculus* (mouse), *Danio rerio* (zebrafish), *Drosophila melanogaster* (fruit fly), and *Caenorhabditis elegans* (nematode) are compared with *Homo sapiens*. The ordinate indicates generation time (in days), reflecting suitability for genetic studies, while the x axis shows evolutionary distance from humans, expressed as time since the last common ancestor. For each species, additional attributes relevant to behavioral research are listed: body weight, lifespan, number of protein coding genes (with percentage of human homologues), and estimated number of neurons. Together, these comparisons illustrate the tradeoffs between phylogenetic proximity to humans, nervous system complexity, and experimental tractability. Adapted from White (2022).

Although anatomically simple, *C. elegans* displays a broad repertoire of well-defined and context dependent behaviors, including chemotaxis, foraging, egg laying, feeding, and escape responses (Schafer 2005). These behaviors are regulated by a compact but functionally diverse nervous system that is subject to modulation by conserved signaling molecules such as serotonin, dopamine, octopamine, and neuropeptides (Bargmann 1998; Alkema et al. 2005; Flavell et al. 2013). Recent peptidomic mapping has further expanded our understanding of neuromodulation in *C. elegans*, revealing a dense neuropeptidergic connectome that coordinates activity across circuits and contributes to dynamic state regulation (Ripoll-Sánchez et al. 2023). Such neuromodulatory systems enable behavioral

flexibility without the need for an expansive neuronal network. From a systems perspective, the worm's nervous system can be thought of as comprising layered behavioral modules, where global states gate access to specific motor outputs in a context dependent manner (Robson and Li 2022). This organization makes it possible to study how behavioral priorities are encoded and reconfigured in real time.

In the sections that follow, the neural and molecular mechanisms underlying feeding and foraging will be described in greater detail.

1.5. *C. elegans* Feeding Behavior and Associated Behavioral States

Feeding behavior in *C. elegans* is tightly orchestrated by a compact and well characterized neuromuscular system centered around the pharynx. This a specialized organ that acts as a pump to draw in bacterial food and also contains a grinder which consists of hardened discs that break open the bacterial cells before they are passed into the intestine (Albertson and Thompson 1976). The pharynx consists of 80 nuclei, including 20 neurons organized into a largely autonomous subnetwork, which makes it an ideal model for dissecting the neural basis of feeding (White et al. 1986; Avery and Horvitzt 1989; Cook et al. 2020).

The anatomical and functional simplicity of the pharyngeal system allows for highly resolved analysis of how specific neuromodulators tune the timing and strength of motor output. For instance, direct optogenetic or pharmacological manipulation of pharyngeal neurons can induce or suppress feeding in the absence of food, demonstrating the capacity of these modulators to override sensory input when internal state dictates (Dallière et al. 2017).

Pumping involves coordinated contractions initiated by motor neurons such as MC, which are activated by mechanical stimulation from food and serotonin signaling (Raizen and Avery 1994). M3 neurons control the timing of relaxation, while M4 drives isthmus peristalsis critical for food transport (Avery and Horvitz 1987) Neurotransmitters including acetylcholine, glutamate, serotonin, and octopamine modulate the circuit. Among them, serotonin plays a

key role by acting on receptors like SER-7 and MOD-1 to modulate pharyngeal excitability and suppress locomotion during feeding states (Hobson et al. 2006; Dag et al. 2023). The presence of food triggers serotonin release from the NSM neurons, which in turn acts on multiple serotonin receptors, including SER-7 and SER-5, to increase the excitability of pharyngeal muscles and promote sustained pumping (Flavell et al. 2013; Dag et al. 2023). Beyond direct control of pharyngeal activity, serotonin also shapes food seeking behavior by promoting transitions from exploration to local search and by maintaining quiescence when food is abundant. The serotonin gated chloride channel MOD-1 is involved in this process, contributing to behavioral transitions by modulating downstream motor circuits (Ranganathan et al. 2001b).

Dopaminergic signaling also contributes to feeding related behaviors such as the enhanced slowing response when well fed animals encounter bacteria, dopamine released from mechanosensory neurons triggers a transient locomotor deceleration (Sawin et al. 2000). Octopamine on the other hand modulates aversive responses and acts antagonistically to serotonin inhibiting pharyngeal pumping. This likely reflects its role in mediating starvation induced foraging behavior (Rogers et al. 2001).

Feeding behavior in *C. elegans* does not occur in isolation but is embedded in a broader foraging strategy that includes dynamic switching between two global behavioral states: roaming and dwelling. Roaming is characterized by sustained forward movement and sparse turning, allowing broad exploration of the environment, while dwelling is marked by slower movement and frequent reversals, optimizing local exploitation of food resources (Fujiwara et al. 2002; Flavell et al. 2013, 2020; Dag et al. 2023). These states are regulated by neuromodulators such as serotonin and the neuropeptide PDF, which act in opposition to coordinate transitions based on environmental input and internal cues. Sustained serotonergic activity in the NSM neuron promotes dwelling, while PDF released from AVB neurons promotes roaming by inhibiting NSM via feedback inhibition (Flavell et al. 2013, 2020; Dag et al. 2023).

In *C. elegans*, food sensing relies on a complex network of sensory neurons capable of detecting a wide range of chemical and mechanical cues. Among these, amphid neurons such as AWA, AWB, AWC, ASH, ASE, and ASI play key roles. AWA and AWC are involved in sensing attractive volatile odors associated with bacterial food, while ASE detects water-soluble attractants like salts and amino acids (Bargmann et al. 1993; Sengupta et al. 1996). ASH neurons detect aversive cues, contributing to food quality assessment and avoidance of harmful environments (Kaplan and Horvitz 1993). The inner labial neurons IL1 and IL2, though less extensively studied than amphid neurons, have been implicated in mechanosensory and chemosensory processing (Lee et al. 2012). They are thought to play a role in head movement coordination and local search behaviors, particularly under starvation or stress conditions (Lee et al. 2012). Outer labial (OL) neurons have been proposed to contribute to mechanosensory responses, including potential roles in sensing food texture (Britz et al. 2021).

Starvation strongly modulates food sensing and foraging behavior in *C. elegans*. In starved animals, the gain of chemosensory responses is enhanced, increasing sensitivity to food related odors (Ryan et al. 2014; Bello et al. 2021). ASI neurons, for example, integrate metabolic state and food availability via insulin like signaling, while AWA and AWC activity is potentiated under starvation to increase odor guided foraging (Ryan et al. 2014; Bello et al. 2021). IL2 neurons have also been reported to influence foraging plasticity and starvation induced behaviors (Lee et al. 2012; Zaslaver et al. 2015).

From an evolutionary perspective, the diversity of nematode feeding strategies ranging from bacterial feeders like *C. elegans* to predatory species like *P. pacificus* is paralleled by variations in pharyngeal morphology, neuromodulatory and circuit connectivity (Chiang et al. 2006; Rivard et al. 2010; Hong et al. 2019). *C. elegans* thus provides a neurobehavioral reference point for studying how conserved circuits support divergent strategies across nematode lineages.

1.6. *Pristionchus pacificus*: A Model for Evolutionary Divergence Studies

The nematode *P. pacificus* has emerged as a powerful satellite model to *C. elegans*, offering a complementary perspective on the evolution of development, behavior, and plasticity. Despite diverging from *C. elegans* approximately 200 million years ago (Dieterich et al. 2008; Howard et al. 2022), *P. pacificus* shares many key biological features with its more established counterpart. It is similarly small, self fertilizing, and fast growing, with a fully sequenced genome and extensive genetic tools, including CRISPR mediated gene editing and transgenesis (Hong and Sommer 2006; Rödelsperger et al. 2014; Witte et al. 2015; Han et al. 2020; Sommer and Lightfoot 2022)). A complete connectome has also been reconstructed, further enhancing its suitability for neurobiological comparisons (Bumbarger et al. 2013; Cook et al. 2025a).

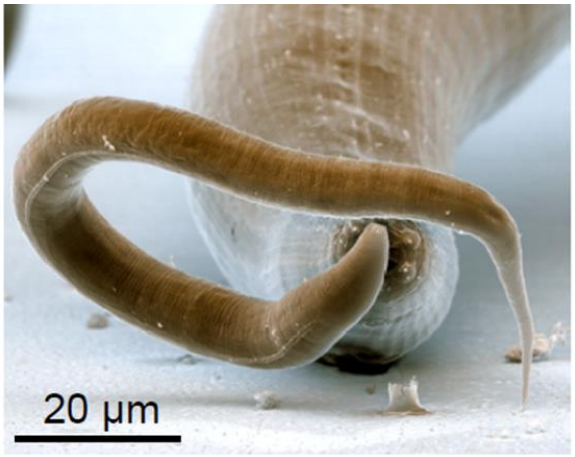

Fig. 4. Scanning electron micrograph showing *P. pacificus* (background), a predatory nematode equipped with teeth-like mouthparts, alongside a *C. elegans* larva (foreground), which represents one of its natural prey species. Adapted from Eren et al. (2024).

Unlike *C. elegans*, which thrives on the bacteria associated with decaying vegetation, *P. pacificus* exhibits a necromenic lifestyle, persisting in a stress resistant dauer stage on living scarab beetles and resuming development upon the host's death (Herrmann et al. 2006). This ecological association exposes it to a diverse and competitive environment, prompting adaptations in morphology and behavior (Sommer and Lightfoot 2022). Central to these adaptations is a striking case of developmental plasticity: *P. pacificus* can switch

between two distinct mouth forms stenostomatous (St), with a single blunt tooth, and eurystomatous (Eu), with two prominent teeth suited for predation on other nematodes (Ragsdale et al. 2013). This dimorphism is influenced by environmental cues such as culture density, nutrient availability, and hormonal signals including dafachronic acid, and is regulated by a genetic network involving *eud-1*, *nhr-40*, and chromatin remodelers (Bento et al. 2010; Kieninger et al. 2016; Serobyan et al. 2016; Werner et al. 2017; Piskobulu et al. 2025).

Predatory feeding in *P. pacificus* is a contact-dependent behavior requiring physical interactions between predator and prey (Wilecki et al. 2015). Sensory cilia exposed to the environment play a crucial role in this detection, with the RFX transcription factor *daf-19* being essential for ciliogenesis and prey recognition (Moreno et al. 2018, 2019). Moreover, mechanosensory and chemosensory inputs converge onto IL2 neurons, whose exposed ciliated endings enable prey contact detection (Roca et al. 2025). Loss of *daf-19* disrupts this process, highlighting the importance of sensory cilia in the initiation of predation (Roca et al. 2025).

Alongside this, tooth function is essential for the execution of predation. Structural integrity and proper development of the dorsal and subventral teeth rely on cuticle remodeling enzymes (Sun et al. 2023). Mutations in *chs-2*, which encodes a chitin synthase, or in astacin metalloproteases lead to malformed teeth covered by an uncut layer of cuticle, rendering them nonfunctional (Ishita et al. 2023; Sun et al. 2023). These findings underscore that predation in *P. pacificus* is not simply a behavioral novelty but is supported by specific molecular and morphological adaptations of the feeding apparatus.

Neuromodulators have also been shown to play a critical role in coordinating the predatory sequence. Serotonin orchestrates the temporal coupling between pharyngeal pumping and tooth movement, ensuring effective penetration of prey cuticles upon initiation of predation (Okumura et al. 2017). In serotonin deficient mutants, this coupling is lost, leading to reduced predation success (Okumura et al. 2017; Ishita et al. 2021). Thus, 5-HT not only modulates internal states but also directly facilitates motor coordination between

independently controlled muscular systems (Ishita et al. 2021). In addition, *P. pacificus* also exhibits substantial behavioral complexity associated with its predatory feeding. These include kin discrimination, social interactions as well as context sensitive decision making strategies that differ from those of *C. elegans* (Wilecki et al. 2015; Lightfoot et al. 2019; Quach and Chalasani 2020; Hiramatsu and Lightfoot 2023).

Therefore, *P. pacificus* illustrates the broader value of comparative model clades in evolutionary biology. While model organisms have proven adept at understanding conserved features of the nervous system, they fail to capture the full range of biological variation or evolutionary innovation. Instead, the pairing of new tractable species that have divergent life histories, ecologies, and behaviors alongside well studied model organisms enables researchers to distinguish conserved principles from lineage specific adaptations. Such comparative approaches and the establishment of model clades not only refine the interpretation of data from canonical models but also open new avenues for uncovering how evolutionary innovation is shaped by gene networks, neural circuits, and morphology across species.

1.7. Thesis Aim

The evolution of novel behaviors poses one of the most compelling questions in neurobiology: How do changes at the molecular and circuit level give rise to behavioral innovations? This thesis explores the evolution and mechanistic underpinnings of predatory behavior in the nematode *Pristionchus pacificus* as a model for the evolutionary neurobiology of aggression and tries to answer the following questions.

Which molecular and neural mechanisms contribute to predatory behavior in *P. pacificus*? This includes identifying specific neurons and neuromodulators that modulate predatory aggression in response to internal and external cues. How do the sensory neurons and the modulatory pathways coordinate transitions to predatory behavior? Which receptors receive these signals and how do these modulatory inputs bias the animal toward predatory versus non predatory behavioral states. In addition, what evolutionary changes in neural circuitry and gene expression distinguish *Pristionchus pacificus* from *Caenorhabditis*

elegans? In this thesis, I address these questions through a comparative analysis and aim to identify specific processes that have diverged across evolutionary time scales that may have contributed to the emergence of predatory aggression in *P. pacificus*.

To address these questions, the study combines genetic tools such as CRISPR/Cas9 mediated gene editing and transgenic reporters to manipulate and monitor specific components of the nervous system involved in aggression. Behavioral analyses are performed using automated tracking and machine learning based classification, enabling quantitative assessment of predatory responses across different genetic and experimental contexts.

By focusing on a behavior that differs markedly between two experimentally tractable nematodes, this thesis seeks to contribute to a broader understanding of how neuromodulatory systems support behavioral flexibility, and how neural adaptations shape behavioral divergence. The findings are expected to complement existing models of behavioral evolution by offering a detailed case study situated at the interface of genetics, neuroscience and ethology.

2. Materials and Methods

2.1. Nematode Husbandry and Strains

2.1.1. Strain Maintenance

All strains used in this study are listed in Table S1. *Caenorhabditis elegans* and *Pristionchus pacificus* were cultured at 20 °C on standard Nematode Growth Medium (NGM) plates seeded with *Escherichia coli* OP50.

2.1.2. Generation of Transgenic Strains

The *Ppa-myo-2p::*RFP (JWL27) strain was generated following a previously established protocol (Han et al. 2020). A 1231 bp fragment upstream of the predicted start codon of the *Ppa-myo-2* gene was amplified by PCR and cloned into the pZH009 plasmid containing codon optimized TurboRFP using NEBuilder HiFi DNA Assembly Master Mix (New England Biolabs). Transcriptional reporter constructs for *Ppa-tbh-1*, *Ppa-tdc-1*, *Ppa-ser-3*, *Ppa-ser-6*, and *Ppa-lgc-55* were generated by cloning promoter regions of 1958 bp, 1585 bp, 1996 bp, 1996 bp, and 1917 bp respectively into TurboRFP or GFP expression vectors. Dr. Jun Liu and Dr. Wolfgang Bönigk contributed to cloning plasmids for the transgenic lines. Injection mixes contained 10 ng/µl of digested reporter construct, 10 ng/µl of *Ppa-egl-20p:*:GFP co-injection marker, and 60 ng/µl of digested genomic carrier DNA. Dr. Marianne Roca, Fumie Hiramatsu, and Dr. James W. Lightfoot performed microinjections for strain construction. Young adult hermaphrodites were injected in the gonads and screened for transgenic animals using an Axio Zoom V16 epi-fluorescence microscope (Zeiss). Confocal imaging was performed with a Leica SP8 system. Dr. Luis Alvarez acquired confocal images of the *ser-3, ser-6*, and *lgc-55* reporter lines.

2.1.3. Stable Integration of Transgenic Lines via UV Irradiation

Ppa-myo-2p::RFP was integrated into the *P. pacificus* genome as previously described (Eren et al. 2022). 10 NGM plates, each seeded with approximately 20 transgenic animals, were irradiated at 0.050 J/cm² using a UV crosslinker (CL-3000, Analytik Jena). After 3–4 days, fluorescent F1 progeny were isolated and transferred individually to 120 plates. F2 animals were screened, and plates with ≥75% fluorescent offspring were selected for further

propagation. Individual integrated lines with 100% transmission were maintained and subsequently outcrossed four times to minimize background mutations.

2.2. High Throughput Behavioral Imaging Setup

Fluorescent imaging of *Ppa-myo-2p::*RFP animals was conducted at 1× magnification on an Axio Zoom V16 (Zeiss) using a Basler acA3088-57um camera with 15 ms exposure. Animals were recorded at 30 frames per second for 10 minutes unless stated otherwise. Animals visible in the field of view for at least 60 seconds were included in analyses.

2.3. Nematode Husbandry and Predatory Assay Design

Caenorhabditis elegans prey were cultured on OP50 seeded plates until starvation, yielding large numbers of L1 larvae. Larvae were harvested by washing plates with M9 buffer, filtering through 20 µm filters, centrifugation, and pipetting 4 µl of pellet onto 6 cm unseeded NGM assay plates. A copper ring (1.5 cm × 1.5 cm) was used to confine the area of observation. Forty young adult *P. pacificus* predators of the eurystomatous morph were starved for 2 hours prior to introduction into the arena. Animals were allowed to acclimate for 15 minutes before acquiring 10 minute behavioral recordings.

2.4. Bacterial Food Source Assay Design

For bacterial tracking assays, 300 µl of an *E. coli* OP50 culture was spotted onto 6 cm NGM plates and incubated for 24 hours prior to use. The same copper arena was applied to restrict movement. Forty young adult *P. pacificus* animals, starved for 2 hours, were introduced into the arena. Following a 15 minute recovery period, recordings were conducted for 10 minutes.

2.5. Manual Predation Assays (Corpse Assay)

Predation behavior was assessed using a standardized corpse-counting assay. Starved *C. elegans* prey were prepared by washing and filtering OP50 seeded cultures to isolate L1 larvae. A 1 µL pellet of larvae was placed on a 6 cm unseeded NGM plate. Five adult *P. pacificus* or *Allodiplogaster sudhausi* predators (confirmed to be eurystomatous)

were transferred to the plate. After a 2-hour interaction period, prey corpses were manually counted.

2.6. Automated Behavioral Tracking and Classification

2.6.1. Automated Behavioral Tracking Using Pharaglow

Automated analysis of animal behavior was conducted using the Python based analysis suite PharaGlow (Bonnard et al. 2022). This tool performs a three-stage tracking procedure: first, it detects the center of mass (COM) and resolves overlapping individuals; second, it constructs continuous trajectories by linking these detections over time; and third, it extracts morphological features including the centerline, body contour, and body width, which enable quantification of pharyngeal pumping behavior. The resulting dataset includes spatial coordinates and straightened images for each tracked animal. Pumping events were identified by computing the inverted skew of fluorescence intensity across the pharyngeal region, a feature sensitive to lumen opening and muscular contraction.

The behavioral classification framework used in this study was developed in collaboration with Leonard Boger, a fellow PhD student in our lab. He was primarily responsible for the design, implementation, and optimization of the machine learning algorithms, including the feature engineering, UMAP embedding, clustering, and classifier training.

2.6.2. Feature Engineering and Data Curation

Initial behavioral metrics extracted by PharaGlow included COM coordinates, body centerline, pumping rate, and skew of fluorescence intensity (as a proxy for pharyngeal activity). From these primary measurements, two additional behavioral descriptors were derived: locomotor velocity and head angle. Velocity was calculated as the displacement of COM over a 2 second interval (60 frames), and head angle was defined as the angular deviation between the direction of movement and the animal’s anterior body axis. The head axis vector was determined from the first to fifth sampling point along the normalized centerline.

To characterize the temporal dynamics of these behaviors, wavelet decomposition was performed using the pywt package with a Gaussian (gaus5) wavelet. The highest frequency component detected was used as a summary feature. For skew, scales corresponding to ~1.3 Hz and ~3.9 Hz were included directly, reflecting frequencies typical of pharyngeal pumping. For velocity, only one scale (~0.8 Hz) was selected. The final feature set consisted of nine behaviorally relevant variables.

To minimize the impact of tracking artifacts, frames containing overlapping animals were excluded. Overlap was identified by detecting frame-wise body area measurements exceeding 1.5 times the mean for that recording.

2.6.3. Manual Annotation of Behavioral States

A subset of behavioral videos was manually annotated by an expert observer using LabelStudio. Sequences were classified into one of four categories: 'biting', 'feeding', 'exploration', or 'quiescence', based on established behavioral definitions (Wilecki et al. 2015). Labels were assigned by inspecting the velocity and pumping traces in combination with video playback. For unlabeled recordings, only recording context was used as a label either "on OP50" or "on *C. elegans* larvae".

2.6.4. Data Preprocessing and Normalization

Before clustering or classification, the raw feature data was preprocessed using a custom pipeline implemented with the sklearn library. Lagged versions of key features (velocity, instantaneous pumping, head angle, mean pumping) were added with shifts of ±5, ±10, and ±15 frames to capture short-term temporal dependencies. Features were then averaged using a 1-second (30 frame) rolling window and down-sampled to 1 Hz. Labels were down-sampled using the most frequent class within each 1-second window. To reduce edge effects from smoothing, the first and last second of each recording were excluded.

The resulting dataset was transformed with a Yeo-Johnson power transform to reduce skewness and scaled using a robust normalization strategy. These transformation parameters were learned from the training set and applied consistently to all new data.

2.6.5. Unsupervised Clustering using UMAP and HDBSCAN

The preprocessed dataset comprising 106 animals recorded during assays with either larvae or bacterial food was embedded into a three-dimensional space using Uniform Manifold Approximation and Projection (UMAP; Python umap module). The parameters used were: n neighbors = 70, min dist = 0, repulsion strength = 4, negative sample rate = 15, disconnection distance = 0.85, and n components = 3. The resulting embedding was subjected to hierarchical density-based spatial clustering (HDBSCAN), with the number of behavioral clusters determined by optimizing the silhouette score. To assign behavioral meaning to each cluster, overlap with manually annotated behavioral labels was evaluated, and feature distributions were inspected to confirm cluster identities. Visual inspection of the original video recordings was used for final confirmation of behavioral state assignments.

2.6.6. Supervised Behavioral State Classification with XGBoost

The embedded and clustered data were then used to train a supervised XGBoost classifier for behavioral state prediction. Nine out of the 106 videos were excluded from training and reserved as a test set. These were selected to reflect the overall distribution of behaviors in the training set. Hyperparameter optimization was conducted using Bayesian search and cross-validation. The training data were split using stratified group shuffle splitting, treating each recording as a single group to preserve independence. Once the optimal parameters were identified, a final model was trained using the full training set. Classifier performance was evaluated by comparing predictions on the held-out test set to the HDBSCAN-derived labels using standard performance metrics. To avoid low-confidence predictions, a probability threshold of 50% was applied; predictions below this threshold were labeled as “None”. This approach excluded only 1.2% of frames (not counting excluded start and end segments), providing high confidence behavioral classification.

2.6.7. Validation of Clustering on an Independent Dataset

To assess the generalizability of the clustering, the full analysis pipeline was applied to an independent validation dataset containing 254 animals. This validation dataset was

subsampled to match the original training set in the distribution of frames from bacteria and larval conditions. All UMAP parameters were kept consistent to ensure comparability.

2.7. Molecular and Genetic Techniques

2.7.1. CRISPR/Cas9 Genome Editing

CRISPR based mutagenesis in *P. pacificus* was carried out following previously established protocols (Witte et al. 2015). Gene specific CRISPR RNAs (crRNAs) targeting early exons were synthesized (IDT) and annealed with tracrRNA at 95 °C, then allowed to cool to room temperature. The duplex RNA was complexed with purified Cas9 protein (IDT) and diluted in TE buffer to final working concentrations of 18.1 µM sgRNA and 12.5 µM Cas9. Microinjections were performed into the gonads of young adult hermaphrodites. P0 animals were removed after 12–24 hours, and F1 progeny were isolated and genotyped by Sanger sequencing following a 24-hour egg-laying period. Supplementary Tables 1 and 2 list all mutant lines, sgRNA sequences, and primers used. Dr. Marianne Roca, Fumie Hiramatsu, and Dr. James W. Lightfoot performed microinjections for strain construction.

2.7.2. Quantification of Transgene Copy Number and Expression (qPCR)

Quantification of transgene copy number and expression via qPCR was performed by our collaborator Ziduan Han (Northwest A & F University, China). Ziduan was responsible for experimental design, DNA/RNA extraction, primer validation, and execution of the qPCR and RT-qPCR assays.

To quantify transgene copy number and assess expression of the *Ppa-myo-2p::RFP* construct in the UV-integrated JWL27 line, DNA and RNA were extracted from *P. pacificus* hermaphrodites. Thirty J4 to young adult animals from non-starved plates were collected for DNA extraction using the NEB Monarch DNA Kit (final elution volume: 35 µL). For RNA extraction, a full plate of non-starved animals was processed with the Zymo RNA Mini Kit (elution volume: 30 µL).

Quantitative PCR (qPCR) and reverse transcription qPCR (RT qPCR) were performed to determine transgene copy number and transcript abundance. For copy number estimation,

primers targeting the RFP sequence were compared against two single copy reference genes, *Ppa-gpd-3* and *Ppa-csg-1*. To assess *Ppa-myo-2p::RFP* transcript levels, RFP expression was compared to endogenous *Ppa-myo-2* mRNA using two independent primer pairs. DNA samples were diluted 1:10, while RNA samples were used undiluted. All assays were run with three technical replicates and two biological replicates.

2.7.3. Cellular Resolution Gene Expression Analysis via Hybridization Chain Reaction (HCR) RNA-FISH

To visualize gene expression at cellular resolution, RNA fluorescent in situ hybridization was performed using Hybridization Chain Reaction (HCR) in *P. pacificus*. The protocol was adapted from published methods to improve tissue permeability, including an extended Proteinase K treatment (200 µg/mL for 1 hour at room temperature)(Ramadan and Hobert 2024).

Worms were hybridized overnight at 37 °C in probe hybridization buffer with 200 pmol of each probe set. Dual HCR labeling was used to simultaneously detect *Ppa-tbh-1* (X1-488) and *Ppa-tdc-1* (X2-647), or *Ppa-klp-6* (X1-488) and *Ppa-ser-3* (X2-647). Triple labeling combined *Ppa-ser-3* (B2, Alexa Fluor 546), *Ppa-ser-6* (B3, Alexa Fluor 488), and *Ppa-lgc-55* (B1, Alexa Fluor 647).

2.7.4. Phylogenetic Analysis of Neuromodulatory Genes

To reconstruct the evolutionary history of genes involved in neuromodulator biosynthesis and signaling, reciprocal best BLAST hits were identified between *P. pacificus* and *C. elegans* genome assemblies. Amino acid sequences were aligned and phylogenies were inferred using the Maximum Likelihood method under the JTT substitution model. The best fitting tree was selected based on the highest log likelihood score. Initial trees for heuristic search were generated using Neighbor Joining and BioNJ algorithms. Branch lengths represent the number of substitutions per site. All analyses were performed using MEGA X (Kumar et al. 2018).

2.8. Pharmacological and Pharmacogenetic Manipulations

2.8.1. Exogenous Application of Neuromodulators

To test the effect of exogenous biogenic amines, predation assays were conducted on agar plates supplemented with 2 mM tyramine or octopamine (Sigma). Neuromodulator solutions were added to freshly autoclaved NGM cooled to 55 °C. Plates were poured and allowed to solidify. *P. pacificus* animals expressing *Ppa-myo-2p::*RFP were pre incubated on unseeded drug supplemented plates for 2 hours, then transferred to predation assay plates containing *C. elegans* L1 larvae and the same neuromodulatory supplement.

2.8.2. Generation of *Ppa-klp-6p::*HisCl Line for Neuronal Silencing

To achieve conditional neuronal silencing of IL2 neurons, a codon optimized version of the *C. elegans* histamine gated chloride channel (HisCl1) was expressed under the *Ppa-klp-6* promoter (2 kb upstream region) (Pokala 2014). The construct (*Ppa-klp-6p::*HisCl) was co-injected with *Ppa-egl-20p::*GFP (co-injection marker) and genomic carrier DNA (PstI-HF digested) into the gonads of young adults. Transgenic animals were maintained as extrachromosomal arrays and selected based on GFP expression.

2.8.3. Preparation of Histamine Assay Plates for Chemogenetic Silencing

To enable pharmacogenetic silencing via HisCl, NGM was supplemented with 10 mM histamine dihydrochloride as described previously (Pokala et al. 2014).1 M histamine stock solution was prepared in sterile distilled water and added to NGM cooled to ~60 °C (5 mL per 500 mL agar). Plates were poured and stored for use within one week. These histamine-supplemented plates were used during the 2 hour starvation phase prior to behavioral testing and throughout the assay period.

2.8.4. Behavioral Assay for IL2 Neuron Silencing

To assess the role of IL2 neurons in predatory behavior, eurystomatous *Ppa-klp-6p::*HisCl young adults were starved for 2 hours on 10 mM histamine-supplemented NGM plates. They were then transferred to a histamine containing assay plate seeded with *C.*

elegans L1 larvae. Following a 15 minute acclimation period, predator behavior was recorded for 10 minutes using a camera mounted stereomicroscope.

2.9. Phenotypic Quantification

2.9.1. Quantification of Egg Laying

Adult hermaphrodites (day 3 post hatching) were individually transferred to OP50 seeded NGM plates. Eggs laid over a 24 hour period were manually counted, and adults were transferred daily to fresh plates for a total of five days or until egg laying ceased.

2.9.2. Quantification of Worm Size and Growth Rate

To monitor developmental growth, synchronized J2 larvae were placed on NGM plates with bacteria. At 24, 48, and 72 hours, animals were transferred to unseeded NGM plates and imaged using an Axio Zoom V16 microscope (Zeiss) with a Basler acA3088-57um camera. Body area was quantified using the WormSizer plugin for ImageJ/Fiji.

2.9.3. Mouth Form Scoring

Mouth-form phenotyping was performed using high magnification stereomicroscopy (150×). Young adult worms from synchronized cultures were scored as eurystomatous (Eu) or stenostomatous (St) based on visible dentition. For behavioral assays, only Eu animals were selected.

2.10. Statistical Analysis

2.10.1. Statistical Tests for Behavioral and Phenotypic Data

All statistical comparisons including analyses of behavioral state metrics (such as relative occupancy time, mean bout duration, and transition probabilities) and corpse counts from predation assays were performed using a two-tailed Mann–Whitney U test. For multiple comparisons, a Bonferroni correction was applied to control the family wise error rate. Reported p-values are corrected accordingly and are detailed along with sample sizes in Supplementary Table 3.

2.10.2. Boxplot Conventions and Significance Reporting

Boxplots follow Tukey's convention: the central line indicates the median, the box represents the interquartile range (IQR), and whiskers extend to 1.5 times the IQR. Statistical significance is denoted as follows: $p < 0.05$ (*), $p < 0.01$ (**), $p < 0.001$ (***), and $p < 0.0001$ (****).

3. Results

3.1. Development of a Behavioral State Classification Framework

To quantitatively analyze the aggressive and predatory behaviors of *P. pacificus*, we first developed a high throughput framework for automated behavioral tracking and classification. This required generating a stable transgenic reporter line to visualize the pharyngeal dynamics that are central to feeding behaviors, and then creating a machine learning pipeline to identify and predict distinct behavioral states from the tracking data.

3.1.1. Generation of Transgenic *Ppa-myo-2p*::RFP Line

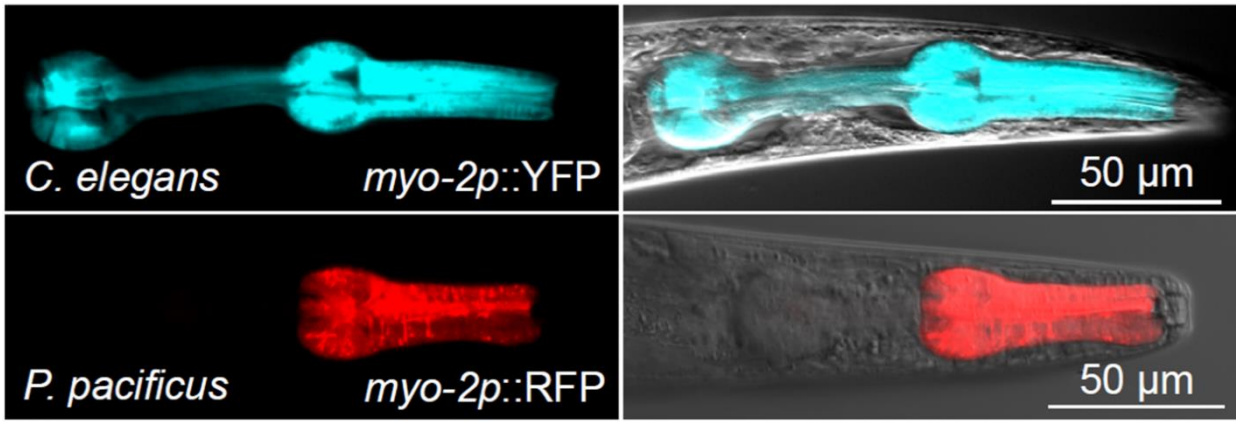

Fig. 5: Expression *myo-2p::*YFP in C. elegans compared to *myo-2p::*RFP expression in P. pacificus.

The nematode pharynx is a neuromuscular organ essential for feeding, and in *C. elegans*, targeting a fluorophore to the pharyngeal muscle has proven highly effective for dissecting feeding and locomotion behaviors (Bonnard et al. 2022). To apply a similar methodology to *P. pacificus*, we generated a transgenic line expressing TurboRFP under the control of the endogenous *Ppa-myo-2* promoter (**Fig. 5**). We observed substantially lower levels of *Ppa-myo-2* expression in the terminal bulb of the *P. pacificus* pharynx compared to *C. elegans* (**Fig.5**), which likely reflects anatomical differences between the species. Specifically, members of the Diplogastridae, including *P. pacificus*, lack the hardened grinder structure present in *C. elegans* and instead exhibit an expanded terminal bulb occupied by large pharyngeal gland cells (Harry et al. 2022). Despite this divergence in pharyngeal

architecture and transgene expression pattern, the fluorescent signal remained sufficient to enable robust tracking of both pharyngeal pumping and locomotion.

The initial extrachromosomal array was integrated into the genome using UV irradiation to ensure stable expression and 100% transmission of the reporter (Eren et al. 2022). We established that the integration resulted in approximately 32-45 copies of the *Ppa-myo-2p::*RFP transgene (**Fig. 6**).

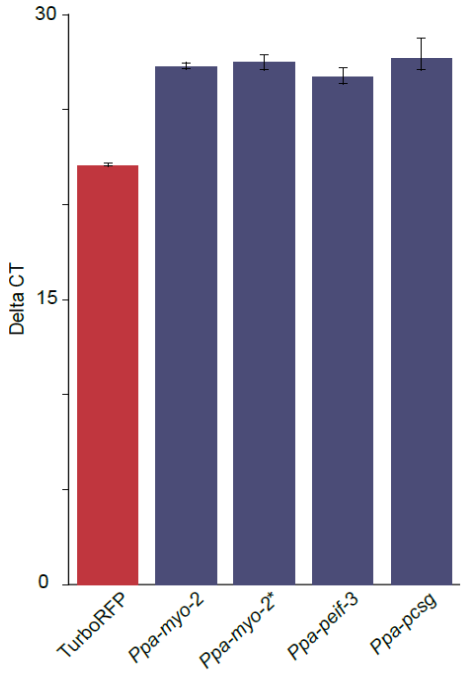

Fig. 6: qPCR analysis of RFP copy number. RFP qPCR reveals 5.5 less cycles of RFP compared to two different primer pairs specific to the *Ppa-myo-2* gene and two known single copy genes *Ppa-csg-1* and *Ppa-eif-3* indicating ~32-45 copies of *Ppa-myo-2p::*RFP are integrated into the P. pacificus genome in strain JWL27.

To ensure this genetic modification did not interfere with the behaviors under investigation, we performed a series of phenotypic assessments. The integrated line showed no adverse effects on key traits related to predation and overall health. Predatory behavior, measured via standard corpse assays, was unaffected in the transgenic line compared to wildtype animals (**Fig. 7A**). Likewise, other critical life history traits, including growth rate and the frequency of the phenotypically plastic predatory (eurystomatous) mouth morph, were also unaffected by the transgene integration (**Fig. 7B, C**). While a small but statistically

significant reduction in fecundity was observed (**Fig. 7D**), this was not expected to impact the short term behavioral assays planned for this study. Thus, the integrated JWL27 (*Ppa-myo-2p::*RFP) strain provided a reliable and behaviorally neutral tool for dissecting feeding and locomotion behaviors during high throughput behavioral tracking experiments.

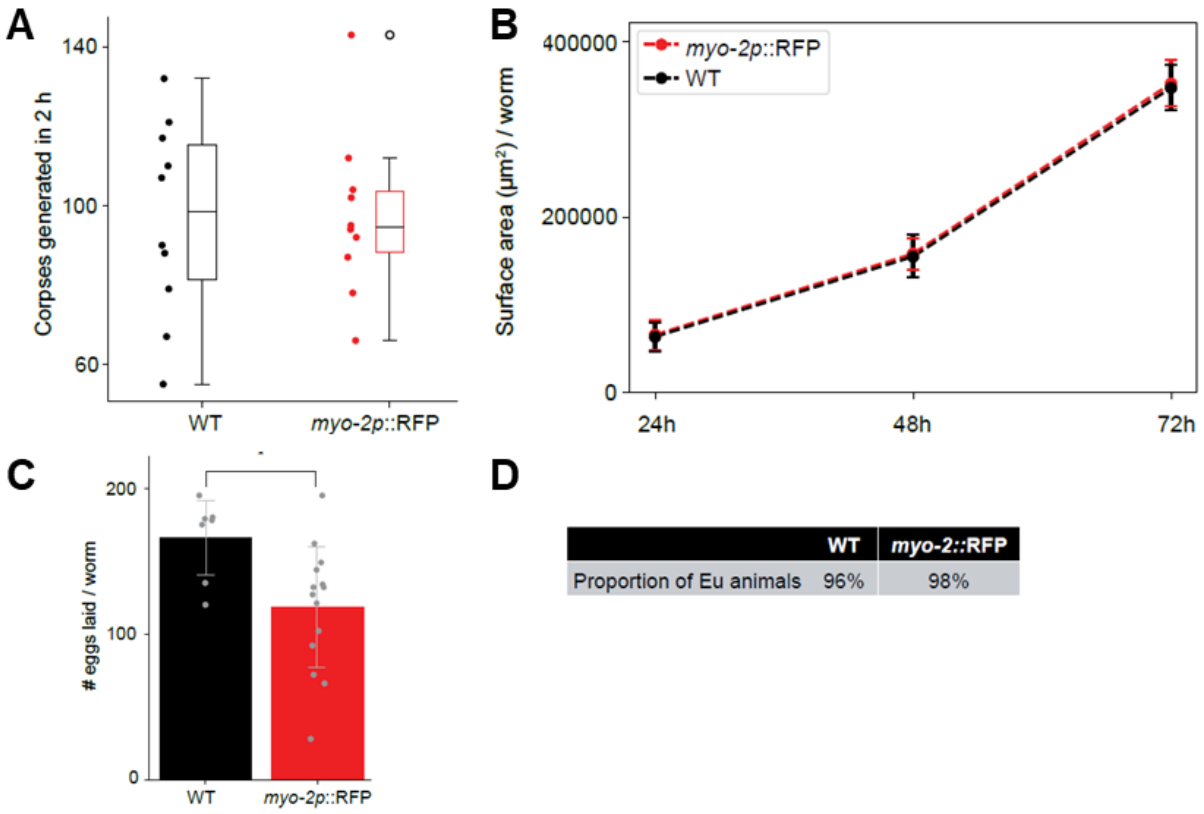

Fig. 7: Predatory behavior is unaffected in the *Ppa-myo-2p*::RFP integrated line. (**A**) Standard corpse assays with 5 young adult *P. pacificus* predators placed onto assay plates containing an abundance of *C. elegans* larvae to predate on for 2 h. 10 replicates were conducted for wildtype and *Ppa-myo-2p*::RFP. (**B**) Growth rate and (**C**) phenotypically plastic mouth morph frequency are unaffected in the *Ppa-myo-2p*::RFP integration line. Eurystomatous (Eu) is the predatory mouth form in *P. pacificus*. (**D**) There is a small reduction in fecundity associated with the *Ppa-myo-2p*::RFP integration. Significance was assessed using a Mann-Whitney U-test ($p = 0.015$).

3.1.2. High Throughput Behavioral Tracking and Feature Extraction

Using the *Ppa-myo-2p::*RFP line, we established an imaging pipeline to track the behavior of many animals simultaneously. Predators were placed in an arena containing either an abundance of *C. elegans* larvae as prey or a lawn of *E. coli* OP50 bacteria as a non-prey food source (**Fig. 8**). Videos of freely moving animals were recorded at 30 frames per second using an epifluorescence microscope.

Fig. 8: High throughput behavioral tracking experiment setup (**A**) For the predatory assay predators are placed in an arena containing abundance of *C. elegans* larvae as prey and videos of freely moving animals were recorded under an epi fluorescence microscope (**B**) Predatory *P. pacificus* animal expressing *myo-2p::*RFP and surrounded by larval *C. elegans* prey.

From these recordings, we used the image analysis tool PharaGlow to extract multiple initial behavioral features, including the animals' center of mass coordinates, centerline, and pharyngeal pumping events based on the skew of fluorescence intensity.

3.1.3 Machine Learning Classification of Behavioral States

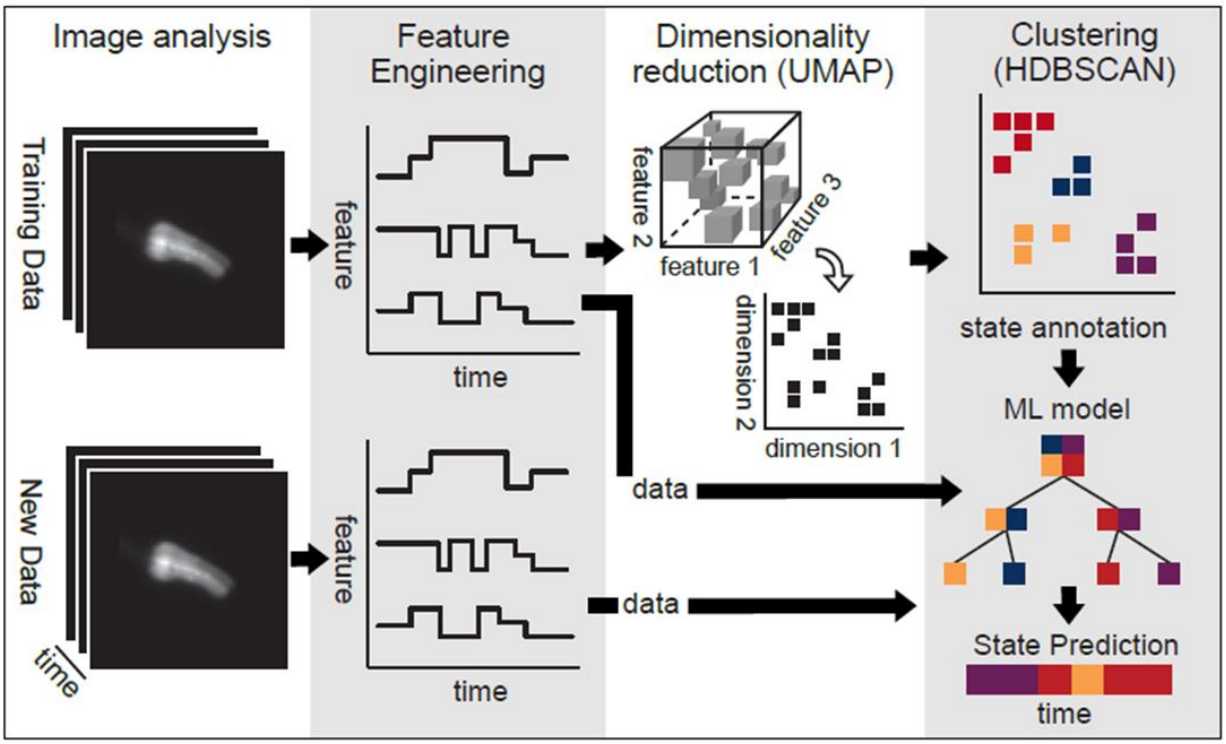

Fig. 9: Schematic of the machine learning pipeline used to classify behavioral states.

To achieve an unbiased classification of behavior, we developed a machine learning pipeline that combined low dimensional embedding and hierarchical clustering. From the initial behavioral metrics, we engineered a set of features designed to capture the key dynamics of locomotion and feeding. To capture the temporal dynamics of these features, we also included wavelet transformations and time lagged features in our final feature set. The behavioral data from 106 animals was first embedded into a 3 dimensional space using Uniform Manifold Approximation and Projection (UMAP) (**Fig. 10A**). We then applied HDBSCAN clustering to this embedding, which robustly identified six distinct behavioral states (**Fig 10B**).

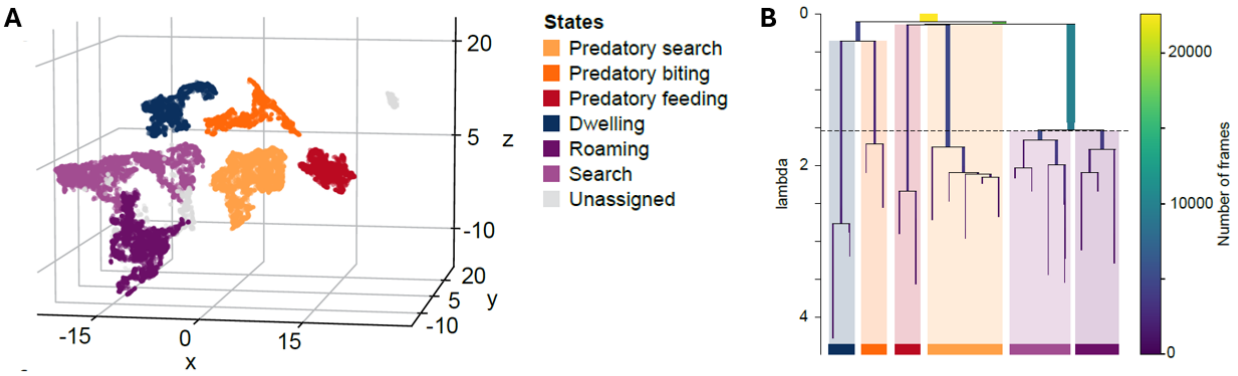

Fig. 10: Hierarchical clustering of UMAP embedded behavioral features. **(A)** UMAP embedding of behavioral features. Colors indicate the six behavioral states identified by hierarchical clustering **(B)** Colors correspond to the individual clusters that are later identified as behavioral states. The horizontal line indicates where the hierarchical tree was cut.

To interpret these computationally defined states, we correlated them with labels from an expert human annotator and the environmental context (prey vs. bacteria) (**Fig. 11**). This process identified states corresponding to canonical nematode behaviors such as 'roaming' and 'dwelling'. Crucially, it also revealed three novel behavioral states that were almost exclusively observed in the presence of prey larvae: ‘predatory search’, ‘predatory biting’, and ‘predatory feeding’ (**Fig. 11**). To ensure these states were not artifacts of a single dataset, we validated the pipeline on a second, independent dataset, which robustly recapitulated the same six behavioral clusters (**Fig. 12**).

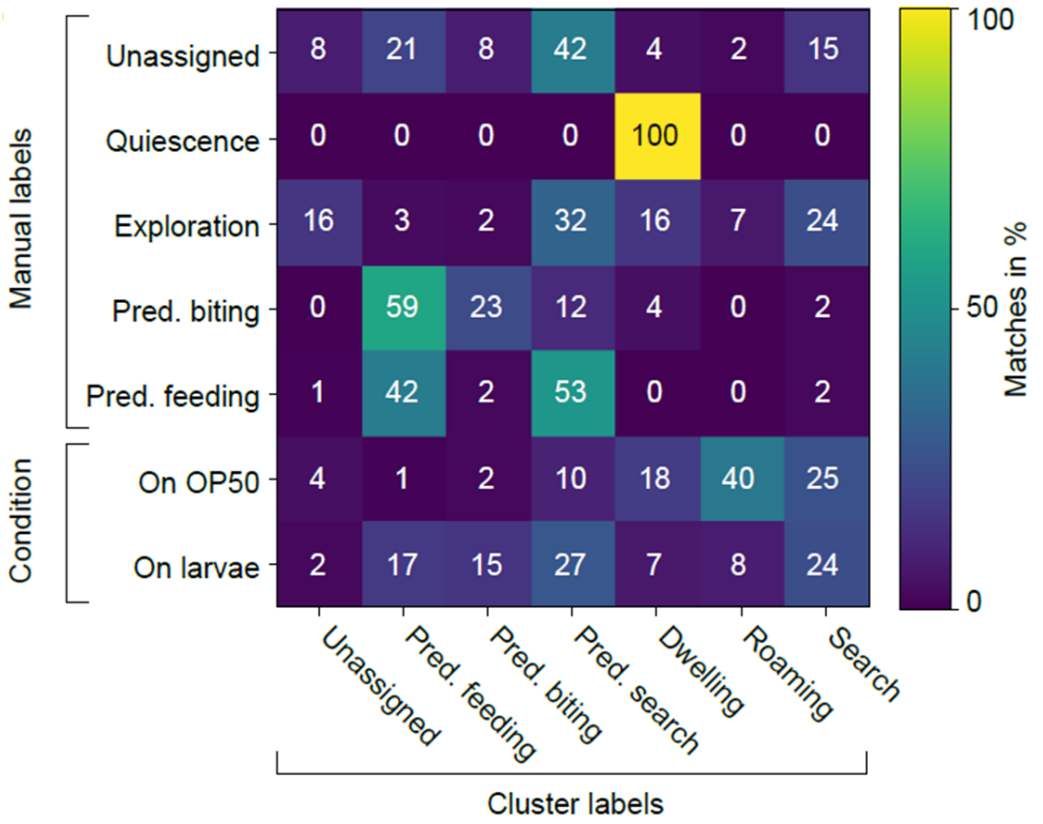

Fig. 11: Confusion matrix between the human expert annotator, condition, and the cluster labels. Unlabeled data is included by condition as either 'On larvae' or 'On OP50'. The latter was used to identify condition specific states.

Finally, to allow for the prediction of these states in new, unseen data, we trained an XGBoost multiclass classifier on the clustered data. The resulting model demonstrated high performance on a held-out test set, achieving over 95% accuracy and recall in predicting the cluster labels (**Fig. 13A, B**). The most informative behavioral features for cluster identity were found to be velocity, pharyngeal pumping rate, and head swing amplitude, which describes the angle between the nose tip and the direction of movement (**Fig. 13C**). Ultimately, this framework allowed for the successful prediction of behavioral states in unrestrained animals, transforming our approach from manual observation to high throughput, quantitative analysis.

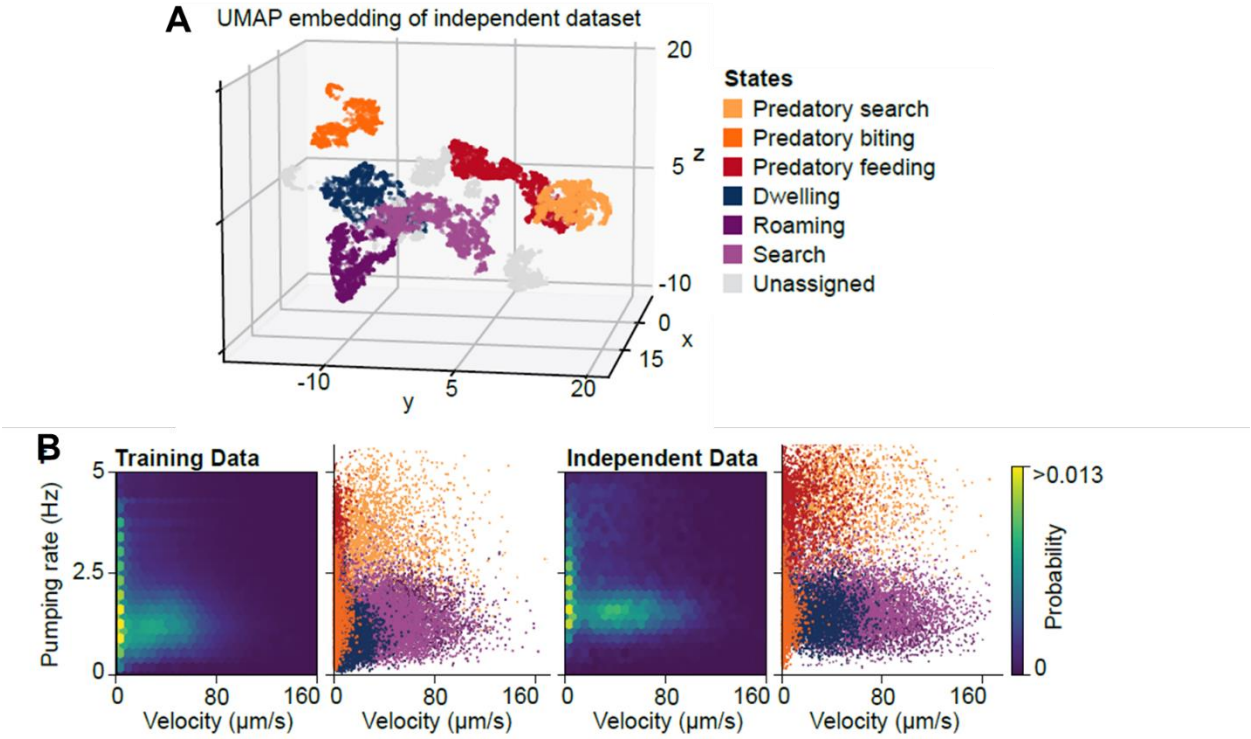

Fig. 12. Cluster validation on a second independent dataset using the same set of parameters for dimensionality reduction. **(A)** UMAP embedding of behavioral features on a second independent dataset. Colors indicate the six behavioral states recapitulated by hierarchical clustering. **(B)** Probability density map of velocity and pumping rate for the original dataset used to cluster the behavioral states (left) and an independent dataset to confirm robustness of the state detection.

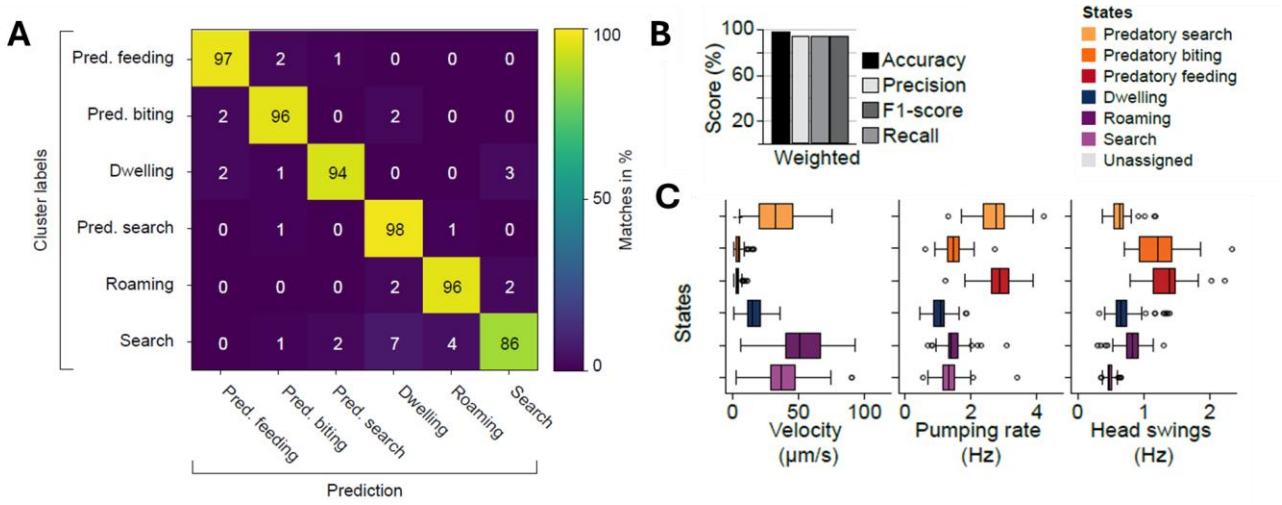

Fig. 13. Cluster validation on a second independent dataset using the same set of parameters for dimensionality reduction. **(A)** Confusion matrix comparing the cluster labels and the predicted labels using the model. **(B)** Performance metrics of the behavioral state classifier on novel, unseen data using weighted metrics. **(C)** Distribution of key behavioral features in each state. Each point in the box plots corresponds to the mean value per state and per tracked animal. Box plots follow Tukey's rule with the box from first to third quartiles, and a line at the median. The fliers denote 1.5 x interquartile range.

3.2. Predatory Aggression is Modulated by Sensory Context and Internal Drive

Having established a robust pipeline for classifying behavior, we next applied this framework to investigate how the predatory repertoire of *P. pacificus* is modulated by different environmental contexts. We compared the behavior of animals in the presence of either larval prey (*C. elegans*) or a standard bacterial food source (*E. coli* OP50) to understand how sensory cues associated with prey shape the occupancy, duration, and transitions of behavioral states.

3.2.1. Context Dependent Behavioral State Occupancy

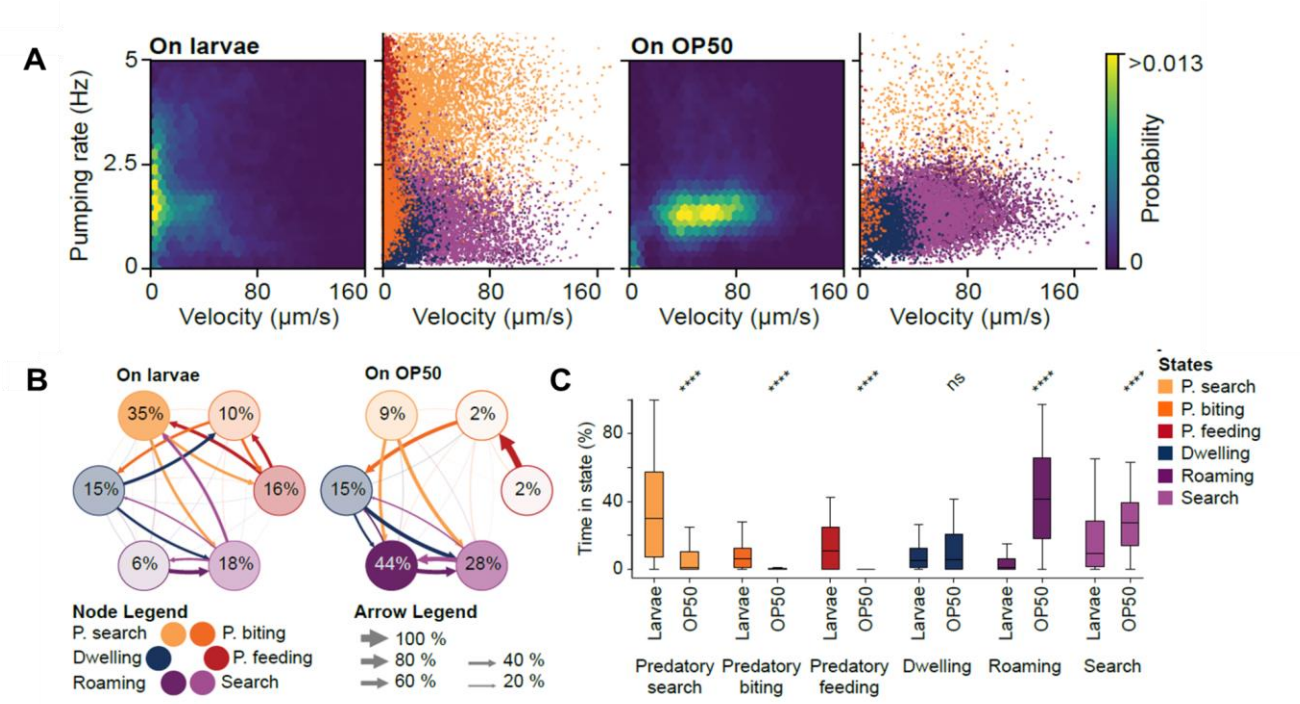

Fig. 14. Automatic classification of behavioral data reveals context-dependent predation drive **(A)** Probability density map of velocity and pumping rate for animals on larval prey or OP50 bacteria. Scatter plots indicate the corresponding state assignments. **(B)** Average transition rates between behavioral states for animals on larval prey and bacterial food, respectively. Numbers in circles indicate the fraction of time per state. Arrow thickness indicates the transition rate normalized to out-going transitions. **(C)** Mean fraction of time spent in each behavioral state per animal. Box plots follow Tukey's rule with the box from first to third quartiles, and a line at the median. The fliers denote 1.5 x interquartile range. Statistics, sample size and p values available in Supplementary Table 3. See methods for statistics.

The behavioral repertoire of *P. pacificus* was profoundly influenced by the available food source. Joint probability density plots of the two most descriptive features velocity and pharyngeal pumping rate revealed distinct behavioral signatures depending on the context (**Fig. 14A**). When exposed to prey larvae, animals preferentially occupied predation related states, which are characterized by specific combinations of movement and pharyngeal activity. Conversely, when placed on a bacterial lawn, predators spent more time in states associated with higher speeds and lower pumping rates, consistent with general foraging (**Fig. 14A**).

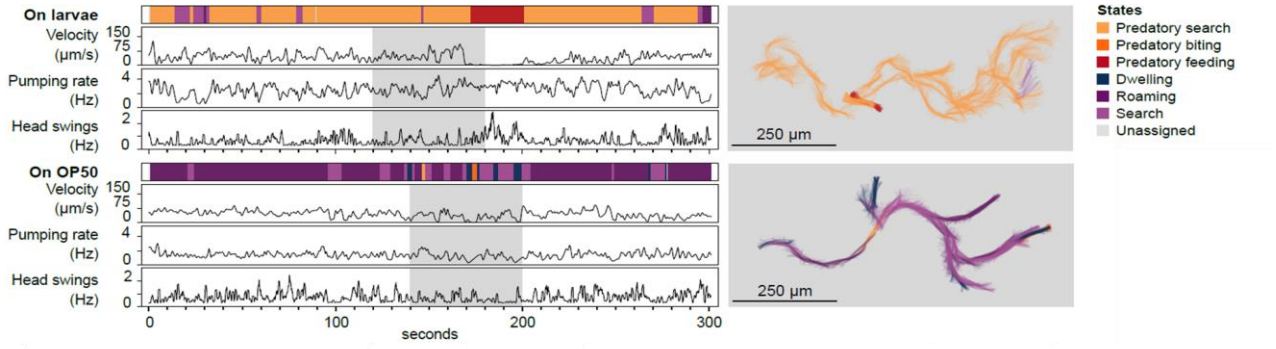

Fig. 15. Ethograms, velocity, pumping rate, and head swings for a representative animal on larval prey (top) or bacterial food (bottom). Pharyngeal centerline as colored by the assigned behavioral state. The tracks shown correspond to the grey regions.

This environmental influence was particularly evident in the type of exploratory behavior exhibited. We identified two distinct search states: a general ‘search’ state more prominent on bacterial food, and a ‘predatory search’ state almost exclusively observed in the presence of prey. The ‘predatory search’ state is distinguished by exaggerated head swing amplitudes, a motor pattern likely adapted for locating and targeting prey (**Fig. 15**). While the total time spent in each state was highly dependent on the sensory context, the average duration of a given behavioral state remained largely consistent across conditions (**Fig. 14B, C**). Therefore, the presence of prey cues acts as a potent switch, altering the animal's propensity to enter and transition between predatory states rather than changing the intrinsic timescale of the behaviors themselves. The total time spent in predatory states thus serves as a reliable measure of aggressive drive.

3.2.2. Decoupling Aggressive and Nutritional Drives in Predation

The identification of distinct ‘biting’ and ‘feeding’ states provided an opportunity to computationally dissect the motivations underlying predation. We designed an assay to disentangle the aggressive drive from the nutritional drive. Predators were placed in an arena containing both prey larvae and an abundant bacterial lawn. We hypothesized that if predation were solely driven by hunger, the presence of an easily accessible food source (bacteria) would reduce attacks on prey. While the total number of biting events remained

relatively consistent between conditions, animals exposed to both bacteria and larvae spent significantly less time in the feeding state (**Fig. 16**). Crucially, the probability of transitioning from a 'biting' event to a 'feeding' event was significantly reduced compared to the larvae only condition (**Fig. 16B, C**). This demonstrates that a greater proportion of predatory contacts are purely aggressive and not linked to consumption when an alternative food source is available. These findings confirm that 'predatory biting' serves a distinct aggressive function to eliminate competitors, which can be decoupled from the nutritional drive to feed. This expanded behavioral complexity in *P. pacificus* represents a significant evolutionary divergence from the canonical roaming and dwelling states described for *C. elegans (Flavell et al. 2020)*.

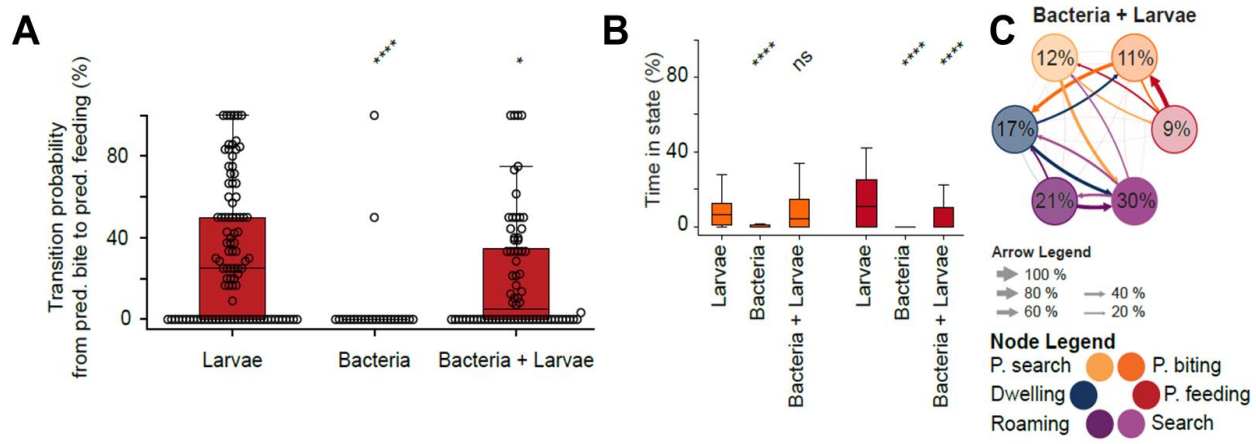

Fig. 16. Behavioral state prediction and aggression validation for animals in predatory or a bacterial food context **(A)** Transition probability that a *P. pacificus* animal transitions from 'predatory biting' to 'predatory feeding' (nutritional drive). Analysis conducted with *P. pacificus* surrounded with larval prey, a lawn of bacteria or both bacteria and larval prey. **(B)** Mean fraction of time spent in 'predatory biting' and 'predatory feeding' behavioral states per animal. Box plots follow Tukey's rule with the box from first to third quartiles, and a line at the median. The fliers denote 1.5 x interquartile range. Statistics, sample size and p values available in Supplementary Table 3. **(C)** Average transition rates between behavioral states for predators surrounded by larval prey and a bacterial food source simultaneously. The number in circles indicates the average state duration and the arrow size indicates the transition rate normalized to outgoing transitions.

3.3. Neuromodulatory Control of Predatory Aggression

Persistent behavioral states are often stabilized by distinct neuromodulatory systems that can act antagonistically to orchestrate mutually exclusive patterns of behavior (Flavell et al. 2013). To investigate whether such mechanisms are involved in establishing and maintaining the aggressive predatory states in *P. pacificus*, we conducted a targeted screen of mutants in the four major monoaminergic pathways.

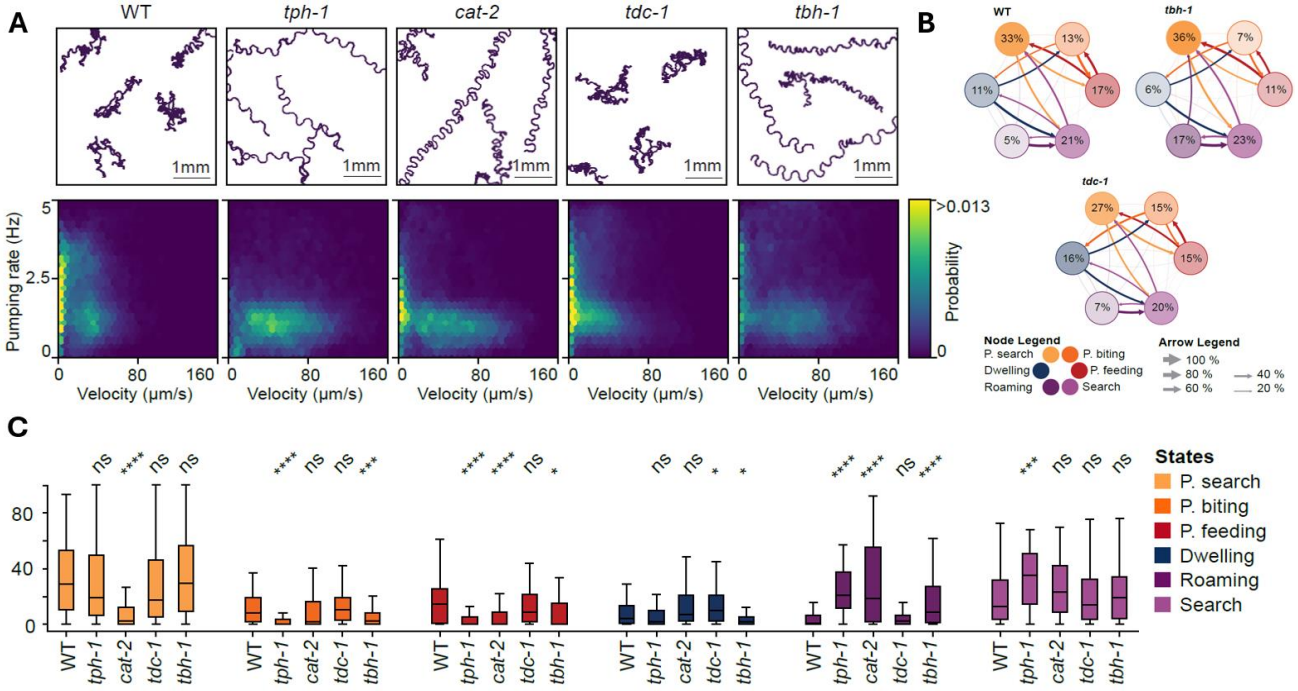

Fig. 17. Noradrenergic system modulate predatory aggression **(A)** Example animal tracks for wildtype (WT), *tph-1, cat-2, tdc-1,* and *tbh-1* mutants with probability density map of velocity and pumping rate for animals corresponding to the respective genotypes. **(B)** Average transition rates between behavioral states for WT, *tdc-1*, and *tbh-1* mutants on larval prey. The number in circles indicates the average state duration as in (C) and the arrow size indicates the transition rate normalized to outgoing transitions. **(C)** Time spent in each behavioral state normalized to the total track duration. Box plots follow Tukey's rule with the box from first to third quartiles, and a line at the median. The fliers denote 1.5 x interquartile range. Significance was assessed using a Mann-Whitney U-test with a Bonferroni correction for multiple comparisons if required.

We generated mutants for the key biosynthesis enzymes of serotonin (*Ppa-tph-1*), dopamine (*Ppa-cat-2*), and octopamine (*Ppa-tbh-1*) using CRISPR/Cas9 as well as *Ppa-tdc-1*, which is required for the synthesis of both tyramine and octopamine (**Fig. 17**). All four genes have clear one to one orthology with their *C. elegans* counterparts (**Fig. 18C**). Each mutant was crossed into the *Ppa-myo-2p*::RFP background, and their behavior in the presence of prey was analyzed using our established high throughput tracking and classification pipeline.

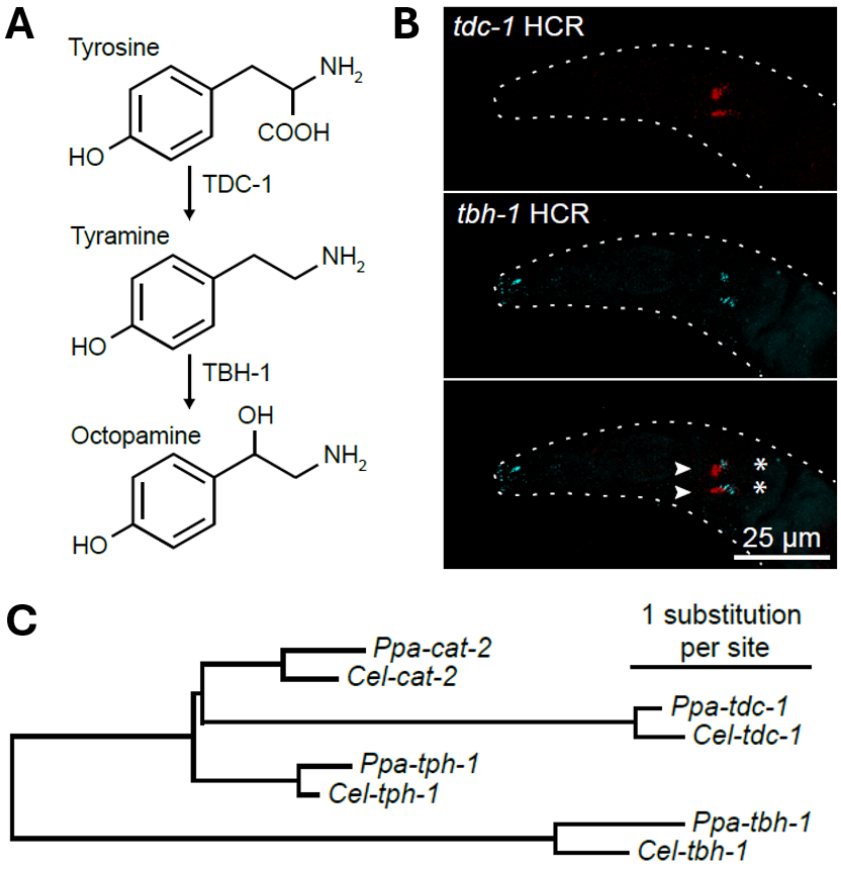

Fig. 18. *P.pacificus* neurons that synthesize the enzymes involved in tyramine (TDC-1) and octopamine synthesis (TBH-1) **(A)** Synthesis pathway of tyramine and octopamine from the precursor tyrosine. The enzymes involved in tyramine (TDC-1) and octopamine synthesis (TBH-1) act in the same pathway. **(B)** mRNA of tdc-1 (red) and tbh-1 (cyan) and colocalization visualized using HCR. Arrows indicates putative pair of RIM neurons while * indicates putative pair of RIC neurons. See methods for statistics. **(C)** Phylogenetic analysis of genes encoding neuromodulator biosynthesis enzymes from *P. pacificus* and *C. elegans*. The tree supports a single orthologous relationship between species.

Analysis of serotonin deficient *Ppa-tph-1* mutants revealed a strong decrease in predation, consistent with previous findings for its role in coordinating the mechanics of tooth and pharyngeal pumping during attacks (Okumura et al. 2017; Ishita et al. 2021). These mutants also exhibited an increase in roaming behaviors, similar to observations in *C. elegans* (**Fig. 17**). Dopamine deficient *Ppa-cat-2* mutants also showed altered motor patterns but, notably, did not exhibit a decrease in the 'predatory biting' state. Instead, we observed a reduction in 'predatory search' and 'predatory feeding' states (**Fig. 17**). Given dopamine's role in foraging and reward in *C. elegans*, this suggests that in *P. pacificus*, dopamine may be required for initiating feeding after a successful kill, possibly as part of a food reward signal.

The most striking results came from the noradrenergic pathway mutants. Animals deficient in octopamine synthesis (*Ppa-tbh-1*) showed a significant reduction in the 'predatory biting' state and fewer transitions into this state, indicating that octopamine is a key promoter of predatory aggression in *P. pacificus* (**Fig. 17**).

3.3.1. Tyramine and Octopamine Function Antagonistically to Regulate Predatory Drive

Intriguingly, mutants lacking the enzyme TDC-1, which is required for the biosynthesis of both tyramine and its downstream product octopamine, maintained predatory associated states at wildtype levels (**Fig. 17, Fig.18A**). This surprising result suggests that the additional loss of tyramine suppresses the predation defect caused by the loss of octopamine. This finding was corroborated by the analysis of *Ppa-tdc-1; Ppa-tbh-1* double mutants maintained predatory associated states at wildtype levels (**Fig. 19**).

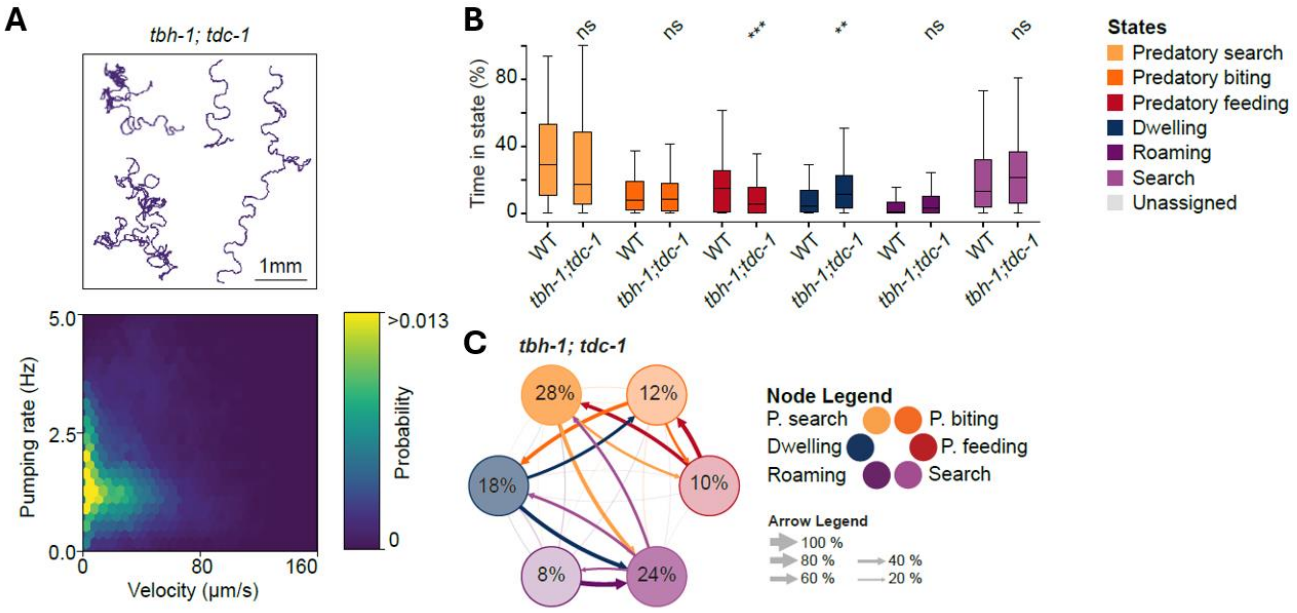

Fig. 19. Phenotype analysis of *tbh-1; tdc-1* double mutant. **(A)** Example tracks and probability density map of velocity and pumping rate for the *tbh-1; tdc-1* double mutant. **(B)** Relative time in each behavioral state for WT versus the *tbh-1; tdc-1* double mutant. **(C)** The average transition rates between behavioral states for the *tbh-1; tdc-1* double mutant.

To confirm this antagonistic relationship, we performed pharmacological rescue experiments. Exogenous application of tyramine to wildtype animals was sufficient to induce docile, nonpredatory behavioral states (**Fig. 20**). Conversely, applying exogenous octopamine not only maintained high levels of predation in wildtype animals but also fully rescued the low aggression phenotype of *Ppa-tbh-1* mutants (**Fig. 21**).

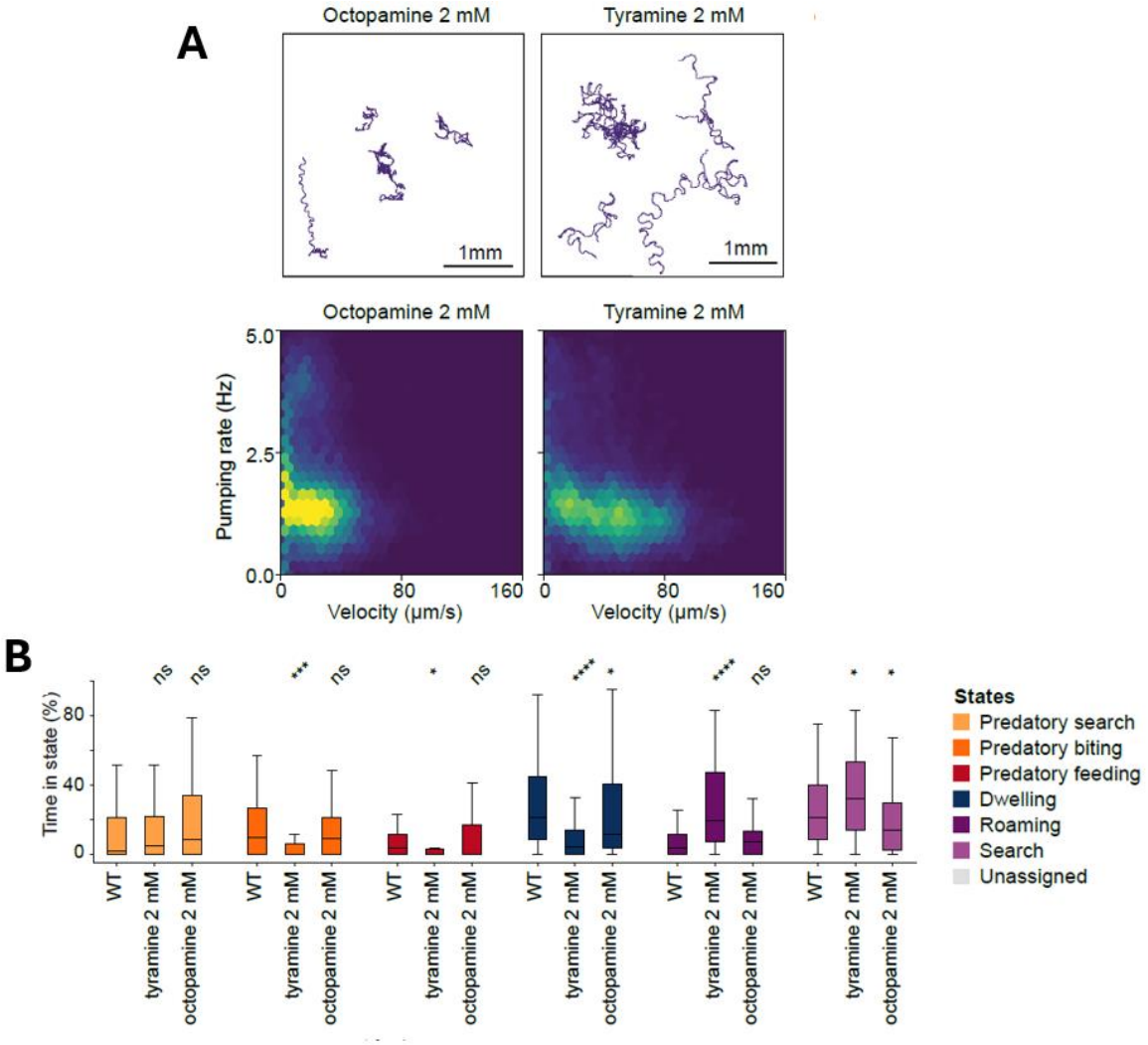

Fig. 20. Behavioral state prediction for exogenous application of octopamine and tyramine. **(A)** Example tracks and probability density map of velocity and pumping rate for animals exposed to 2 mM octopamine or tyramine, respectively. **(B)** Relative time in each behavioral state for WT animals compared to animals on 2 mM octopamine or tyramine.

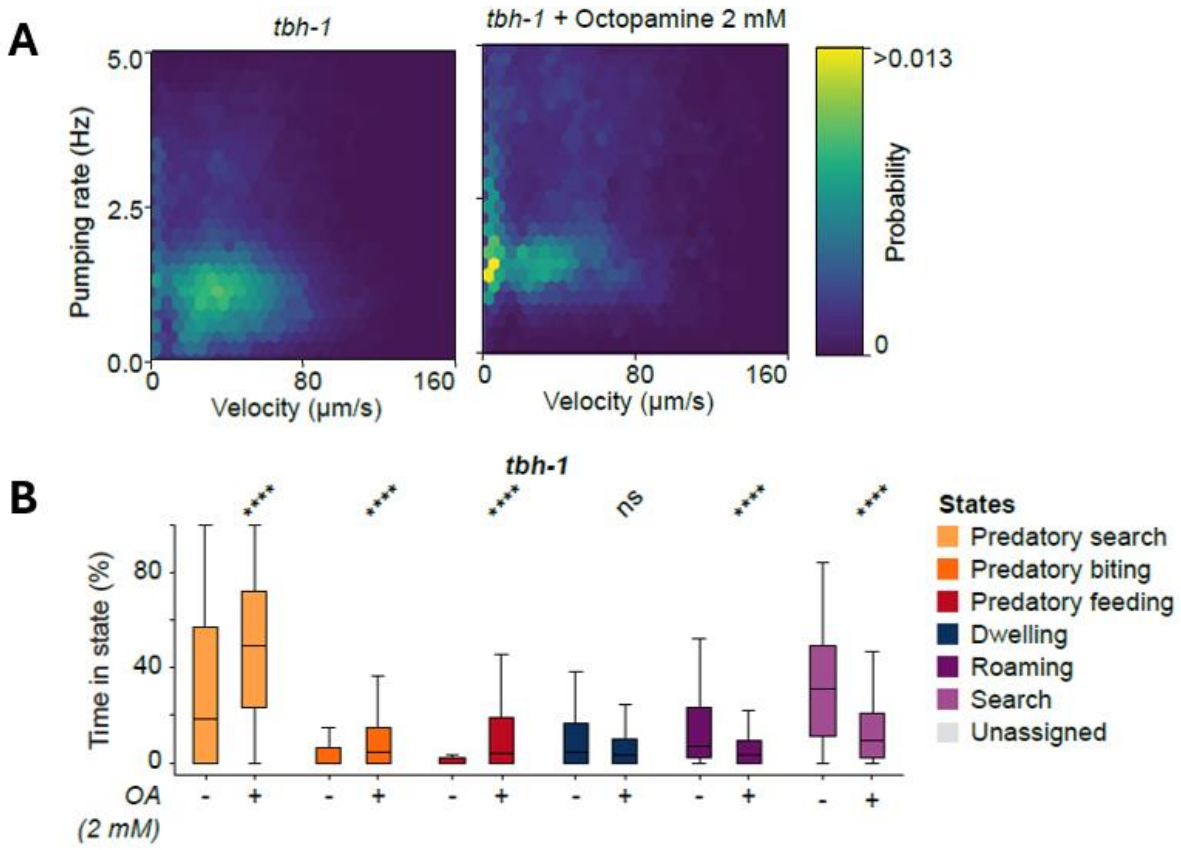

Fig. 21. Behavioral state prediction for exogenous application of octopamine to *Ppa-tbh-1* mutant **(A)** Probability density map of velocity and pumping rate for *Ppa-tbh-1* mutants exposed to 2 mM octopamine **(B)** Relative time in each behavioral state for *tbh-1* mutants compared to *tbh-1* mutants supplemented with 2 mM exogenous octopamine.

Taken together, these results suggest that octopamine promotes an aggressive state necessary for robust predatory biting, while tyramine acts antagonistically to establish a docile, nonpredatory state. This functional antagonism effectively operates as a neuromodulatory switch, allowing *P. pacificus* to control a complex, evolutionarily novel behavior that is absent in *C. elegans*. Having established this divergent function, we next sought to determine the neural circuits regulating these distinct behaviors.

In *C. elegans*, the tyraminergic interneurons RIM and RIC are the sole expressors of *Cel-tdc-1*, while the RIC neurons additionally express *Cel-tbh-1*, making them the only

octopaminergic neurons in the animal (Alkema et al. 2005). To investigate whether the expression of these enzymes is conserved in *P. pacificus*, we utilized hybridization chain reaction (HCR) to visualize their transcripts at cellular resolution. We found that the neuronal expression pattern of the biosynthesis genes is remarkably conserved between the two species. Similar to *C. elegans*, *Ppa-tdc-1* transcripts were detected in two pairs of neurons whose soma positions are consistent with the putative *P. pacificus* RIM (anterior) and RIC (posterior) neurons (Cook et al. 2025b). Furthermore, *Ppa-tbh-1* transcripts co-localized exclusively with the posterior *Ppa-tdc-1*-positive neuron pair, which we identify as the RIC neurons (**Fig. 18B**).

This striking conservation of the biosynthesis circuitry suggests that the novel, antagonistic roles of tyramine and octopamine in regulating predation in *P. pacificus* are not due to changes in which neurons produce these neuromodulators. Therefore, we hypothesized that the evolutionary divergence in function must lie downstream, in the circuits that receive and interpret these signals. This led us to next investigate the expression and function of the tyramine and octopamine receptor circuits.

3.4. Receptor Level Dissection of Noradrenergic Modulation

The evolutionary conservation of the noradrenergic biosynthesis circuitry between *P. pacificus* and *C. elegans* suggested that the novel, antagonistic functions of octopamine and tyramine in predation are a result of divergence in their downstream receptor networks. To test this hypothesis, we next sought to identify the specific receptors mediating these opposing effects and to map their expression patterns within the nervous system.

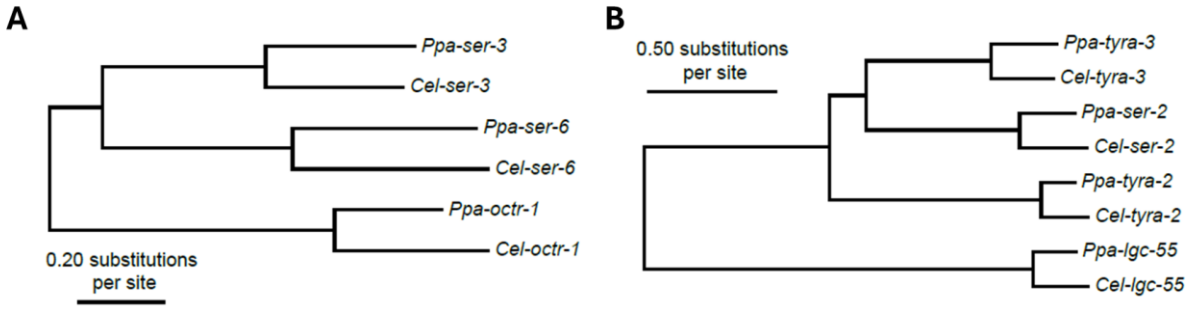

Fig. 22. Phylogenetic analysis of octopamine and tyramine receptors **(A)** Phylogenetic analysis of octopamine receptor genes from *P. pacificus* and *C. elegans*. The tree supports a single orthologous relationship between species. **(B)** Phylogenetic analysis of tyramine receptor genes from *P. pacificus* and *C. elegans*. The tree supports a single orthologous relationship between species.

3.4.1. Functional Analysis Identifies Receptors for Aggression and Docility

We first identified *P. pacificus* orthologs of known tyramine and octopamine receptors from *C. elegans* through phylogenetic analysis (**Fig. 22**). From this analysis, we selected key candidates for functional investigation, including the octopamine receptors *Ppa-octr-1*, *Ppa-ser-3*, and *Ppa-ser-6*, and the tyramine receptors *Ppa-tyra-2*, *Ppa-tyra-3*, *Ppa-ser-2*, and *Ppa-lgc-55*. We generated loss of function mutants for each of these receptors using CRISPR/Cas9 genome editing and analyzed their predatory behavior using our established machine learning pipeline.

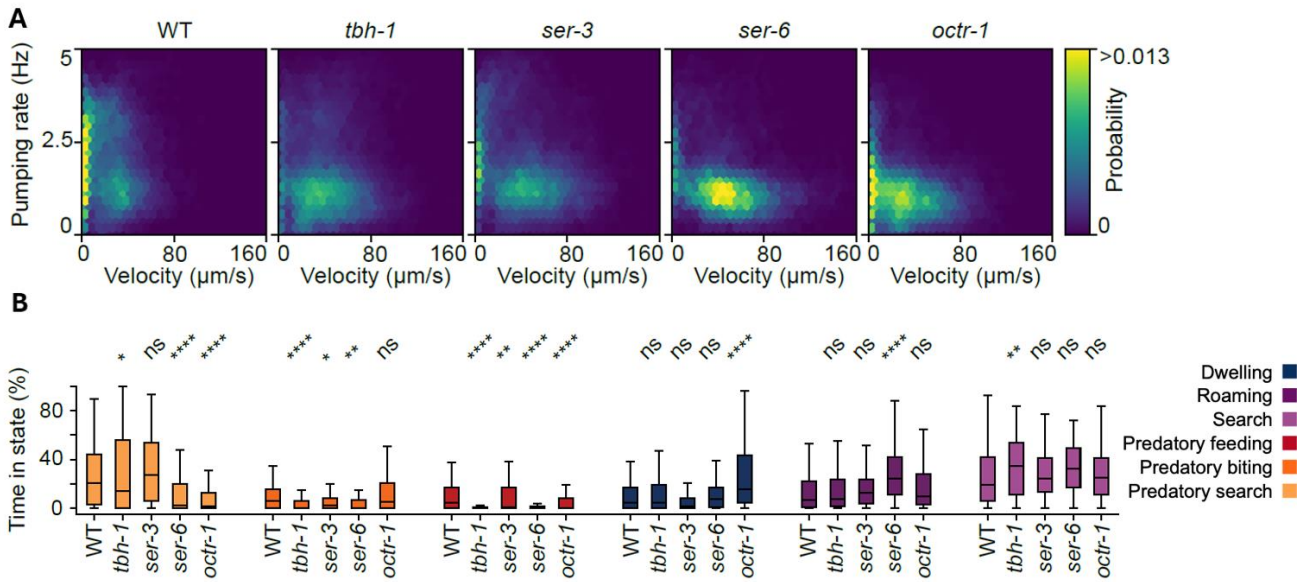

Fig. 23. Octopamine receptors gate aggressive state entry **(A)** Probability density map of velocity and pumping rate for WT, *tbh-1* and the octopamine receptors *ser-3*, *ser-6* and *octr-1*. *ser-3* and *ser-6* mutations reduce predatory biting similar to *tbh-1* mutation. **(B)** Relative time in each behavioral state for all genotypes in (A). All statistics are comparing mutants to WT.

The behavioral profiling of these receptor mutants revealed distinct and opposing functional roles. Mutants for the octopamine receptors *Ppa-ser-3* and *Ppa-ser-6* exhibited a significant reduction in the 'predatory biting' state, phenocopying the octopamine deficient *Ppa-tbh-1* mutants and confirming their role in promoting aggression (**Fig. 23**). Conversely, mutants for the tyramine receptor *Ppa-lgc-55* showed a striking increase in 'predatory biting', phenocopying the tyramine-deficient *Ppa-tdc-1* mutants and confirming its role in suppressing aggression (**Fig. 24**). No significant predatory defects were observed in the other receptor mutants tested. These results demonstrate that the antagonistic effects of octopamine and tyramine are mediated by distinct sets of receptors: Ppa-SER-3 and Ppa-SER-6 are essential for the aggression promoting effects of octopamine, while Ppa-LGC-55 is required for the aggression suppressing action of tyramine.

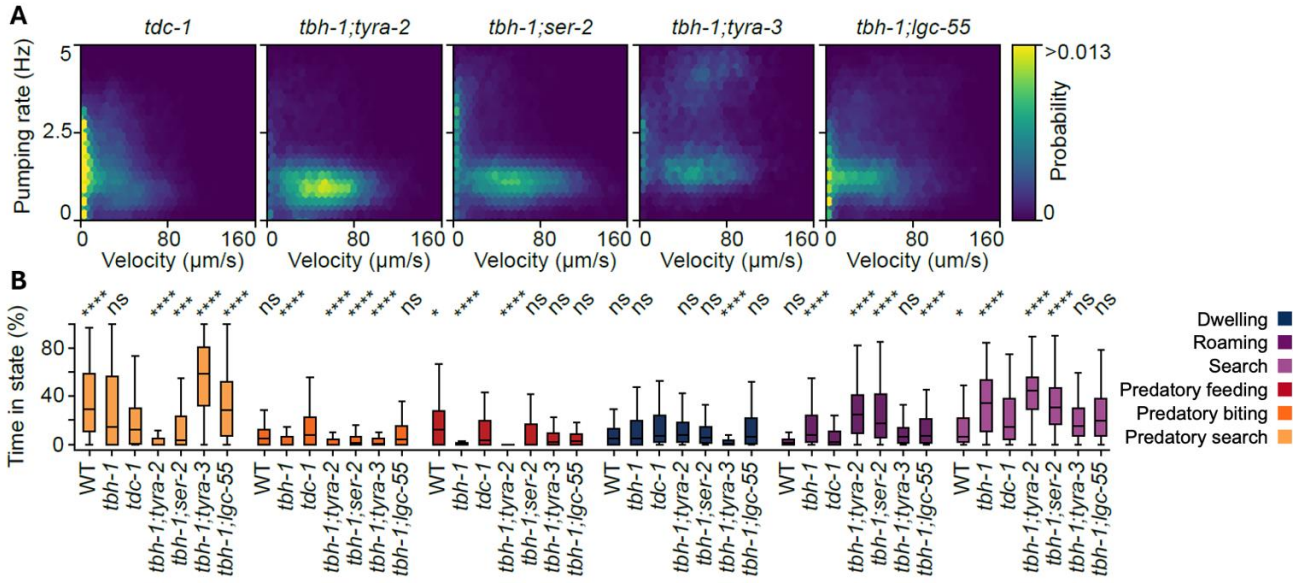

Fig. 24. Tyramine receptors gate aggressive state exit **(A)** Probability density map of velocity and pumping rate for *tdc-1* and the tyramine receptors *tyra-2*, *ser-2*, *tyra-3*, and *lgc-55*, all in the *tbh-1* background. **(B)** Relative time in each behavioral state for all genotypes in (A). All statistics are comparing mutants to *tdc-1* to detect aggression rescue phenotypes. Box plots follow Tukey's rule with the box from first to third quartiles, and a line at the median. The fliers denote 1.5 x interquartile range. See methods for statistics.

3.4.2. Divergent Receptor Expression Patterns Underlie Functional Rewiring of Neuromodulatory Circuits

Having identified the key receptors, we next investigated their neuronal expression patterns to understand how the underlying circuits have evolved. Using transcriptional reporters, we mapped the localization of the aggression promoting and aggression suppressing receptors in the *P. pacificus* head and compared these to the corresponding receptor expression in *C. elegans*.

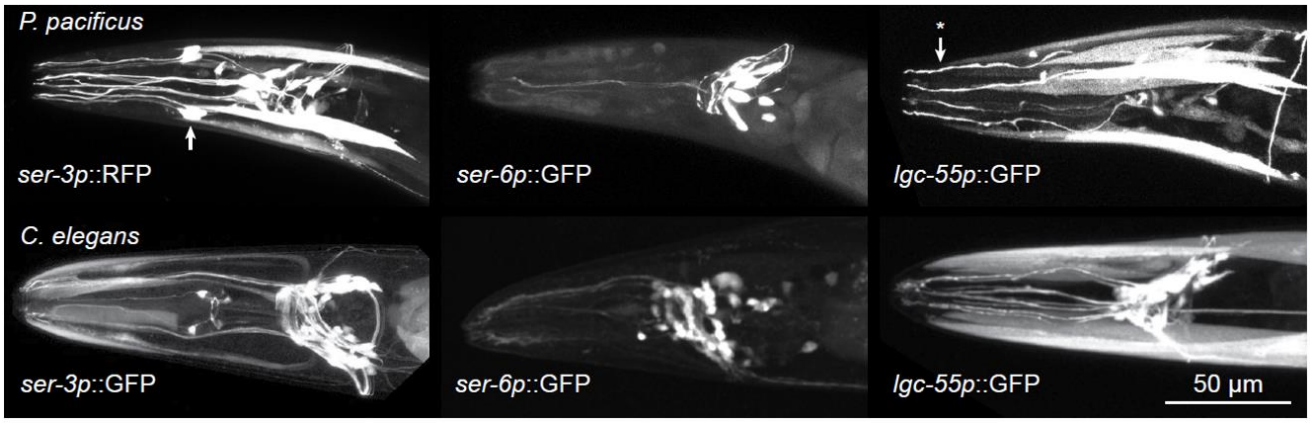

Fig. 25. Comparative expression pattern analysis for the octopamine receptors *ser-3* and *ser-6*, as well as the tyramine receptor *lgc-55* in *P. pacificus* (top) and *C. elegans* (bottom). Arrow indicates putative IL1 and IL2 neurites. Arrow with * indicates putative OL cell neurites.

This analysis revealed a striking evolutionary divergence in receptor expression. In *P. pacificus*, the aggression promoting octopamine receptors *Ppa-ser-3* and *Ppa-ser-6* are co-expressed in a small number of head sensory neurons. Most prominently, the six IL2 neurons, whose sensory endings are exposed to the external environment express the *Ppa-ser-3* octopamine receptor in *P. pacificus* but not in *C. elegans* (**Fig. 25**). In contrast, the aggression suppressing tyramine receptor *Ppa-lgc-55* is expressed in a distinct, nonoverlapping set of sensory neurons, including the OLs (**Fig. 25**).

This evolutionary rewiring of receptor expression provides candidates for a circuit level mechanism for the functional regulation of the novel predatory aggression we observe. By targeting octopamine and tyramine signaling to distinct, nonoverlapping sensory pathways, the noradrenergic system in *P. pacificus* has been adapted to drive opposing behavioral states critical for regulating its novel predatory behavior. In particular, the localization of aggression promoting octopamine receptors to the environmentally exposed IL2 neurons positions these cells as key mediators of prey detection and the initiation of aggressive attacks.

3.5. The IL2 Sensory Neurons are Essential for Predatory Aggression

Our finding that the aggression promoting octopamine receptor *Ppa-ser-3* is expressed in the IL2 sensory neurons implicated these cells as a key node in the predatory circuit. In *C. elegans*, these neurons are known to have environmentally exposed sensory endings and are involved in sensory modulation and nictation behavior, but they do not express octopamine receptors (Lee et al. 2012). In *P. pacificus*, the IL2 neurons are similarly positioned as the first point of contact between predator and prey, making them prime candidates for mediating the initiation of an attack (**Fig. 26**). We therefore sought to directly test their role in predation through targeted neuronal silencing.

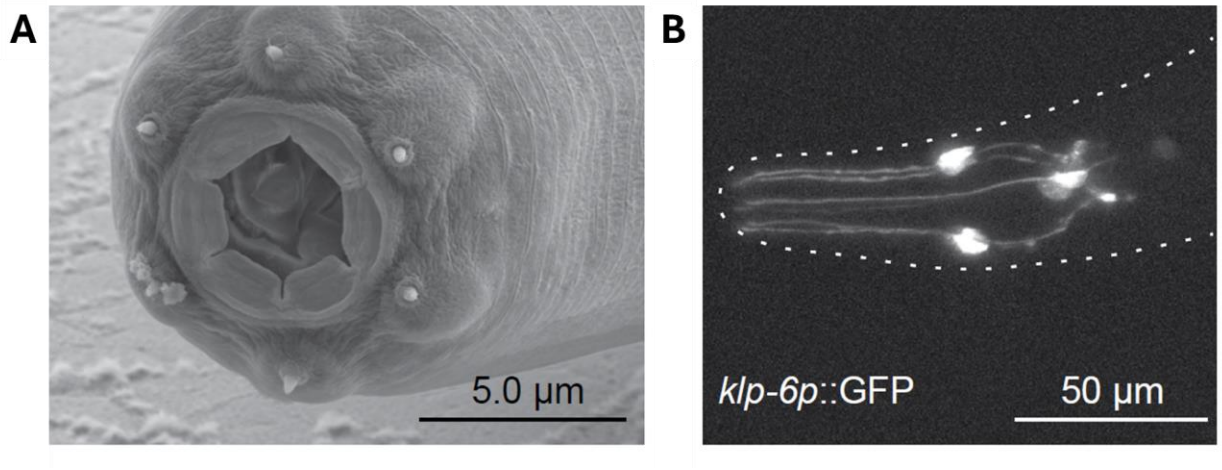

Fig. 26. IL2 neurons in *P. pacificus* **(A)** SEM image of the *P. pacificus* face. Six sensory endings from the IL2 neurons circle the mouth opening and are candidates for prey detection. **(B)** *klp-6::*GFP expression is specifically localized to IL2 neurons in *P. pacificus*.

3.5.1. Targeted Silencing of IL2 Neurons Using the Ppa-klp-6 Promoter

To specifically manipulate the IL2 neurons, we first needed to validate a specific genetic driver. In *C. elegans*, the promoter of the kinesin gene *Cel-klp-6* drives robust and exclusive expression in the six IL2 sensory neurons. We confirmed that a reporter construct using the orthologous *Ppa-klp-6* promoter also resulted in strong and specific expression in the IL2 neurons of *P. pacificus* (**Fig. 26B**).

With this specific driver in hand, we generated a transgenic line expressing the histamine gated chloride channel (HisCl) under the control of the *Ppa-klp-6* promoter. This pharmacogenetic tool allows for the inducible and reversible silencing of targeted neurons upon the exogenous application of histamine.

3.5.2. IL2 Silencing Decreases Predatory State Occupancy and Reduces Aggressive Drive

Upon silencing the IL2 neurons by placing the transgenic animals on histamine supplemented plates, we observed a substantial and significant decrease in all predatory behaviors. The total time spent in all three predation-associated states ‘predatory search’, ‘predatory biting’, and ‘predatory feeding’ was reduced compared to control animals (**Fig. 27A, B**).

Furthermore, the overall dynamics of the predatory sequence were disrupted. Analysis of the behavioral ethogram revealed that transitions from non-predatory states into the ‘predatory biting’ state were far less frequent in animals with silenced IL2 neurons (**Fig. 27C**). This demonstrates that the IL2 neurons are not only involved in executing predatory actions but are also critical for initiating the aggressive state itself. Taken together, these results confirm that the IL2 sensory neurons are an essential component of the neural circuitry governing predatory aggression in *P. pacificus*.

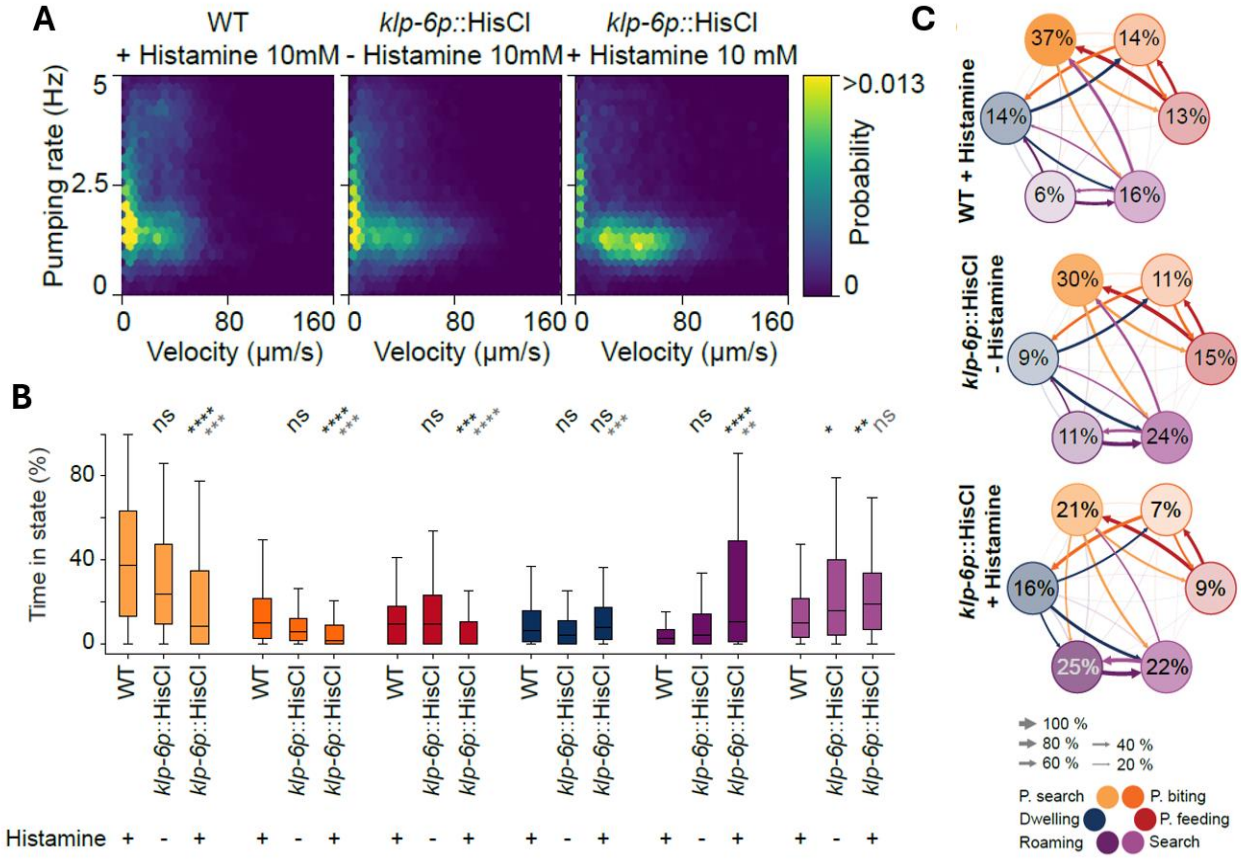

Fig. 27. Phenotype analysis of genetically silenced IL2 neurons. **(A)** Probability density map of velocity and pumping rate after genetic silencing of IL2 neurons. Plots show WT + 10 mM histamine and *klp-6p::*HisCl without histamine controls and *klp-6p::*HisCl + 10 mM histamine silencing conditions. **(B)** Relative time in each behavioral state for all conditions in (A). Box plots follow Tukey's rule with the box from first to third quartiles, and a line at the median. The fliers denote 1.5 x interquartile range. Statistics in black compared to WT while statistics in grey compare to *klp-6p::*HisCl without Histamine controls. **(C)** Average transition rates between behavioral states for WT + 10 mM Histamine, *klp-6p::*HisCl without histamine and *klp-6p::*HisCl + 10 mM histamine silencing conditions. The number in circles indicates the average state duration as in (A), and the arrow size indicates the transition rate normalized to outgoing transitions.

3.6. The Role of Octopamine in Predatory Aggression is an Ancient Evolutionary Innovation

While *P. pacificus* is the most well studied member of the Diplogastridae family, nearly all described species within this taxon are capable of predatory aggression (Wilecki et al. 2015). Given that octopamine and its receptors are essential for these behaviors in *P. pacificus*, we sought to investigate the evolutionary origins of this neuromodulatory association by examining a basal member of the family.

3.6.1. Phylogenetic Context and the Basal Predator *Allodiplogaster sudhausi*

To place our findings in a broader evolutionary context, we examined the function of octopamine in *Allodiplogaster sudhausi*, a large, free living nematode species that occupies a basal position within the Diplogastridae family (**Fig. 28A**). Similar to *P. pacificus*, *A. sudhausi* possesses teeth like structures and is a highly predatory and cannibalistic species, making it an ideal outgroup for assessing the conservation of the mechanisms underlying predation (Wighard 2024, **Fig. 28B**).

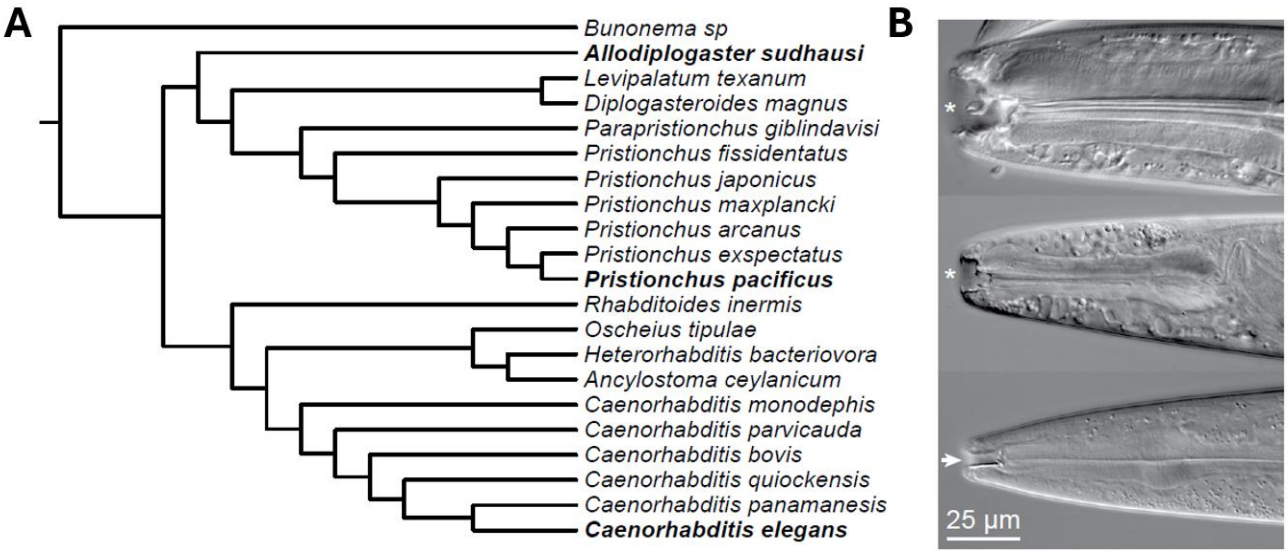

Fig. 28. *A. sudhausi* and *P. pacificus* predatory nematodes in Diplogastridae family. **(A)** Schematic phylogeny illustrating the evolutionary relationships among nematodes. **(B)** DIC mouth images of the predatory *A. sudhausi* and *P. pacificus* with mouths containing teeth like structures (*) and the microbial feeder *C. elegans* with an empty buccal cavity (arrow).

3.6.2. Functional Role of Octopamine in Aggression is Conserved in *A. sudhausi*

To investigate a conserved role for octopamine in promoting predatory aggression across the Diplogastridae, we generated loss of function mutants in the octopamine biosynthesis gene, *Asu-tbh-1*, in *A. sudhausi* using CRISPR/Cas9. We then performed manual corpse assays, exposing *C. elegans* larvae to either wildtype or *Asu-tbh-1* mutant predators.

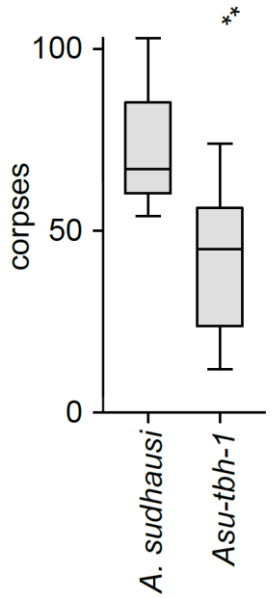

Fig. 29. Functional role of octopamine in promoting aggression in *A. sudhausi.* **(A)** Corpse assays of *A. sudhausi* WT compared to *Asu-tbh-1* mutants which show reduced predatory aggression. *C. elegans* corpses were counted after 2 h exposure to 5 predators.

Consistent with our findings in *P. pacificus*, the *Asu-tbh-1* mutants produced significantly fewer *C. elegans* corpses compared to wildtype predators (**Fig. 29**). This reduction in killing efficiency indicates a conserved requirement for octopamine in mediating predatory interactions. These results suggest that the functional role of octopamine in promoting aggression is an ancient trait that likely evolved early in the Diplogastridae lineage, coinciding with the origin of predation in this family.

3.6.3. An Evolutionary Model for the Noradrenergic Regulation of Aggression in Diplogastridae

Based on the collective findings of this study, we propose an evolutionary model in which an antagonistic noradrenergic circuit was co-opted to regulate predatory aggression in the Diplogastridae. In this model, octopamine and tyramine act as a neuromodulatory switch to control the transition between aggressive and docile internal states. Octopamine promotes a state of heightened aggression, while tyramine acts antagonistically to induce passivity. This switch is implemented at the level of distinct head sensory neurons, including the IL2 neurons, which are gated by specific octopamine and tyramine receptors. When an aggressive state is active, sensory input from these neurons, triggered by contact with prey, is translated into a predatory attack. We propose that this neuromodulatory mechanism evolved early in the Diplogastridae lineage, providing the foundation for the diverse and widespread predatory behaviors observed throughout this family.

4. Discussion

4.1. Reconstructing evolutionary change through comparative neuroethology

Understanding the evolution of behavior represents one of the most dynamic and integrative frontiers in biology. It links molecular and genetic variation to neuronal circuit function, ecological context, and ultimately to organismal fitness (Krakauer et al. 2017). Crucially, how these behavioral changes occur over evolutionary timescales is poorly understood, but likely depends on modifications to gene regulation, neuromodulatory systems, or circuit connectivity (Marder and Goaillard 2006; Marder 2012; Roberts et al. 2022). By examining the genetic and neuronal bases of behavioral novelties, it becomes possible to identify both the conserved mechanisms and the lineage-specific innovations that give rise to adaptive diversity (Jourjine and Hoekstra 2021). Together, with their distinct behaviors and evolutionary divergence, *C. elegans* and *P. pacificus* offer a tractable and powerful system to investigate this phenomenon (Bargmann 2012; Witte et al. 2015; Cook et al. 2019, 2020, 2025b).

Using these nematode systems, we combined high throughput tracking with semi-supervised behavioral state labeling, cell type resolved perturbations, and receptor mapping to reconstruct how *P. pacificus* aggression, a behavior absent from *C. elegans*, is regulated and evolved. Initial experiments established that wildtype *P. pacificus* engage in persistent states associated with predatory aggression only in the presence of potential prey and this was observed across repeated trials (**Fig. 14** and **Fig. 16**). Genetic and pharmacological manipulations revealed an antagonistic role for octopamine and tyramine: loss of octopamine synthesis reduced prey search and attack probability, whereas loss of tyramine maintains wildtype levels of predatory aggression (**Fig. 17, Fig. 20** and **Fig. 21**). At the circuit level, we identified the IL2 sensory neurons as a node where prey cues and octopaminergic gain control interact; acute IL2 silencing reduced predatory search, biting, and feeding (**Fig. 27**). Together, these results support a model in which octopamine acting via the SER-3 receptor expressed in IL2 and partner neurons as well as SER-6 expressed in additional head neurons releases an aggression biased drive for prey tracking and biting, whereas tyramine acting via

LGC-55 ion channels provides a brake that enables switching toward foraging when conditions favor it (**Fig. 23** and **Fig. 24**).

Thus, neuromodulators and their receptors provide a flexible substrate through which circuits can be rewired, allowing new behaviors to emerge without wholesale changes to architecture.

4.2. Aggression interfaces with predation, cannibalism, and territoriality

Quantitative behavioral assays revealed structured transitions among predatory search, biting, and feeding against larval prey (**Fig. 14**). When prey were presented together with a bacterial food source, bite rates remained similar to prey only assays, whereas predatory feeding decreased and was delayed, indicating that a substantial fraction of bites reflects an aggression biased action rather than an immediate nutritional drive. This is consistent with the previously identified territorial exclusion and resource defense (Quach and Chalasani 2020) (**Fig. 16**). Aggression in *P. pacificus* manifests as a neuromodulated internal state that often co-occurs with predation, cannibalism, and territorial interactions, rather than a single reflexive motor act (**Fig. 16** and **Fig. 17**). This architecture echoes other invertebrate systems where octopamine shapes territoriality in social insects (Roeder 2005), cannibalism and predation in arachnids (Widmer et al. 2005; Flock and Carlson 2019), and contest behavior in crustaceans (Kravitz and Huber 2003), and parallels Drosophila where aggression depends on octopamine together with additional monoamines, hormones, and neuropeptides (Vrontou et al. 2006; Zhou et al. 2008; Wang and Anderson 2010). Our pharmacological and genetic interventions identify octopamine and tyramine as principal regulators of an aggressive state in *P. pacificus*, placing this nematode within a broader phylogenetic pattern of noradrenergic control over aggressive action selection, while leaving room for additional modulators (e.g. dopamine, neuropeptides, pheromones) and internal drives (hunger, satiety) to further shape behavioral interactions. (**Fig. 17. Fig. 20** and **Fig. 21**).

4.3. Evolutionary divergence of noradrenergic function: from independence in *C. elegans* to antagonism in *P. pacificus*

In *C. elegans*, tyramine predominantly gates escape and reversal behaviors while octopamine promotes fasting associated arousal programs, with limited evidence for direct antagonism between the two (Alkema et al. 2005; Churgin et al. 2017; Liu et al. 2019; Florman and Alkema 2022). Notably, antagonistic interactions between these amines are documented in other invertebrates: in *Drosophila* larvae, tyramine and octopamine drive opposite changes in locomotion (Saraswati et al. 2004); in honey bees, octopamine increases locomotor activity whereas tyramine decreases it (Fussnecker et al. 2006). In *P. pacificus*, we uncovered a tightly coupled, opponent relationship: loss of octopamine synthesis (*tbh-1* mutants) diminished the predatory biting, whereas loss of tyramine synthesis together with loss of octopamine synthesis (*tdc-1* mutants) enhanced the predatory biting, consistent with a push and pull architecture (**Fig. 17**). These findings were reinforced through the addition of exogenous tyramine that biased animals toward non-aggressive foraging, while exogenous octopamine rescued deficits in *tbh-1* mutants and shifted state occupancy toward aggression (**Fig. 20** and **Fig. 21**). Importantly *tdc-1* mutants lacking tyramine and, via substrate removal, octopamine still executed predatory bites with wildtype kinematics and rates (**Fig. 17**). These findings suggest these modulators act on transitions between states rather than on the motor execution of biting. Furthermore, in this species, the basal behavioral state is one of aggression, which is subsequently shaped and modulated by the action of these neurotransmitters.

An additional design feature is biochemical: tyramine is the immediate biosynthetic precursor of octopamine (tdc-1 → tbh-1; **Fig. 18A**). In a system where the two signals act antagonistically, increasing TBH-1 activity converts more tyramine into octopamine, simultaneously elevating octopamine while depleting tyramine. This coupled push and pull could sharpen and hasten switches in state control by producing high contrast changes in their neuromodulatory activity. Conversely, reducing TBH-1 activity should raise tyramine and lower octopamine, biasing exit from aggression. Thus, this pathway architecture offers a natural, rapid mechanism for antagonistic state regulation (**Fig. 18A**). Together these results

indicate that the evolutionary coupling of octopamine and tyramine in *P. pacificus* did not simply regulate aggression; but also resulted in a bidirectional control axis that can be tuned on short timescales and by environmental context.

4.4. Circuit level substrate: receptor rewiring, not transmitter source reallocation

Reporter transgenes and HCR staining revealed the expression of the biosynthetic enzymes is conserved, *tdc-1* in RIM/RIC and *tbh-1* in RIC neurons, arguing against a transmitter source switch as the basis for functional divergence between species (**Fig. 18B,** (Alkema et al. 2005; Pirri et al. 2009). In both *C. elegans* and *P. pacificus*, RIM and RIC are paired head interneurons whose somata lie near the nerve ring and whose processes make extensive chemical and electrical contacts onto first order interneurons and head motor neurons (Cook et al. 2019, 2025b). In *C. elegans*, RIM releases tyramine during reversals to suppress head oscillations and facilitate coordinated escape (Alkema et al. 2005; Pirri et al. 2009), whereas RIC serves as the principal octopaminergic source recruited during fasting/arousal to bias foraging and locomotor choices (Suo et al. 2006). Morphologically and at the level of marker expression, the *Pristionchus* orthologs share this organization (**Fig. 18B,** (Alkema et al. 2005; Pirri et al. 2009), placing the noradrenergic transmitter sources upstream of head sensory and premotor circuits. This conservation implies that evolutionary divergence in predatory control arose not by changing which neurons make tyramine and octopamine, but by altering where their receptors are expressed and which sensory streams they gate.

Behavioral analyses of CRISPR generated mutants in octopamine and tyramine receptor genes support a requirement for these receptors in regulating the aggressive behavioral state. A focused CRISPR screen across octopamine receptor candidates showed that *ser-3* and *ser-6*, but not *octr-1*, recapitulated the *tbh-1* phenotype, indicating that octopamine's pro-aggressive effects are mediated predominantly through SER-3/SER-6 (**Fig. 23**). Mechanistically, SER-3/SER-6 are Gq/Gs-biased GPCRs; when expressed on head sensory neurons, their activation is expected to increase cellular excitability and sensory gain by engaging PLCβ/IP_3–DAG/PKC pathways that depolarize the membrane,

raising cAMP/PKA signaling that phosphorylates voltage gated channels and release machinery (Suo et al. 2006; Petrascheck et al. 2007; Mills et al. 2012). The net effect is a lower threshold and steeper slope (higher gain) of the neuron's input–output function, making neurons more likely to cross decision thresholds for state entry in response to the same prey cues. By contrast, OCTR-1 is Gi/o-coupled and would be expected to inhibit adenylyl cyclase and/or recruit GIRK-like K^+ currents, consistent with the absence of a *tbh-1*-like phenotype in *octr-1* mutants (Harris et al. 2010).

In parallel, a CRISPR screen of tyramine receptors in the *tbh-1* background revealed that only loss of *lgc-55* restored predation toward the *tdc-1* like predatory level and indicating tyramine acts via the LGC-55 chloride channel to suppress aggression (**Fig. 24**). Consistent with the rescue logic in *tdc-1*, LGC-55 encodes a tyramine-gated Cl^- channel that mediates tyramine dependent inhibition (Pirri et al., 2009).

Reporter transgenes of the octopamine and tyramine receptor genes that regulates the aggression has shown that receptor distributions are extensively remodeled in *P. pacificus*: octopamine responsive GPCRs, in particular SER-3 is enriched across head sensory neurons, including IL1 and IL2 that project to first order interneurons implicated in orienting and local search respectively (Lee et al. 2012; Cook et al. 2025b) (**Fig. 25**). Additionally, while the tyramine-gated chloride channel LGC-55 populates partially distinct sensory classes compared with *C. elegans* including OL neurons (**Fig. 25**). OL sensilla comprise six neurons in two subclasses: four OLQs that are mechanosensory controlling gentle nose touch (Chatzigeorgiou and Schafer 2011) and two OLLs that are mechanosensory and additionally cold sensitive (Fan et al. 2021).

By functionally, redistributing receptors on sensory neurons, this alters the gain with which prey cues enter central decision nodes, thereby moving the system between states without altering synaptic anatomy of motor circuits. This mechanism may explain how identical sensory inputs can evoke divergent outcomes depending on the changing behavioral state. It also suggests why behavioral novelties may arise rapidly as altering cis-

regulatory elements that govern receptor placement may suffice to reweight gate thresholds without jeopardizing neuromodulatory homeostasis.

4.5. IL2 neurons as a node for prey detection and state gating

We identified IL2 sensory neurons as a pivotal entry point where prey cues and octopaminergic gain control converge to promote aggressive state entry (**Fig. 25**). SER-3 expression in IL2 positions octopamine to amplify prey evoked input, and concurrent studies show that *P. pacificus* IL2 neurons express mechanosensory and chemosensory receptors required for efficient prey detection, indicating convergence of detection and modulation within the same node (Roca et al. 2025). Acute silencing of IL2 via histamine gated chloride channels reduced predatory search, biting, and feeding, demonstrating necessity for both initiation and maintenance of the aggressive state (**Fig. 27**). These data support a model in which IL2 integrates prey contact with octopaminergic bias to tip action selection toward aggression. Within this model, IL2 acts as a conditional relay. In a docile modulatory background, identical prey contact fails to reach the threshold for state transition, whereas in an octopamine biased background, the same input crosses threshold and commits the system to the aggressive trajectory with stereotyped motor execution. What makes IL2 suited to gate state transitions? Morphologically, IL2's ciliated endings are positioned to sample close range mechanochemical cues generated during prey contact, and their axonal projections intersect early with interneurons that influence head sweep biasing and local exploitation (Lee et al. 2012; Cook et al. 2025b). Functionally, IL2 silencing reduces the predatory state entry, even when other sensory neurons remained intact (**Fig. 27**). Thus, the IL2 neurons potentially occupy a privileged position as both detector and gatekeeper, coupling prey-derived cues with neuromodulatory context to determine whether predatory aggressive behavior is engaged.

4.6. An ancient association: octopamine and aggression across Diplogastridae

Predatory aggression is widespread across Diplogastrids, suggesting that noradrenergic control may have deep evolutionary roots in this family (**Fig. 28**). In the basal predatory species *Allodiplogaster sudhausi*, disruption of the octopamine biosynthesis

enzyme *tbh-1* also reduced killing efficiency in standardized corpse assays in this species. This mirrors its pro-aggressive role in *P. pacificus* (**Fig. 29**). Accordingly, phylogenetic mapping places this association early in Diplogastrid evolution. These comparative results argue that octopaminergic promotion of aggressive states is an ancient feature of this family of predatory nematodes. This association of octopamine and aggressive is not only specific to nematodes as it is also observed in numerous other invertebrates including insects, arachnids and crustaceans (Kravitz and Huber 2003; Vrontou et al. 2006; Zhou et al. 2008; Wang and Anderson 2010).

4.7. Possible circuit and receptor mechanisms underlying an opponent switch regulating predatory biting

While our findings establish a role for tyramine and octopamine in modulating predatory states, there are also broader, unresolved mechanisms. In this section, I speculate on additional neuromodulatory pathways and circuit-level adaptations that may influence these behaviors and further underlie evolutionary shifts in behavioral control.

Octopamine, acting via SER-3/SER-6 receptors expressed in IL2 and IL1 and partner neurons, enhances the gain of prey evoked pathways to promote predatory search and biting (**Fig. 23** and **Fig. 25**). In *C. elegans*, the dendrites of the IL1 and IL2 neurons are tightly bundled by the same inner labial sheath glia and are known to be extensively coupled by gap junctions (White et al. 1986). Given that the IL1 and IL2 dendrites in *P. pacificus* are similarly enclosed within a shared sheath (Cook et al. 2025b), and considering the remarkable conservation of neural circuitry between these species (Bumbarger et al. 2013), it is highly probable that the IL1 and IL2 neurons are also electrically coupled in *P. pacificus*. Such coupling would enable synchronous recruitment and amplification of input during octopaminergic drive, positioning IL2 as the critical convergence hub for inputs that trigger predatory engagement. Indeed, recent work has also identified prey detection specific mechanosensory and chemosensory receptors in the IL2 neurons (Roca et al, 2025). Furthermore, in both *C. elegans* and *P. pacificus* only a single connection links the somatic nervous system with the pharyngeal nervous system. This occurs through the ring

interneuron, RIP on the somatic side and the pharyngeal interneuron I1 (Bumbarger et al. 2013). Crucially, the IL2 sensory neurons synapse directly onto RIP and therefore provides a route through which octopamine can bias head sensory inputs toward pharyngeal motor synchrony, effectively gating entry into the predatory biting state. Additionally, in *P. pacificus*, I1 has been shown to be under serotonergic control and required for coordinating pharyngeal pumping with tooth movements (Okumura et al. 2017; Ishita et al. 2021) while in *C. elegans* this neuron is instead only cholinergic indicating further neuromodulatory divergence across this circuit.

For the tyraminergic induction of the docile state, we identified the tyramine-gated chloride channel LGC-55 expressed on the distinct sensory classes of neurons including OL neurons (**Fig. 24** and **Fig. 25**). Because LGC-55 activation is inhibitory, tyramine may hyperpolarize OL neurons and dampen their mechanosensory drive (Pirri et al. 2009). In adult *P. pacificus*, a subset of OL neurons (OLQ) also forms chemical synapses directly onto RIP (Cook et al. 2025b). OL neurons also provide excitatory input to IL1 and IL2, which themselves make direct synapses onto RIP (Cook et al. 2025b). Thus, inhibiting OLs could reduce RIP drive via two routes: directly, by weakening OLQ→RIP transmission; and indirectly, by reducing OL evoked excitation of IL1/IL2 that converge on RIP. Because RIP is the sole synaptic bridge between the somatosensory and pharyngeal nervous systems, RIP is well placed to integrate prey evoked mechanosensory cues.

4.8. Broader mechanistic implications: towards general principles and cross-species relevance

The findings presented in this thesis, while focused on a comparative nematode model system, offer insights into fundamental principles of neuromodulation, circuit evolution, and behavioral control that resonate across the animal kingdom, including in mammals. By dissecting the evolutionary steps towards a complex behavior, we hope to identify generalizable rules that govern how nervous systems adapt to new ecological challenges.

In *P. pacificus*, octopamine may increase the readiness of IL2 neurons, lowering their threshold so that prey cues more reliably drive entry into the aggressive state (**Fig. 23, Fig.**

25 and **Fig. 27**). This is consistent with the well described role for neuromodulators which act as gain control mechanisms at key sensory interface (Widmer 2005). This also includes in the noradrenergic system which is thought equivalent to invertebrate octopamine. In mammals, the noradrenergic system, originating from the locus coeruleus, is critical for regulating enduring behavioral modes like vigilance, exploitation, and defense, which have distinct kinetics and neural footprints (Aston-Jones and Cohen 2005; Bouret and Sara 2005; Sara 2009). An analogous role is played by early sensory relays and limbic-hypothalamic hubs that convert ethologically salient cues into enduring internal modes. For example, chemosensory inputs routed to medial amygdala and hypothalamus control social and aggressive states (Falkner et al. 2014; Chen and Hong 2018), or superior colliculus–periaqueductal gray pathways are critical for threat evaluation (Tovote et al. 2016; Shang et al. 2018). The shared architectural principle is that neuromodulators act at the initial stages of sensory processing to bias the computation that links cue detection to the selection of a persistent internal state.

The second major principle highlighted by our work is that "receptor-map rewiring," rather than transmitter-source relocation, is a potent and perhaps common mechanism for behavioral evolution. Across taxa, changes in the deployment of neuromodulator receptors have been causally linked to behavioral evolution. For example, species and population differences in vasopressin receptor (AVPR1A) expression in the brains of vole species, correlates with switching between polygamous and monogamous and parental care social structures (Hammock and Young 2006; Donaldson and Young 2008). Additionally, developmental programs and experience can retune receptor expression patterns, thereby modifying the degree to which modulatory signals influence sensory–limbic gating. In mammals, for instance, adrenergic receptor expression and signaling shift dynamically with stress and arousal, particularly in prefrontal (Ramos and Arnsten 2007; Arnsten 2009; McEwen and Morrison 201), and β-adrenergic receptor density and coupling changes across aging (Amenta et al. 1991; Ricci et al. 1995). Together, these observations provide a mechanistic rationale for how receptor variability can remodel behaviors.

4.9. Conclusions, limitations, and outlook

Our results indicate that predation, cannibalism, and territoriality in *P. pacificus* are controlled by a modulatory system in which octopamine and tyramine act in opposition to bias access to distinct behavioral states. This framework explains the context-dependence of predatory responses, maintains separable control of hunger and aggression drives, and accounts for why identical sensory cues can elicit different behaviors depending on the animal's current state.

The principal limitations of our study lie in technical resolution and available tools. At the circuit level, we lack CRISPR knock-in lines with endogenously tagged receptors, which would allow visualization of receptor proteins under their native regulation. Importantly, *P. pacificus* also does not yet have the full suite of optogenetic and activity imaging tools that would enable precise causal testing of necessity and sufficiency of the identified neural circuit components. Compared to *C. elegans*, this constrains how finely we can dissect receptor dynamics, downstream partners, and synaptic interactions.

Looking ahead, several complementary avenues of research present themselves. Endogenous reporter tagging of receptor components will provide a more precise view of protein localization and dynamics. Calcium imaging of neurons expressing SER-3, SER-6, and LGC-55 receptors, along with the octopaminergic and tyraminergic RIM and RIC cells, could directly link neuronal activity to state transitions and behavioral outcomes. Optogenetic activation of IL2, RIM, and RIC neurons would further validate their roles and help dissect the circuitry underlying the evolution of predatory aggression. In parallel, RNA-seq analysis of receptor and neuromodulator expression across diverse wild isolates could reveal natural variation in the predatory aggression system. Finally, comparative studies in other predatory nematodes outside of the Diplogastrids will be essential to determine whether the link between octopamine and aggression represents a unique evolutionary innovation or a recurring theme across nematode clades.

In summary, noradrenergic circuits balance aggressive behavioral states in the Diplogastridae family and are associated with the evolution of complex behavioral traits. More broadly, our findings underscore that neuromodulatory systems provide a powerful substrate for behavioral innovation, linking molecular change to behavioral adaptations and contributing to general principles of how nervous systems evolve.

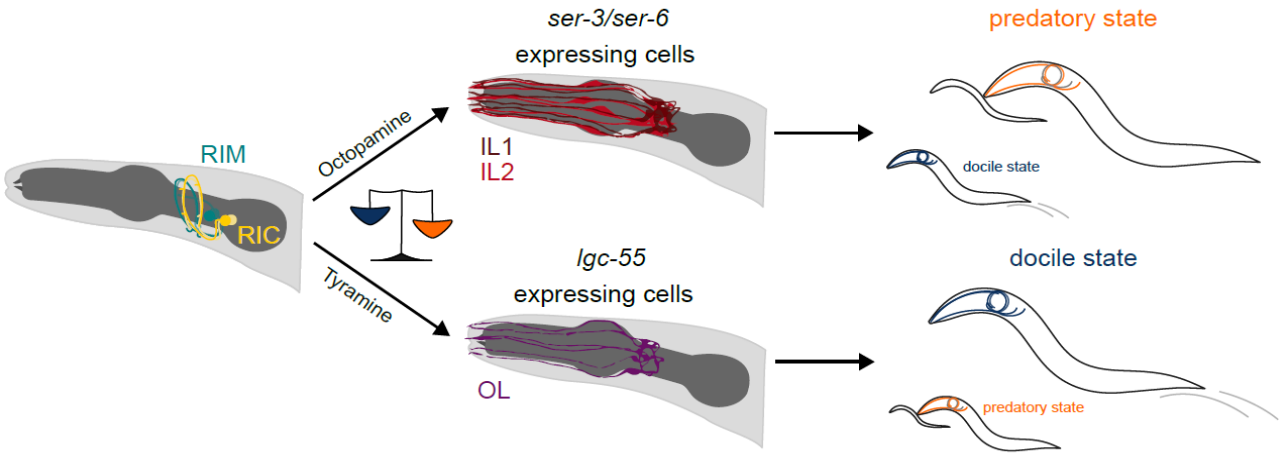

Fig. 30. Proposed model of the antagonistic octopamine/tyramine regulation driving aggressive versus docile behavioral states.

5. Abstract

Behaviors are adaptive traits shaped by natural selection. Nevertheless, the genetic, molecular, and neural modifications that underlie behavioral innovations remain poorly understood. Here, I identify specialized adaptations linked to the evolution of invertebrate aggression by leveraging a comparative nematode framework, *Pristionchus pacificus* versus *Caenorhabditis elegans,* to dissect the evolution of predatory aggression and its interface with territoriality and feeding. We combined high throughput tracking with a semi-supervised behavioral state labeling pipeline, cell type resolved perturbations, receptor mapping, and targeted CRISPR screens. Quantitative analyses revealed that octopamine and tyramine function as an antagonistic pair at the molecular level: *tbh-1* loss (↓octopamine) reduced entry into the predatory state, *tdc-1* loss (↓tyramine and ↓octopamine) rescued this effect. Furthermore, exogenous octopamine and tyramine also shifted state occupancy in opposite directions. Behavioral assays of CRISPR mutants showed that mutations in the octopamine receptors *ser-3/ser-6* phenocopied *tbh-1* deficits, whereas mutations in the tyramine associated ion channel, *lgc-55* mirrored the rescue observed in *tdc-1*. Crucially, we found that while the neurotransmitter source remained conserved across species, the receptor expression has been rewired with differential expression observed across head sensory neurons. Notably, *P. pacificus* specific SER-3 expression is detected in IL2 sensory neurons and functional silencing of these reduces predatory search, biting, and feeding. This establishes the IL2 neurons as a sensory hub for prey detection and state gating. Comparative tests across another basal Diplogastrid species indicate that octopamine's pro-aggressive role is conserved within this family. Thus adaptations in noradrenergic circuits emerges as a central mechanism for shaping the evolution of aggressive behavioral states in nematodes.

6. List of Figures

7. List of tables

8. References

Albertson DG, Thompson JN. The pharynx of Caenorhabditis elegans. Philos Trans R Soc Lond B, Biol Sci. 1976;275(938):299–325.

Alkema MJ, Hunter-Ensor M, Ringstad N, Horvitz HR. Tyramine Functions Independently of Octopamine in the Caenorhabditis elegans Nervous System. Neuron. 2005;46(2):247–60.

Allen AM, Sokolowski MB. Expression of the foraging gene in adult Drosophila melanogaster. J Neurogenet. 2021;35(3):192–212.

Amenta F, Zaccheo D, Collier WL. Neurotransmitters, neuroreceptors and aging. Mech Ageing Dev. 1991;61(3):249–73.

Arnsten AFT. Stress signalling pathways that impair prefrontal cortex structure and function. Nat Rev Neurosci. 2009;10(6):410–22.

Asahina K, Watanabe K, Duistermars BJ, Hoopfer E, González CR, Eyjólfsdóttir EA, et al. Tachykinin-Expressing Neurons Control Male-Specific Aggressive Arousal in Drosophila. Cell. 2014;156(1–2):221–35.

Aston-Jones G, Cohen JD. AN INTEGRATIVE THEORY OF LOCUS COERULEUS-NOREPINEPHRINE FUNCTION: Adaptive Gain and Optimal Performance. Annu Rev Neurosci. 2005;28(1):403–50.

Avery L, Horvitz HR. A cell that dies during wild-type C. elegans development can function as a neuron in a ced-3 mutant. Cell. 1987;51(6):1071–8.

Avery L, Horvitzt HR. Pharyngeal pumping continues after laser killing of the pharyngeal nervous system of C. elegans. Neuron. 1989;3(4):473–85.

Baldwin MW, Toda Y, Nakagita T, O'Connell MJ, Klasing KC, Misaka T, et al. Evolution of sweet taste perception in hummingbirds by transformation of the ancestral umami receptor. Science. 2014;345(6199):929–33.

Bargmann CI. Neurobiology of the Caenorhabditis elegans Genome. Science. 1998;282(5396):2028–33.

Bargmann CI. Beyond the connectome: How neuromodulators shape neural circuits. BioEssays. 2012;34(6):458–65.

Bargmann CI, Hartwieg E, Horvitz HR. Odorant-selective genes and neurons mediate olfaction in C.

elegans. Cell. 1993;74(3):515–27.

Bello MD, Pérez-Escudero A, Schroeder FC, Gore J. Inversion of pheromone preference optimizes foraging in C. elegans. eLife. 2021;10:e58144.

Bendesky A, Kwon YM, Lassance JM, Lewarch CL, Yao S, Peterson BK, et al. The genetic basis of parental care evolution in monogamous mice. Nature. 2017;544(7651):434–9.

Benichov JI, Benezra SE, Vallentin D, Globerson E, Long MA, Tchernichovski O. The Forebrain Song System Mediates Predictive Call Timing in Female and Male Zebra Finches. Curr Biol. 2016;26(3):309–18.

Bento G, Ogawa A, Sommer RJ. Co-option of the hormone-signalling module dafachronic acid–DAF-12 in nematode evolution. Nature. 2010;466(7305):494–7.

Benzer S. BEHAVIORAL MUTANTS OF Drosophila ISOLATED BY COUNTERCURRENT DISTRIBUTION. Proc Natl Acad Sci. 1967;58(3):1112–9.

Bonnard E, Liu J, Zjacic N, Alvarez L, Scholz M. Automatically tracking feeding behavior in populations of foraging C. elegans. eLife. 2022;11:e77252.

Bouret S, Sara SJ. Network reset: a simplified overarching theory of locus coeruleus noradrenaline function. Trends Neurosci. 2005;28(11):574–82.

Brainard MS, Doupe AJ. What songbirds teach us about learning. Nature. 2002;417(6886):351–8.

Branson K, Robie AA, Bender J, Perona P, Dickinson MH. High-throughput ethomics in large groups of Drosophila. Nat Methods. 2009;6(6):451–7.

Brenner S. THE GENETICS OF CAENORHABDITIS ELEGANS. Genetics. 1974;77(1):71–94.

Briggman KL, Abarbanel HDI, Jr. WBK. Optical Imaging of Neuronal Populations During Decision-Making. Science. 2005;307(5711):896–901.

Britz S, Markert SM, Witvliet D, Steyer AM, Tröger S, Mulcahy B, et al. Structural Analysis of the Caenorhabditis elegans Dauer Larval Anterior Sensilla by Focused Ion Beam-Scanning Electron Microscopy. Front Neuroanat. 2021;15:732520.

Bumbarger DJ, Riebesell M, Rödelsperger C, Sommer RJ. System-wide Rewiring Underlies Behavioral Differences in Predatory and Bacterial-Feeding Nematodes. Cell. 2013;152(1–2):109–19.

Camhi JM. Neuroethology : nerve cells and the natural behavior of animals. 1941.

Capecchi MR. The new mouse genetics: Altering the genome by gene targeting. Trends Genet. 1989;5(3):70–6.

Chalfie M, Tu Y, Euskirchen G, Ward WW, Prasher DC. Green Fluorescent Protein as a Marker for Gene Expression. Science. 1994;263(5148):802–5.

Chatzigeorgiou M, Schafer WR. Lateral Facilitation between Primary Mechanosensory Neurons Controls Nose Touch Perception in C. elegans. Neuron. 2011;70(2):299–309.

Chen P, Hong W. Neural Circuit Mechanisms of Social Behavior. Neuron. 2018;98(1):16–30.
Chiang JTA, Steciuk M, Shtonda B, Avery L. Evolution of pharyngeal behaviors and neuronal functions in free-living soil nematodes. J Exp Biol. 2006;209(10):1859–73.

Churgin MA, McCloskey RJ, Peters E, Fang-Yen C. Antagonistic Serotonergic and Octopaminergic Neural Circuits Mediate Food-Dependent Locomotory Behavior in Caenorhabditis elegans. J Neurosci. 2017;37(33):7811–23.

Coleman RT, Morantte I, Koreman GT, Cheng ML, Ding Y, Ruta V. A modular circuit coordinates the diversification of courtship strategies. Nature. 2024;635(8037):142–50.

Consortium* TC elegans S. Genome Sequence of the Nematode C. elegans: A Platform for Investigating Biology. Science. 1998;282(5396):2012–8.

Cook SJ, Crouse CM, Yemini E, Hall DH, Emmons SW, Hobert O. The connectome of the Caenorhabditis elegans pharynx. J Comp Neurol. 2020;528(16):2767–84.

Cook SJ, Jarrell TA, Brittin CA, Wang Y, Bloniarz AE, Yakovlev MA, et al. Whole-animal connectomes of both Caenorhabditis elegans sexes. Nature. 2019;571(7763):63–71.

Cook SJ, Kalinski CA, Loer CM, Memar N, Majeed M, Stephen SR, et al. Comparative connectomics of two distantly related nematode species reveals patterns of nervous system evolution. bioRxiv. 2025a;:2024.06.13.598904.

Cook SJ, Kalinski CA, Loer CM, Memar N, Majeed M, Stephen SR, et al. Comparative connectomics of two distantly related nematode species reveals patterns of nervous system evolution. Science. 2025b;389(6759):eadx2143–eadx2143.

Dag U, Nwabudike I, Kang D, Gomes MA, Kim J, Atanas AA, et al. Dissecting the functional organization of the C. elegans serotonergic system at whole-brain scale. Cell. 2023;186(12):2574-2592.e20.

Dai H, Chen Y, Chen S, Mao Q, Kennedy D, Landback P, et al. The evolution of courtship behaviors through the origination of a new gene in Drosophila. Proc Natl Acad Sci. 2008;105(21):7478–83.

Dallière N, Holden-Dye L, Dillon J, O'Connor V, Walker RJ. Oxford Research Encyclopedia of Neuroscience 2017.

Dankert H, Wang L, Hoopfer ED, Anderson DJ, Perona P. Automated monitoring and analysis of social behavior in Drosophila. Nat Methods. 2009;6(4):297–303.

Dieterich C, Clifton SW, Schuster LN, Chinwalla A, Delehaunty K, Dinkelacker I, et al. The Pristionchus pacificus genome provides a unique perspective on nematode lifestyle and parasitism. Nat Genet. 2008;40(10):1193–8.

Donaldson ZR, Young LJ. Oxytocin, Vasopressin, and the Neurogenetics of Sociality. Science. 2008;322(5903):900–4.

Eren GG, Roca M, Han Z, Lightfoot JW. Genomic integration of transgenes using UV irradiation in Pristionchus pacificus. microPublication Biol. 2022;2022:10.17912/micropub.biology.000576.
Evarts EV. Relation of pyramidal tract activity to force exerted during voluntary movement. J Neurophysiol. 1968;31(1):14–27.

Falkner AL, Dollar P, Perona P, Anderson DJ, Lin D. Decoding Ventromedial Hypothalamic Neural Activity during Male Mouse Aggression. J Neurosci. 2014;34(17):5971–84.

Fan Y, Zou W, Liu J, Al-Sheikh U, Cheng H, Duan D, et al. Polymodal Functionality of C. elegans OLL Neurons in Mechanosensation and Thermosensation. Neurosci Bull. 2021;37(5):611–22.

Fire A, Xu S, Montgomery MK, Kostas SA, Driver SE, Mello CC. Potent and specific genetic interference by double-stranded RNA in Caenorhabditis elegans. Nature. 1998;391(6669):806–11.

Flavell SW, Pokala N, Macosko EZ, Albrecht DR, Larsch J, Bargmann CI. Serotonin and the Neuropeptide PDF Initiate and Extend Opposing Behavioral States in C. elegans. Cell. 2013;154(5):1023–35.

Flavell SW, Raizen DM, You YJ. Behavioral States. Genetics. 2020;216(2):315–32.

Flock T, Carlson BE. Exogenous octopamine increases antipredator aggression in scorpions (Centruroides vittatus). J Arachnol. 2019;47(3):392–5.

Florman JT, Alkema MJ. Co-transmission of neuropeptides and monoamines choreograph the C. elegans escape response. PLoS Genet. 2022;18(3):e1010091.

Frisch K von. The dance language and orientation of bees. Harvard University Press.; 1967.
Fujiwara M, Sengupta P, McIntire SL. Regulation of Body Size and Behavioral State of C. elegans by Sensory Perception and the EGL-4 cGMP-Dependent Protein Kinase. Neuron. 2002;36(6):1091–102.

Fussnecker BL, Smith BH, Mustard JA. Octopamine and tyramine influence the behavioral profile of locomotor activity in the honey bee (Apis mellifera). J Insect Physiol. 2006;52(10):1083–92.

Hammock EAD, Young LJ. Oxytocin, vasopressin and pair bonding: implications for autism. Philos Trans R Soc B: Biol Sci. 2006;361(1476):2187–98.

Han Z, Lo WS, Lightfoot JW, Witte H, Sun S, Sommer RJ. Improving Transgenesis Efficiency and CRISPR-Associated Tools Through Codon Optimization and Native Intron Addition in Pristionchus Nematodes. Genetics. 2020;216(4):genetics.303785.2020.

Harris G, Mills H, Wragg R, Hapiak V, Castelletto M, Korchnak A, et al. The Monoaminergic Modulation of Sensory-Mediated Aversive Responses in Caenorhabditis elegans Requires Glutamatergic/Peptidergic Cotransmission. J Neurosci. 2010;30(23):7889–99.

Harry CJ, Messar SM, Ragsdale EJ. Comparative reconstruction of the predatory feeding structures of the polyphenic nematode Pristionchus pacificus. Evol Dev. 2022;24(1–2):16–36.

Hernández DG, Rivera C, Cande J, Zhou B, Stern DL, Berman GJ. A framework for studying behavioral evolution by reconstructing ancestral repertoires. eLife. 2021;10:e61806.

Herrmann M, Mayer WE, Sommer RJ. Nematodes of the genus Pristionchus are closely associated with scarab beetles and the Colorado potato beetle in Western Europe. Zoology. 2006;109(2):96–108.

Hiramatsu F, Lightfoot JW. Kin-recognition and predation shape collective behaviors in the cannibalistic nematode Pristionchus pacificus. PLOS Genet. 2023;19(12):e1011056.

Hobson RJ, Hapiak VM, Xiao H, Buehrer KL, Komuniecki PR, Komuniecki RW. SER-7, a Caenorhabditis elegans 5-HT7-like Receptor, Is Essential for the 5-HT Stimulation of Pharyngeal Pumping and Egg Laying. Genetics. 2006;172(1):159–69.

Hodgkin AL, Huxley AF. A quantitative description of membrane current and its application to conduction and excitation in nerve. J Physiol. 1952;117(4):500–44.

Hong RL, Riebesell M, Bumbarger DJ, Cook SJ, Carstensen HR, Sarpolaki T, et al. Evolution of neuronal anatomy and circuitry in two highly divergent nematode species. bioRxiv. 2019;595025.

Hong RL, Sommer RJ. Chemoattraction in Pristionchus Nematodes and Implications for Insect Recognition. Curr Biol. 2006;16(23):2359–65.

Howard RJ, Giacomelli M, Lozano-Fernandez J, Edgecombe GD, Fleming JF, Kristensen RM, et al. The Ediacaran origin of Ecdysozoa: integrating fossil and phylogenomic data. J Geol Soc. 2022;179(4):jgs2021-107.

Hoyle G. The Scope of Neuroethology. 1984.
Huber F. Central nervous control of sound production in crickets and some speculations on its evolution, Evolution. 1962.

Inagaki HK, Ben-Tabou de-Leon S, Wong AM, Jagadish S, Ishimoto H, Barnea G, et al. Visualizing Neuromodulation In Vivo: TANGO-Mapping of Dopamine Signaling Reveals Appetite Control of Sugar Sensing. Cell. 2012;148(3):583–95.

Ishita Y, Chihara T, Okumura M. Different combinations of serotonin receptors regulate predatory and bacterial feeding behaviors in the nematode Pristionchus pacificus. G3. 2021;11(2):jkab011.

Ishita Y, Onodera A, Ekino T, Chihara T, Okumura M. Co-option of an Astacin Metalloprotease Is Associated with an Evolutionarily Novel Feeding Morphology in a Predatory Nematode. Mol Biol Evol. 2023;40(12):msad266.

Jourjine N, Hoekstra HE. Expanding evolutionary neuroscience: insights from comparing variation in behavior. Neuron. 2021;109(7):1084–99.

Kabra M, Robie AA, Rivera-Alba M, Branson S, Branson K. JAABA: interactive machine learning for automatic annotation of animal behavior. Nat Methods. 2013;10(1):64–7.

Kandel ER. The Molecular Biology of Memory Storage: A Dialogue Between Genes and Synapses. Science. 2001;294(5544):1030–8.

Kaplan JM, Horvitz HR. A dual mechanosensory and chemosensory neuron in Caenorhabditis elegans. Proc Natl Acad Sci. 1993;90(6):2227–31.

Katz B, Miledi R. The effect of calcium on acetylcholine release from motor nerve terminals. Proc R Soc Lond Ser B Biol Sci. 1965;161(985):496–503.

Kieninger MR, Ivers NA, Rödelsperger C, Markov GV, Sommer RJ, Ragsdale EJ. The Nuclear Hormone Receptor NHR-40 Acts Downstream of the Sulfatase EUD-1 as Part of a Developmental Plasticity Switch in Pristionchus. Curr Biol. 2016;26(16):2174–9.

Kindt KS, Quast KB, Giles AC, De S, Hendrey D, Nicastro I, et al. Dopamine Mediates Context-Dependent Modulation of Sensory Plasticity in C. elegans. Neuron. 2007;55(4):662–76.

Krakauer JW, Ghazanfar AA, Gomez-Marin A, MacIver MA, Poeppel D. Neuroscience Needs Behavior: Correcting a Reductionist Bias. Neuron. 2017;93(3):480–90.

Kravitz EA, Huber R. Aggression in invertebrates. Curr Opin Neurobiol. 2003;13(6):736–43.
Krogh A. The Progress of Physiology. Science. 1929;70(1809):200–4.

Kumar S, Stecher G, Li M, Knyaz C, Tamura K. MEGA X: Molecular Evolutionary Genetics Analysis across Computing Platforms. Mol Biol Evol. 2018;35(6):1547–9.

Kutsukake M, Komatsu A, Yamamoto D, Ishiwa-Chigusa S. A tyramine receptor gene mutation causes a defective olfactory behavior in Drosophila melanogaster. Gene. 2000;245(1):31–42.

Lee H, Choi M kyu, Lee D, Kim H sung, Hwang H, Kim H, et al. Nictation, a dispersal behavior of the nematode Caenorhabditis elegans, is regulated by IL2 neurons. Nat Neurosci. 2012;15(1):107–12.

Li W, Kang L, Piggott BJ, Feng Z, Xu XZS. The neural circuits and sensory channels mediating harsh touch sensation in Caenorhabditis elegans. Nat Commun. 2011;2(1):315.

Lightfoot JW, Dardiry M, Kalirad A, Giaimo S, Eberhardt G, Witte H, et al. Sex or cannibalism: Polyphenism and kin recognition control social action strategies in nematodes. Sci Adv. 2021;7(35):eabg8042.

Lightfoot JW, Wilecki M, Rödelsperger C, Moreno E, Susoy V, Witte H, et al. Small peptide–mediated self-recognition prevents cannibalism in predatory nematodes. Science. 2019;364(6435):86–9.

Liu H, Qin LW, Li R, Zhang C, Al-Sheikh U, Wu ZX. Reciprocal modulation of 5-HT and octopamine regulates pumping via feedforward and feedback circuits in C. elegans. Proc Natl Acad Sci. 2019;116(14):7107–12.

Lorenz K. The comparative method in studying innate behavior patterns. Symposia of the Society for Experimental Biology. 1950;4.

Lorenz K. On Aggression. 1966.

Marder E. Neuromodulation of Neuronal Circuits: Back to the Future. Neuron. 2012;76(1):1–11.

Marder E, Goaillard JM. Variability, compensation and homeostasis in neuron and network function. Nat Rev Neurosci. 2006;7(7):563–74.

McEwen BS, Morrison JH. The Brain on Stress: Vulnerability and Plasticity of the Prefrontal Cortex over the Life Course. Neuron. 2013;79(1):16–29.

Mills H, Wragg R, Hapiak V, Castelletto M, Zahratka J, Harris G, et al. Monoamines and neuropeptides interact to inhibit aversive behavior in Caenorhabditis elegans. EMBO J. 2012;31(3):667–78.

Moreno E, Lenuzzi M, Rödelsperger C, Prabh N, Witte H, Roeseler W, et al. DAF-19/RFX controls ciliogenesis and influences oxygen-induced social behaviors in Pristionchus pacificus. Evol Dev. 2018;20(6):233–43.

Moreno E, Lightfoot JW, Lenuzzi M, Sommer RJ. Cilia drive developmental plasticity and are essential for efficient prey detection in predatory nematodes. Proc Royal Soc B. 2019;286(1912):20191089.

Moulin B, Rybak F, Aubin T, Jallon JM. Compared Ontogenesis of Courtship Song Components of Males from the Sibling Species, D. melanogaster and D. simulans. Behav Genet. 2001;31(3):299–308.

Nelson ME, MacIver MA. Sensory acquisition in active sensing systems. J Comp Physiol A. 2006;192(6):573–86.

Okumura M, Wilecki M, Sommer RJ. Serotonin Drives Predatory Feeding Behavior via Synchronous Feeding Rhythms in the Nematode Pristionchus pacificus. G3 Genes Genomes Genetics. 2017;7(11):3745–55.

Petrascheck M, Ye X, Buck LB. An antidepressant that extends lifespan in adult Caenorhabditis elegans. Nature. 2007;450(7169):553–6.

Pirri JK, McPherson AD, Donnelly JL, Francis MM, Alkema MJ. A Tyramine-Gated Chloride Channel Coordinates Distinct Motor Programs of a Caenorhabditis elegans Escape Response. Neuron. 2009;62(4):526–38.

Piskobulu V, Athanasouli M, Witte H, Feldhaus C, Streit A, Sommer RJ. High Nutritional Conditions Influence Feeding Plasticity in Pristionchus pacificus and Render Worms Non-Predatory. J Exp Zoöl Part B: Mol Dev Evol. 2025;344(2):94–111.

Pokala N, Liu Q, Gordus A, Bargmann CI. Inducible and titratable silencing of Caenorhabditis elegans neurons in vivo with histamine-gated chloride channels. Proc Natl Acad Sci. 2014;111(7):2770–5.

Quach KT, Chalasani SH. Intraguild predation between Pristionchus pacificus and Caenorhabditis elegans: a complex interaction with the potential for aggressive behavior. J Neurogenet. 2020;34(3–4):404–19.

Ragsdale EJ, Müller MR, Rödelsperger C, Sommer RJ. A Developmental Switch Coupled to the Evolution of Plasticity Acts through a Sulfatase. Cell. 2013;155(4):922–33.

Raizen DM, Avery L. Electrical activity and behavior in the pharynx of caenorhabditis elegans. Neuron. 1994;12(3):483–95.

Ramadan YH, Hobert O. Visualization of gene expression in Pristionchus pacificus with smFISH and in situ HCR. microPublication Biol. 2024;2024:10.17912/micropub.biology.001274.

Ramos BP, Arnsten AFT. Adrenergic pharmacology and cognition: Focus on the prefrontal cortex. Pharmacol Ther. 2007;113(3):523–36.

Ranganathan R, Sawin ER, Trent C, Horvitz HR. Mutations in the Caenorhabditis elegans serotonin reuptake transporter MOD-5 reveal serotonin-dependent and -independent activities of fluoxetine. J Neurosci : Off J Soc Neurosci. 2001a;21(16):5871–84.

Ranganathan R, Sawin ER, Trent C, Horvitz HR. Mutations in the Caenorhabditis elegans Serotonin Reuptake Transporter MOD-5 Reveal Serotonin-Dependent and -Independent Activities of Fluoxetine. J Neurosci. 2001b;21(16):5871–84.

Ricci A, Vega J, Zaccheo D, Amenta F. Dopamine D1like receptors in the thymus of aged rats: A radioligand binding and autoradiographic study. J Neuroimmunol. 1995;56(2):155–60.

Ripoll-Sánchez L, Watteyne J, Sun H, Fernandez R, Taylor SR, Weinreb A, et al. The neuropeptidergic connectome of C. elegans. Neuron. 2023;111(22):3570-3589.e5.

Rivard L, Srinivasan J, Stone A, Ochoa S, Sternberg PW, Loer CM. A comparison of experience-dependent locomotory behaviors and biogenic amine neurons in nematode relatives of Caenorhabditis elegans. BMC Neurosci. 2010;11(1):22.

Roberts RJV, Pop S, Prieto-Godino LL. Evolution of central neural circuits: state of the art and perspectives. Nat Rev Neurosci. 2022;23(12):725–43.

Robson DN, Li JM. A dynamical systems view of neuroethology: Uncovering stateful computation in natural behaviors. Curr Opin Neurobiol. 2022;73:102517.

Roca M, Eren GG, Böger L, Didenko O, Lo W sui, Scholz M, et al. Evolution of sensory systems underlies the emergence of predatory feeding behaviors in nematodes. bioRxiv.

2025;2025.03.24.644997.

Rödelsperger C, Neher RA, Weller AM, Eberhardt G, Witte H, Mayer WE, et al. Characterization of Genetic Diversity in the Nematode Pristionchus pacificus from Population-Scale Resequencing Data. Genetics. 2014;196(4):1153–65.

Roeder T. TYRAMINE AND OCTOPAMINE: Ruling Behavior and Metabolism. Annu Rev Èntomol. 2005;50(1):447–77.

Rogers CM, Franks CJ, Walker RJ, Burke JF, Holden-Dye L. Regulation of the pharynx of Caenorhabditis elegans by 5-HT, octopamine, and FMRFamide-like neuropeptides. J Neurobiol. 2001;49(3):235–44.

Ryan DA, Miller RM, Lee K, Neal SJ, Fagan KA, Sengupta P, et al. Sex, Age, and Hunger Regulate Behavioral Prioritization through Dynamic Modulation of Chemoreceptor Expression. Curr Biol. 2014;24(21):2509–17.

Sara SJ. The locus coeruleus and noradrenergic modulation of cognition. Nat Rev Neurosci. 2009;10(3):211–23.

Saraswati S, Fox LE, Soll DR, Wu C. Tyramine and octopamine have opposite effects on the locomotion of Drosophila larvae. J Neurobiol. 2004;58(4):425–41.

Sawin ER, Ranganathan R, Horvitz HR. C. elegans Locomotory Rate Is Modulated by the Environment through a Dopaminergic Pathway and by Experience through a Serotonergic Pathway. Neuron. 2000;26(3):619–31.

Sayin S, Backer JFD, Siju KP, Wosniack ME, Lewis LP, Frisch LM, et al. A Neural Circuit Arbitrates between Persistence and Withdrawal in Hungry Drosophila. Neuron. 2019;104(3):544-558.e6.

Schafer WR. Deciphering the Neural and Molecular Mechanisms of C. elegans Behavior. Curr Biol. 2005;15(17):R723–9.

Sengupta P, Chou JH, Bargmann CI. odr-10 Encodes a Seven Transmembrane Domain Olfactory Receptor Required for Responses to the Odorant Diacetyl. Cell. 1996;84(6):899–909.

Serobyan V, Xiao H, Namdeo S, Rödelsperger C, Sieriebriennikov B, Witte H, et al. Chromatin remodelling and antisense-mediated up-regulation of the developmental switch gene eud-1 control predatory feeding plasticity. Nat Commun. 2016;7(1):12337.

Shang C, Chen Z, Liu A, Li Y, Zhang J, Qu B, et al. Divergent midbrain circuits orchestrate escape and freezing responses to looming stimuli in mice. Nat Commun. 2018;9(1):1232.

Sommer RJ, Lightfoot JW. Nematodes as Model Organisms. 2022;1–23.
Sulston JE, Horvitz HR. Post-embryonic cell lineages of the nematode, Caenorhabditis elegans. Dev Biol. 1977;56(1):110–56.

Sun S, Witte H, Sommer RJ. Chitin contributes to the formation of a feeding structure in a predatory nematode. Curr Biol. 2023;33(1):15-27.e6.

Suo S, Kimura Y, Tol HHMV. Starvation Induces cAMP Response Element-Binding Protein-Dependent Gene Expression through Octopamine–Gq Signaling in Caenorhabditis elegans. J Neurosci. 2006;26(40):10082–90.

Thistle R, Cameron P, Ghorayshi A, Dennison L, Scott K. Contact Chemoreceptors Mediate Male-Male Repulsion and Male-Female Attraction during Drosophila Courtship. Cell. 2012;149(5):1140–51.

Tinbergen N. The Study of Instinct. 1951.

Tovote P, Esposito MS, Botta P, Chaudun F, Fadok JP, Markovic M, et al. Midbrain circuits for defensive behavior. Nature. 2016;534(7606):206–12.

Vidal-Gadea A, Topper S, Young L, Crisp A, Kressin L, Elbel E, et al. Caenorhabditis elegans selects distinct crawling and swimming gaits via dopamine and serotonin. Proc Natl Acad Sci. 2011;108(42):17504–9.

Vogelstein JT, Park Y, Ohyama T, Kerr RA, Truman JW, Priebe CE, et al. Discovery of Brainwide Neural-Behavioral Maps via Multiscale Unsupervised Structure Learning. Science. 2014;344(6182):386–92.

Vrontou E, Nilsen SP, Demir E, Kravitz EA, Dickson BJ. fruitless regulates aggression and dominance in Drosophila. Nat Neurosci. 2006;9(12):1469–71.

Wang L, Anderson DJ. Identification of an aggression-promoting pheromone and its receptor neurons in Drosophila. Nature. 2010;463(7278):227–31.

Werner MS, Sieriebriennikov B, Loschko T, Namdeo S, Lenuzzi M, Dardiry M, et al. Environmental influence on Pristionchus pacificus mouth form through different culture methods. Sci Rep. 2017;7(1):7207.

White JG, Southgate E, Thomson JN, Brenner S. The structure of the nervous system of the nematode Caenorhabditis elegans. Philos Trans R Soc Lond B, Biol Sci. 1986;314(1165):1–340.

Widmer A, Höger U, Meisner S, French AS, Torkkeli PH. Spider Peripheral Mechanosensory Neurons Are Directly Innervated and Modulated by Octopaminergic Efferents. J Neurosci. 2005;25(6):1588–98.

Wighard S, Witte H, Sommer RJ. Conserved switch genes that arose via whole-genome duplication regulate a cannibalistic nematode morph. Sci Adv. 2024;10(15):eadk6062.

Wilecki M, Lightfoot JW, Susoy V, Sommer RJ. Predatory feeding behavior in Pristionchus nematodes is dependent on phenotypic plasticity and induced by serotonin. J Exp Biol. 2015;218(9):1306–13.

Witte H, Moreno E, Rödelsperger C, Kim J, Kim JS, Streit A, et al. Gene inactivation using the CRISPR/Cas9 system in the nematode Pristionchus pacificus. Dev Genes Evol. 2015;225(1):55–62.
Witvliet D, Mulcahy B, Mitchell JK, Meirovitch Y, Berger DR, Wu Y, et al. Connectomes across development reveal principles of brain maturation. Nature. 2021;596(7871):257–61.

Yang C, Mammen L, Kim B, Li M, Robson DN, Li JM. A population code for spatial representation in the zebrafish telencephalon. Nature. 2024;634(8033):397–406.

Ye D, Walsh JT, Junker IP, Ding Y. Changes in the cellular makeup of motor patterning circuits drive courtship song evolution in Drosophila. Curr Biol. 2024;34(11):2319-2329.e6.

Zaslaver A, Liani I, Shtangel O, Ginzburg S, Yee L, Sternberg PW. Hierarchical sparse coding in the sensory system of Caenorhabditis elegans. Proc Natl Acad Sci. 2015;112(4):1185–9.

Zhang M, Chung SH, Fang-Yen C, Craig C, Kerr RA, Suzuki H, et al. A Self-Regulating Feed-Forward Circuit Controlling C. elegans Egg-Laying Behavior. Curr Biol. 2008;18(19):1445–55.

Zhao H, Li J, Zhang J. Molecular evidence for the loss of three basic tastes in penguins. Curr Biol. 2015;25(4):R141–2.

Zhou C, Rao Y, Rao Y. A subset of octopaminergic neurons are important for Drosophila aggression. Nat Neurosci. 2008;11(9):1059–67.

9. Statement of own contribution

This dissertation was conducted at the Max Planck Institute for Neurobiology of Behavior – caesar. Under the supervision of Dr. James W. Lightfoot, I planned the research program, designed the behavioral assays, developed the receptor mapping strategy, and established the genetics and perturbation logic. I implemented PharaGlow tracking for *P. pacificus* by generating the transgenic line with integrated pharyngeal reporter expression, adapting and setting up the tracking infrastructure in our lab, building the associated imaging and compression pipeline, and optimizing analysis parameters specifically for this species. In addition, I collected and curated the majority of the behavioral recordings; performed pharmacological manipulations; carried out cell type specific perturbations; and generated or outcrossed the CRISPR lines used for receptor tests. I also implemented the semi-supervised behavioral state labeling pipeline, performed statistical analyses, produced all primary figures, and interpreted the results, except where noted below.

Where applicable, I received support as follows: Leonard Böger (PhD student, our lab) led the behavioral classification framework used in this thesis; he designed, implemented, and optimized the machine-learning pipeline (feature engineering, UMAP embedding, clustering, and classifier training) under the supervision of Dr. Monika Scholz, and contributed to statistical evaluation and figure preparation related to ML/behavioral classification. Dr. Marianne Roca, Fumie Hiramatsu, and Dr. James W. Lightfoot performed microinjections for strain construction. Dr. Jun Liu and Dr. Wolfgang Bönigk contributed cloning plasmids for the transgenic lines. Dr. Luis Alvarez acquired confocal images of the *ser-3, ser-6*, and *lgc-55* reporter lines. Dr. Lewis A. Cockram collected behavioral recordings under bacterial plus larval condition. Nurit Zorn contributed to generating CRISPR mutants. Quantification of transgene copy number and expression by qPCR was carried out by Dr. Ziduan Han. Misako Okumura provided the *tbh-1* and *tdc-1* mutant strains. All such contributions are acknowledged in the relevant sections and are consistent with the author contribution statements of associated publications. Raw data used for evaluation were generated by me unless explicitly indicated.

In preparing the written text, I used generative AI tools (“ChatGPT (OpenAI)”) solely to improve readability, grammar, and consistency of style and to draft alternative phrasings. I reviewed and edited all AI assisted passages and take full responsibility for the scientific content and conclusions. I confirm that I wrote this thesis independently and have not used any sources or aids other than those specified by me. I hereby confirm that my thesis complies with the Statement by the Executive Committee of the Deutsche Forschungsgemeinschaft (DFG) on the influence of generative models on science and on the DFG’s funding activities, including transparency of use, human authorship, and responsibility for content.

10. Acknowledgements

First and foremost, to James, thank you for your endless encouragement, for reminding me that growth often comes from trying things out, even when they are messy.

To my thesis advisory committee, Prof. Dr. Ilona Grunwald Kadow and Prof. Dr. Tobias Rose. Thank you for your guidance and constructive critique throughout this dissertation.

To Monika, for offering fresh perspectives and sharing a truly dynamic mind that constantly challenged and inspired me.

To Ezgi, for being a true friend during the loneliest times of COVID and for your immense support in helping me settle in Bonn. I couldn't have asked for a better companion in those challenging days.

To Neo, my loyal companion, for refreshing my mind every evening after long days at the lab and making this journey a little brighter with your presence.

To Altug, for sharing countless good memories, for listening patiently to my "crybaby" moments, and for offering grounded, realistic advice that helped me more than you know.

To my wonderful lab members: Fumie, my worm playmate and source of the warmest hugs; Marianne, for sharing your love of the sea, fantasy and board games; and Leonard, who always appeared like Gandalf whenever the project needed a spark of support, and for being the coolest Kölner I have had the pleasure of knowing.

To my parents, for being the embodiment of resilience and for always being there whenever I needed support.

To my grandparents, for filling my childhood with love and memories that continue to warm my heart.

And finally, to my brother, for being my company during the last year.

11. Appendix

Strain	Background	Genomics	Source
JWL27	PS312	*Ppa-myo-2::TurboRFP* [bnnls1]	This paper
RS2946	PS312	*tph-1(*tu628*)*	Okumura and Wilecki
JWL50	PS312	*tph-1(*tu628*); Ppa-myo-2:: TurboRFP* [bnnls1]	This paper
RS3150	PS312	*cat-2(tu1023)*	Onodera et al.
JWL121	PS312	*cat-2(tu1023); Ppa-myo-2:: TurboRFP* [bnnls1]	This paper
MOK46	PS312	*tbh-1(cbh32)*	Onodera et al.
MOK47	PS312	*tbh-1 (cbh33)*	Onodera et al.
JWL246	PS312	*tbh-1(cbh33); Ppa-myo-2:: TurboRFP* [bnnls1]	This paper
JWL112	PS312	*tbh-1(cbh32); Ppa-myo-2:: TurboRFP* [bnnls1]	This paper
RS3069	PS312	*tdc-1(tu1006)*	Onodera et al.
RS3070	PS312	*tdc-1(tu1007)*	Onodera et al.
JWL245	PS312	*tdc-1(tu1006); Ppa-myo-2:: TurboRFP* [bnnls1]	This paper
JWL122	PS312	*tdc-1(tu1007); Ppa-myo-2:: TurboRFP* [bnnls1]	This paper
JWL134	PS312	*ser-3(bnn115); Ppa-myo-2:: TurboRFP* [bnnls1]	This paper
JWL135	PS312	*ser-6(bnn116); Ppa-myo-2:: TurboRFP* [bnnls1]	This paper
JWL137	PS312	*octr-1(bnn119); Ppa-myo-2:: TurboRFP* [bnnls1]	This paper
JWL144	PS312	*tyra-2(bnn123); tbh-1(cbh32); Ppa-myo-2:: TurboRFP* [bnnls1]	This paper
JWL148	PS312	*ser-2 (bnn125); tbh-1 (cbh32); Ppa-myo-2:: TurboRFP* [bnnls1]	This paper
JWL152	PS312	*lgc-55 (bnn129); tbh-1 (cbh32); Ppa-myo-2:: TurboRFP* [bnnls1]	This paper
JWL155	PS312	*tyra-3 (bnn132); tbh-1 (cbh32); Ppa-myo-2:: TurboRFP* [bnnls1]	This paper
JWL170	PS312	*ser-2(bnn138); tyra-2(bnn139); tyra-3 (bnn132); tbh-1 (cbh32); Ppa-myo-2:: TurboRFP* [bnnls1]	This paper

JWL172	PS312	*tbh-1 (cbh32);tdc-1(tu1007); Ppa-myo-2:: TurboRFP* [bnnls1]	This paper
JWL192	PS312	*Ppa-tbh-1:: TurboRFP; Ppa-tdc-1:: GFP* [bnnEx11]	This paper
JWL205	PS312	*Ppa-ser-3:: TurboRFP; Ppa-ser-6:: GFP* [bnnEx13]	This paper
JWL206	PS312	*Ppa-ser-3:: TurboRFP; Ppa-lgc-55:: GFP* [bnnEx14]	This paper
JWL252	PS312	*Ppa-klp-6::GFP* [bnnEx21]	This paper
JWL257	PS312	*Ppa-klp-6:HisCl* [bnnEx22*]; Ppa-mec-6::GFP; Ppa-myo-2:: TurboRFP* [bnnls1]	This paper
JWL258	PS312	*Ppa-ser-3 (bnn190); Ppa-myo-2:: TurboRFP* [bnnls1]	This paper
RS5678B			Rödelsperger et al.
SJ4103		*myo-3::GFP(mit)* [zcIs14]	*Caenorhabditis* Genetics Center
SB413			Wighard and Witte
VN443		*ser-6::GFP, ceh-17::dsRed, tbh-1::dsRed, pRF4* [vnEx144]	Yoshida et al.
BC11545		*dpy-5(e907); rCesK02F2.6::GFP; pCeh361* [sEx11545]	*Caenorhabditis* Genetics Center
FQ63		lin-15AB(n765) X; lgc-55p::GFP + lin-15(+) [wzIs20]	*Caenorhabditis* Genetics Center
N2			*Caenorhabditis* Genetics Center
GRU101		*myo-2p*::yfp [gnaIs1]	*Caenorhabditis* Genetics Center
JWL270	SB413	*Asu-tbh-1.1* (bnn195) *Asu-tbh-1.2* (bnn196*)*	*This paper*
SB413			Wighard et al.

Table 1: Strain list of animals used in this study

Target gene	Function	Sequence
ser-3(bnn115)	PCR F1	GACAATGAGGCTTCGCTGTG
ser-3(bnn115)	PCR F2 (Sequencing)	GCTGATCAGTTGTCCTTATCGTTACC
ser-3(bnn115)	PCR R2	CGCAATGCTCCTTCTACGAGTG
ser-3(bnn115)	PCR R1	GCCCACTAATTCGTCCGTCG
ser-6(bnn116)	PCR F1	GAGAAGAGAACAGATACAGGGGTG
ser-6(bnn116)	PCR F2 (Sequencing)	GTGGAATAAAGACCATTCCTATTCCAGG
ser-6(bnn116)	PCR R2	CGAATCGAAGAGGAGAATGATAGG
ser-6(bnn116)	PCR R1	GTTGACAATACTGGTATTGAGTCATGG
octr-1(bnn119)	PCR F1	GAGATAATCGTGCTCGGCAACG
octr-1(bnn119)	PCR F2 (Sequencing)	CTCGTGGTCATGACCGTGTAC
octr-1(bnn119)	PCR R2	GCTGCGTTACGCAAAAGTACC
octr-1(bnn119)	PCR R1	GTGCGCTTGTTGGGATAAGAAAG
tyra-2(bnn123)	PCR F1	GGCACGGTAATGAGTATTCGGAAG
tyra-2(bnn123)	PCR F2	CTCGACGGCCTCAATATGGAAC
tyra-2(bnn123)	PCR R2 (Sequencing)	GCGGTTCACTATGGACAACAAC
tyra-2(bnn123)	PCR R1	GTTTCGGAGATGAAGAGGAATAGGG
ser-2 (bnn125)	PCR F1	GGATGAACCATGGACCAGCG
ser-2 (bnn125)	PCR F2	CGATTTTGGGCACTGTTCCAC
ser-2 (bnn125)	PCR R2 (Sequencing)	CCGATGAATCTGATACGCACC
ser-2 (bnn125)	PCR R1	GAGACGAGACCTGGGTCATTTG
lgc-55 (bnn129)	PCR F1	GCAAGCTGCTCATCCAAGG
lgc-55 (bnn129)	PCR F2	CCTCGTCGGGAAATTCAATTGTATG
lgc-55 (bnn129)	PCR R2 (Sequencing)	GATTATCCCTTCGAGAGATGTCCC
lgc-55 (bnn129)	PCR R1	CAATAAGTGCATGATGTGGGAATGG
tyra-3 (bnn132)	PCR F1	CTGCCCCATTTCAGGGAAATG
tyra-3 (bnn132)	PCR F2	GCTCTGCATGGGCTACAATC
tyra-3 (bnn132)	PCR R2 (Sequencing)	GTGAAGCTGGTGGATCATCGG
tyra-3 (bnn132)	PCR R1	GAAACTGCCAGATGCGGAGTAC

Table 2: Sequence of sgRNA and primers used to generate CRISPR knock outs

Population	*Condition*	State	N	Mean Rank	Sum Rank	U1	U2	Mann-Whitney U	p	N tests	bonferroni p	Figure
	WT larvae	pred. feed	131									Fig. 14 C
		pred. bite	131									
		pred. search	131									
		dwelling	131									
		roaming	131									
		search	131									
WT larvae	WT OP50	pred. feed	92	68,91	6340,00	9990,00	2062,00	2062,00	**2,70E-20**	1	**2,70E-20**	Fig. 14 C
		pred. bite	92	74,60	6863,00	9467,00	2585,00	2585,00	**2,86E-14**	1	**2,86E-14**	
		pred. search	92	76,41	7030,00	9300,00	2752,00	2752,00	**2,69E-12**	1	**2,69E-12**	
		dwelling	92	112,36	10337,00	5993,00	6059,00	5993,00	9,45E-01	1	9,45E-01	
		roaming	92	163,88	15077,00	1253,00	10799,00	1253,00	**2,80E-24**	1	**2,80E-24**	
		search	92	135,54	12470,00	3860,00	8192,00	3860,00	**4,85E-06**	1	**4,85E-06**	
	WT	pred. feed	91									Fig. 17 C
		pred. bite	91									
		pred. search	91									
		dwelling	91									
		roaming	91									
		search	91									
WT	*Ppa-tph-1*	pred. feed	56	51,08	2860,50	3831,50	1264,50	1264,50	**1,53E-07**	4	**6,10E-07**	Fig. 17 C
		pred. bite	56	50,14	2808,00	3884,00	1212,00	1212,00	**5,68E-08**	4	**2,27E-07**	
		pred. search	56	68,62	3842,50	2849,50	2246,50	2246,50	2,30E-01	4	9,18E-01	
		dwelling	56	65,47	3666,50	3025,50	2070,50	2070,50	5,58E-02	4	2,23E-01	
		roaming	56	109,54	6134,50	557,50	4538,50	557,50	**1,17E-15**	4	**4,69E-15**	
		search	56	91,34	5115,00	1577,00	3519,00	1577,00	**1,08E-04**	4	**4,31E-04**	
WT	*Ppa-cat-2*	pred. feed	97	75,99	7371,00	6209,00	2618,00	2618,00	**4,76E-07**	4	**1,90E-06**	Fig. 17 C
		pred. bite	97	85,58	8301,00	5279,00	3548,00	3548,00	**1,79E-02**	4	7,17E-02	
		pred. search	97	66,67	6467,00	7113,00	1714,00	1714,00	**2,97E-13**	4	**1,19E-12**	
		dwelling	97	101,60	9855,00	3725,00	5102,00	3725,00	6,44E-02	4	2,58E-01	
		roaming	97	119,14	11557,00	2023,00	6804,00	2023,00	**8,99E-11**	4	**3,60E-10**	
		search	97	102,75	9967,00	3613,00	5214,00	3613,00	**3,19E-02**	4	1,27E-01	
WT	*Ppa-tdc-1*	pred. feed	167	126,48	21122,00	8103,00	7094,00	7094,00	3,76E-01	4	1,50E+00	Fig. 17 C
		pred. bite	167	133,61	22313,50	6911,50	8285,50	6911,50	2,29E-01	4	9,17E-01	
		pred. search	167	122,55	20466,00	8759,00	6438,00	6438,00	**4,27E-02**	4	1,71E-01	
		dwelling	167	138,90	23197,00	6028,00	9169,00	6028,00	**6,06E-03**	4	**2,42E-02**	
		roaming	167	134,53	22466,50	6758,50	8438,50	6758,50	1,34E-01	4	5,37E-01	
		search	167	130,99	21875,00	7350,00	7847,00	7350,00	6,65E-01	4	2,66E+00	
WT	*Ppa-tbh-1*	pred. feed	141	106,88	15070,00	7772,00	5059,00	5059,00	**5,84E-03**	4	**2,34E-02**	Fig. 17 C
		pred. bite	141	103,57	14603,50	8238,50	4592,50	4592,50	**2,15E-04**	4	**8,61E-04**	
		pred. search	141	117,98	16635,00	6207,00	6624,00	6207,00	6,77E-01	4	2,71E+00	
		dwelling	141	106,89	15072,00	7770,00	5061,00	5061,00	**6,31E-03**	4	**2,53E-02**	
		roaming	141	136,95	19309,50	3532,50	9298,50	3532,50	**5,78E-09**	4	**2,31E-08**	
		search	141	121,26	17098,00	5744,00	7087,00	5744,00	1,79E-01	4	7,15E-01	
	WT	pred. feed	91									Fig. 19 B
		pred. bite	91									
		pred. search	91									
		dwelling	91									
		roaming	91									
		search	91									
WT larvae	*Ppa-tbh-1-tdc-1*	pred. feed	219	144,78	31707,00	12312,00	7617,00	7617,00	**9,20E-04**	1	**9,20E-04**	Fig. 19 B
		pred. bite	219	154,88	33918,00	10101,00	9828,00	9828,00	8,49E-01	1	8,49E-01	
		pred. search	219	149,21	32677,50	11341,50	8587,50	8587,50	5,51E-02	1	5,51E-02	
		dwelling	219	165,29	36199,00	7820,00	12109,00	7820,00	**2,80E-03**	1	**2,80E-03**	
		roaming	219	161,29	35322,50	8696,50	11232,50	8696,50	7,08E-02	1	7,08E-02	
		search	219	161,27	35318,50	8700,50	11228,50	8700,50	7,86E-02	1	7,86E-02	
	WT larvae	pred. feed	66									Fig. 20 B
		pred. bite	66									
		pred. search	66									
		dwelling	66									
		roaming	66									
		search	66									
WT larvae	Tyramine 2 mM	pred. feed	78	64,57051282	5036,5	3192,5	1955,5	1955,5	**6,48E-03**	2	**1,30E-02**	Fig. 20 B
		pred. bite	78	61,23717949	4776,5	3452,5	1695,5	1695,5	**2,71E-04**	2	**5,42E-04**	
		pred. search	78	74,73076923	5829	2400	2748	2400	4,77E-01	2	9,53E-01	
		dwelling	78	55,73076923	4347	3882	1266	1266	**1,49E-07**	2	**2,99E-07**	
		roaming	78	89,94871795	7016	1213	3935	1213	**4,60E-08**	2	**9,20E-08**	
		search	78	80,10897436	6248,5	1980,5	3167,5	1980,5	**1,74E-02**	2	**3,48E-02**	
WT larvae	Octopamine 2 mM	pred. feed	143	105,4895105	15085	4649	4789	4649	8,56E-01	2	1,71E+00	Fig. 20 B
		pred. bite	143	105,5979021	15100,5	4633,5	4804,5	4633,5	8,33E-01	2	1,67E+00	
		pred. search	143	109,5244755	15662	4072	5366	4072	1,06E-01	2	2,11E-01	
		dwelling	143	98,61538462	14102	5632	3806	3806	**2,47E-02**	2	**4,94E-02**	
		roaming	143	106,6643357	15253	4481	4957	4481	5,53E-01	2	1,11E+00	
		search	143	98,21328671	14044,5	5689,5	3748,5	3748,5	**1,68E-02**	2	**3,37E-02**	
	Ppa-tbh-1	pred. feed	197									Fig. 21 B
		pred. bite	197									
		pred. search	197									
		dwelling	197									
		roaming	197									
		search	197									
Ppa-tbh-1	*Ppa-tbh-1* + OA	pred. feed	401	336,0162095	134742,5	24855,5	54141,5	24855,5	**9,07E-15**	1	**9,07E-15**	Fig. 21 B
		pred. bite	401	328,8603491	131873	27725	51272	27725	**1,04E-09**	1	**1,04E-09**	
		pred. search	401	334,0785536	133965,5	25632,5	53364,5	25632,5	**2,73E-12**	1	**2,73E-12**	
		dwelling	401	290,7119701	116575,5	43022,5	35974,5	35974,5	7,22E-02	1	7,22E-02	
		roaming	401	270,7593516	108574,5	51023,5	27973,5	27973,5	**5,40E-09**	1	**5,40E-09**	
		search	401	255,4339152	102429	57169	21828	21828	**5,19E-19**	1	**5,19E-19**	

	WT	pred. feed	116								Fig. 23 B
		pred. bite	116								
		pred. search	116								
		dwelling	116								
		roaming	116								
		search	116								
WT	*Ppa-tbh-1*	pred. feed	170	222,37	37803,00	10222,00	23268,00	10222,00	**1,65E-12**	4	**6,60E-12**	Fig. 23 B
		pred. bite	170	221,68	37686,00	10339,00	23151,00	10339,00	**5,28E-11**	4	**2,11E-10**	
		pred. search	170	189,12	32150,50	15874,50	17615,50	15874,50	**3,87E-01**	4	**1,55E+00**	
		dwelling	170	180,57	30697,00	17328,00	16162,00	16162,00	5,61E-01	4	2,25E+00	
		roaming	170	178,11	30278,50	17746,50	15743,50	15743,50	3,21E-01	4	1,29E+00	
		search	170	164,13	27902,00	20123,00	13367,00	13367,00	**8,55E-04**	4	**3,42E-03**	
WT	*Ppa-ser-3*	pred. feed	137	193,63	26527,00	9915,00	17074,00	9915,00	**2,08E-06**	4	**8,33E-06**	Fig. 23 B
		pred. bite	137	184,42	25265,00	11177,00	15812,00	11177,00	**4,62E-03**	4	**1,85E-02**	
		pred. search	137	178,14	24404,50	12037,50	14951,50	12037,50	9,04E-02	4	3,61E-01	
		dwelling	137	148,54	20350,00	16092,00	10897,00	10897,00	**2,44E-03**	4	**9,77E-03**	
		roaming	137	179,47	24587,50	11854,50	15134,50	11854,50	5,85E-02	4	2,34E-01	
		search	137	155,65	21323,50	15118,50	11870,50	11870,50	6,14E-02	4	2,46E-01	
WT	*Ppa-ser-6*	pred. feed	104	151,72	15778,50	10169,50	10318,50	10169,50	8,97E-01	4	3,59E+00	Fig. 23 B
		pred. bite	104	159,36	16573,00	9375,00	11113,00	9375,00	1,90E-01	4	7,61E-01	
		pred. search	104	129,16	13432,50	12515,50	7972,50	7972,50	**1,20E-03**	4	**4,81E-03**	
		dwelling	104	155,01	16121,00	9827,00	10661,00	9827,00	5,59E-01	4	2,23E+00	
		roaming	104	192,37	20006,50	5941,50	14546,50	5941,50	**1,99E-09**	4	**7,96E-09**	
		search	104	155,20	16141,00	9807,00	10681,00	9807,00	5,43E-01	4	2,17E+00	
WT	*Ppa-octr-1*	pred. feed	215	217,16	46690,00	18885,00	23470,00	18885,00	**2,35E-02**	4	9,41E-02	Fig. 23 B
		pred. bite	215	241,29	51876,50	13698,50	28656,50	13698,50	**1,33E-10**	4	**5,31E-10**	
		pred. search	215	177,76	38218,50	27356,50	14998,50	14998,50	**1,38E-07**	4	**5,51E-07**	
		dwelling	215	239,28	51446,00	14129,00	28226,00	14129,00	**4,80E-09**	4	**1,92E-08**	
		roaming	215	215,10	46247,00	19328,00	23027,00	19328,00	1,25E-01	4	5,00E-01	
		search	215	194,25	41763,00	23812,00	18543,00	18543,00	**2,91E-02**	4	1,16E-01	
Ppa-tdc-1	WT	pred. feed	116	198,64	23042,00	11004,00	16256,00	11004,00	**2,58E-03**	6	**1,55E-02**	Fig. 24 B
		pred. bite	116	162,26	18822,00	15224,00	12036,00	12036,00	7,15E-02	6	4,29E-01	
		pred. search	116	209,90	24348,50	9697,50	17562,50	9697,50	**1,02E-05**	6	**6,11E-05**	
		dwelling	116	160,55	18624,00	15422,00	11838,00	11838,00	**4,43E-02**	6	2,66E-01	
		roaming	116	157,18	18233,00	15813,00	11447,00	11447,00	**1,14E-02**	6	6,85E-02	
		search	116	152,67	17709,50	16336,50	10923,50	10923,50	**2,45E-03**	6	**1,47E-02**	
Ppa-tdc-1	*Ppa-tbh-1*	pred. feed	197	175,54	34580,50	31217,50	15077,50	15077,50	**7,83E-12**	6	**4,70E-11**	Fig. 24 B
		pred. bite	197	171,04	33694,00	32104,00	14191,00	14191,00	**6,93E-13**	6	**4,16E-12**	
		pred. search	197	222,18	43769,50	22028,50	24266,50	22028,50	3,82E-01	6	2,29E+00	
		dwelling	197	201,74	39742,50	26055,50	20239,50	20239,50	**2,38E-02**	6	1,43E-01	
		roaming	197	251,23	49492,00	16306,00	29989,00	16306,00	**8,48E-08**	6	**5,09E-07**	
		search	197	247,37	48732,00	17066,00	29229,00	17066,00	**2,51E-06**	6	**1,51E-05**	
	Ppa-tdc-1	pred. feed	235									Fig. 24 B
		pred. bite	235									
		pred. search	235									
		dwelling	235									
		roaming	235									
		search	235									
Ppa-tdc-1	*Ppa-tbh-1-tyra-2*	pred. feed	184	161,23	29667,00	30593,00	12647,00	12647,00	**3,52E-16**	6	**2,11E-15**	Fig. 24 B
		pred. bite	184	162,32	29866,00	30394,00	12846,00	12846,00	**1,66E-13**	6	**9,98E-13**	
		pred. search	184	157,76	29027,00	31233,00	12007,00	12007,00	**6,56E-16**	6	**3,94E-15**	
		dwelling	184	209,53	38554,00	21706,00	21534,00	21534,00	9,44E-01	6	5,67E+00	
		roaming	184	278,28	51203,00	9057,00	34183,00	9057,00	**8,69E-25**	6	**5,22E-24**	
		search	184	272,46	50132,50	10127,50	33112,50	10127,50	**9,38E-21**	6	**5,63E-20**	
Ppa-tdc-1	*Ppa-tbh-1-ser-2*	pred. feed	298	254,77	75922,50	38658,50	31371,50	31371,50	**2,91E-02**	6	1,75E-01	Fig. 24 B
		pred. bite	298	226,41	67469,00	47112,00	22918,00	22918,00	**1,42E-12**	6	**8,52E-12**	
		pred. search	298	243,86	72670,00	41911,00	28119,00	28119,00	**7,19E-05**	6	**4,31E-04**	
		dwelling	298	252,47	75235,00	39346,00	30684,00	30684,00	**1,38E-02**	6	8,28E-02	
		roaming	298	324,25	96627,00	17954,00	52076,00	17954,00	**2,41E-22**	6	**1,45E-21**	
		search	298	304,30	90680,00	23901,00	46129,00	23901,00	**3,04E-10**	6	**1,82E-09**	
Ppa-tdc-1	*Ppa-tbh-1-tyra-3*	pred. feed	60	133,21	7992,50	7937,50	6162,50	6162,50	1,18E-01	6	7,08E-01	Fig. 24 B
		pred. bite	60	103,27	6196,00	9734,00	4366,00	4366,00	**3,69E-06**	6	**2,21E-05**	
		pred. search	60	223,58	13414,50	2515,50	11584,50	2515,50	**1,24E-14**	6	**7,44E-14**	
		dwelling	60	85,22	5113,00	10817,00	3283,00	3283,00	**1,35E-10**	6	**8,12E-10**	
		roaming	60	172,53	10352,00	5578,00	8522,00	5578,00	**1,09E-02**	6	6,52E-02	
		search	60	150,48	9028,50	6901,50	7198,50	6901,50	8,02E-01	6	4,81E+00	
Ppa-tdc-1	*Ppa-tbh-1-lgc-55*	pred. feed	175	195,03	34129,50	22395,50	18729,50	18729,50	1,11E-01	6	6,68E-01	Fig. 24 B
		pred. bite	175	190,44	33327,50	23197,50	17927,50	17927,50	**2,44E-02**	6	1,46E-01	
		pred. search	175	239,09	41840,00	14685,00	26440,00	14685,00	**6,86E-07**	6	**4,11E-06**	
		dwelling	175	194,62	34059,00	22466,00	18659,00	18659,00	1,07E-01	6	6,44E-01	
		roaming	175	238,10	41667,50	14857,50	26267,50	14857,50	**1,15E-06**	6	**6,87E-06**	
		search	175	214,00	37450,00	19075,00	22050,00	19075,00	2,10E-01	6	1,26E+00	
	WT larvae	pred. feed	103									Fig. 27
		pred. bite	103									
		pred. search	103									
		dwelling	103									
		roaming	103									
		search	103									
WT larvae	*Ppa-klp-6::HisCl* - Histamine	pred. feed	107	107,13	11463,00	5336,00	5685,00	5336,00	6,89E-01	2	1,38E+00	Fig. 27
		pred. bite	107	98,00	10485,50	6313,50	4707,50	4707,50	6,76E-02	2	1,35E-01	
		pred. search	107	99,36	10631,00	6168,00	4853,00	4853,00	1,35E-01	2	2,70E-01	
		dwelling	107	96,78	10355,50	6443,50	4577,50	4577,50	**3,33E-02**	2	6,65E-02	
		roaming	107	113,78	12174,50	4624,50	6396,50	4624,50	**4,13E-02**	2	8,26E-02	
		search	107	116,54	12469,50	4329,50	6691,50	4329,50	**7,30E-03**	2	**1,46E-02**	
WT larvae	*Ppa-klp-6::HisCl* + Histamine	pred. feed	104	87,96	9148,00	7024,00	3688,00	3688,00	**5,08E-05**	2	**1,02E-04**	Fig. 27
		pred. bite	104	84,32	8769,50	7402,50	3309,50	3309,50	**1,48E-06**	2	**2,97E-06**	
		pred. search	104	86,53	8999,00	7173,00	3539,00	3539,00	**2,28E-05**	2	**4,55E-05**	
		dwelling	104	107,36	11165,00	5007,00	5705,00	5007,00	4,18E-01	2	8,35E-01	
		roaming	104	123,58	12852,00	3320,00	7392,00	3320,00	**1,88E-06**	2	**3,75E-06**	
		search	104	115,81	12044,00	4128,00	6584,00	4128,00	**4,36E-03**	2	**8,72E-03**	
	Ppa-klp-6::HisCl - Histamine	pred. feed	107									Fig. 27
		pred. bite	107									
		pred. search	107									
		dwelling	107									
		roaming	107									
		search	107									
Ppa-klp-6::HisCl - Histamine	*Ppa-klp-6::HisCl* + Histamine	pred. feed	104	89,91	9351,00	7237,00	3891,00	3891,00	**7,19E-05**	1	**7,19E-05**	Fig. 27
		pred. bite	104	91,89	9556,50	7031,50	4096,50	4096,50	**7,64E-04**	1	**7,64E-04**	
		pred. search	104	90,86	9449,00	7139,00	3989,00	3989,00	**3,68E-04**	1	**3,68E-04**	
		dwelling	104	118,10	12282,50	4305,50	6822,50	4305,50	**4,34E-03**	1	**4,34E-03**	
		roaming	104	119,81	12460,00	4128,00	7000,00	4128,00	**1,12E-03**	1	**1,12E-03**	
		search	104	105,73	10996,00	5592,00	5536,00	5536,00	9,51E-01	1	9,51E-01	
	A. sudhausi	corpses	10									Fig. 29
A. sudhausi	*Asu-tbh-1*	corpses	10	5,5	55	89	11	11	**3,59E-03**	1	**3,59E-03**	Fig. 29

Table 3: p values of the statistical tests